NASA Contractor Report 165720

A COMPARISON OF SOME STATIC AND DYNAMIC MECHANICAL PROPERTIES OF 18x5.5 AND 49x17 TYPE VII AIRCRAFT TIRES AS MEASURED BY THREE TEST FACILITIES

Richard N. Dodge and Samuel K. Clark

THE UNIVERSITY OF MICHIGAN
Ann Arbor, Michigan 48109

Grant NSG-1494
July 1981

National Aeronautics and
Space Administration

Langley Research Center
Hampton, Virginia 23665

TABLE OF CONTENTS

A COMPARISON OF SOME STATIC AND DYNAMIC MECHANICAL PROPERTIES OF 18X5.5 AND 49X17 TYPE VII AIRCRAFT TIRES AS MEASURED BY THREE TEST FACILITIES

Richard N. Dodge and Samuel K. Clark
The University of Michigan

SUMMARY

Mechanical properties of 49x17 and 18x5.5 type VII aircraft tires were measured during static, slow rolling, and high-speed tests, and comparisons were made between data as acquired on indoor drum dynamometers and on an outdoor test track. In addition, mechanical properties were also obtained from scale model tires and compared with corresponding properties from full-size tires. While the tests covered a wide range of tire properties, results seem to indicate that speed effects are not large, scale models may be used for obtaining some but not all tire properties, and that predictive equations developed in NASA TR R-64 are still useful in estimating most mechanical properties.

INTRODUCTION

To analyze adequately the takeoff, landing and taxi characteristics of modern day aircraft, it is essential that landing gear designers have accurate data available on many tire mechanical properties. The measurement of these mechanical properties, however, is an expensive and lengthy process since aircraft tires are usually heavily loaded and operate of high speeds, thus requiring large and costly test equipment to simulate their operating conditions. Only two such facilities exist in the United States for the controlled study of such tire characteristics at realistic speeds and operating conditions: the Landing Loads and Traction Facility at the NASA Langley Research Center, and the Flight Dynamics Laboratory under the Air Force Wright Aeronautical Laboratories at Wright-Patterson Air Force Base (FDL).

At the present time, aircraft landing gear designers are forced to rely on very limited aircraft tire mechanical property data furnished by tire or component manufacturers or by the government laboratories of NASA and the Air Force. Extensive use is still being made of NASA Technical Report R-64, "Mechanical Properties of Aircraft Tires" reference 1, which summarizes the state of knowledge concerning mechanical characteristics of such tires as it existed about 20 years ago, and based almost entirely upon static or very slow rolling data. Almost nothing is currently available which describes the influence of speed on such tire characteristics.

Recognizing the lack of such data, aircraft industry representatives have for some years urged a coherent program for assessing the influence of speed and other dynamic characteristics on aircraft tire mechanical properties, and, further, have urged programs designed to assess the continuing validity of NASA TR R-64 in light of more modern aircraft tire designs. These efforts became focused in the industry committee which is primarily active in this area - the SAE Committee A5. Under the sponsorship of this committee, a program was originated jointly by the Landing Dynamics Office at NASA-Langley and the Flight Dynamics Laboratory at Wright Patterson Air Force Base. These two groups agreed to a co-operative test program generated jointly by them in conjunction with the SAE A5 committee, and The University of Michigan agreed to conduct a modest scale-model tire measurement program to determine the adequacy of scale model techniques in assessing speed and dynamic effects on aircraft tire mechanical properties.

Two Type VII, modern aircraft tire designs were chosen for this program: size 49x17 in a 26-ply rating and size 18x5.5 in a 14-ply rating. The test plan originally prepared to meet the needs of the program is given in Appendix B, and it basically involves evaluating the usual vertical, lateral, fore-and-aft and torsional static characteristics of both tire sizes, together with measurements of slow rolling relaxation length, cornering force, and self aligning torque. In addition, and most important, dynamic vertical load deflection, vertical hysteresis, cornering force and self aligning torque measurements were to be carried out on both tire sizes over a speed range to 100 knots.

Each of these properties has important uses in analyzing operating characteristics of the runway-tire-landing gear interaction in modern aircraft. For example, the vertical load deflection characteristics directly affect landing gear strut design, while lateral and torsional characteristics of the tires are directly related to cornering and yaw response and are thus important to shimmy analysis. Tire fore-and-aft elastic properties affect anti-skid and braking design, and are therefore important in their own right.

The program was initiated in 1975 with the acquisition of the tires through the Aeronautical Systems Division, Wright-Patterson Air Force Base and tests were conducted independently by both NASA-Langley and the Flight Dynamics Laboratory. In 1978, NASA initiated a Research Grant with the University of Michigan to conduct an analysis of the obtained data and to examine various methods for the transformation of the data from the static to the dynamic case. The purpose of this report is to present the results of that effort.

SYMBOLS

Values are given in both SI and U.S. Customary Units.

The measurements were made in U.S. Customary Units.

C_i - Constants relating model spring constants to prototype

D - Outside diameter of free tire

$E \cdot h$ - Tire membrane stiffness

F_x - Fore-and-aft force (ground force parallel to direction of motion)

F_y - Lateral force (perpendicular to direction of motion)

F_z - Vertical force

h - Half-length of the tire-ground contact area (footprint)

K - Spring constant

K_λ - Lateral spring constant

L_y - Yawed-rolling - relaxation length

M_z - Turning or twisting moment about a vertical axis through the wheel center

N - Cornering power

p_o - Inflation pressure at zero vertical load (gage)

Q - Dimensionless force ratio used in relating model forces to prototype forces

V - Horizontal rolling speed

σ_x - Fore-and-aft deflection

σ_y - Lateral deflection

σ_z - Vertical deflection

η - Dimensionless deflection ratio used in relating model deflections to prototype deflections

η_y - Lateral hysteresis parameter

ψ - Yaw angle

TEST FACILITIES AND PROCEDURES

The tires used in this program were 49x17, 26 ply-rating and 18x5.5, 14 ply-rating, Type VII aircraft tires which were selected in quantities of 5 each from Air Force inventory, chosen from the same manufacturer and with closely spaced serial numbers and dates of manufacture. Each of the tires was subjected to three break-in taxi runs of two miles at rated pressure and load. The scale model tires used in this study were designed and built by the University of Michigan which had experience (reference 2) in the modeling of aircraft tires. The scale models were constructed to a 12:1 ratio for the 49x17 tire and to a 4:1 ratio for the 18x5.5 tire. Table 1 provides a summary of pertinent geometric properties of the full-size tires and their corresponding scaled models.

The test plan for each tire is outlined in Appendix B. This plan was used by each facility, although it was not possible for each organization to measure all properties identified in the plan.

NASA Facility.

NASA used the same basic test equipment to determine most of the tire static vertical, lateral, and fore-and-aft stiffness characteristics. This equipment consisted of a bearing plate upon which the test tire rested under a vertical load, and the instrumentation necessary to monitor the various tire loadings and displacements. Tire loadings included the vertical load, which was controlled by the test carriage hydraulic system, and either the lateral or fore-and-aft load which was applied to the bearing plate by means of a hydraulic piston. The

magnitude of the vertical load was measured by load cells under the bearing plate, whereas other loads were measured by a load cell located between the hydraulic piston and a rigid backstop. The displacements were measured with dial gages and motion transducers.

The dynamic tire data obtained by NASA came from tests conducted on the Langley aircraft landing loads and traction facility. A description of this facility can be found in numerous NASA publications, of which reference 3 is a good example. Both test carriages were employed in this program. The large carriage with a speed potential of 110 knots served as the test bed for the 49x17 tire and the small carriage capable of speeds to 120 knots was used in testing the smaller tire. The runway surface for both tires was dry concrete.

The slow-rolling, quasi-static NASA data were obtained with the same facility used to acquire the dynamic data except instead of being propelled by the water jet the carriages were towed over the test section by a tug.

FDL Facility

The Flight Dynamics Laboratory static and slow-rolling quasi-static tests were performed on the flat surface Tire Force Machine (TFM). The basic features of this machine include a tire/wheel assembly housed in a frame containing six load cells through which the loads are applied and the resultant tire forces and moments are reacted, a twenty-foot flat movable test bed, and a computer-controlled automatic data logging system.

The dynamic data were obtained from the computer-controlled, 120-inch dynamometer test apparatus. The major features of this apparatus are a test carriage which supports the tire and is positioned by a servo-controlled hydraulic system, a 120-inch diameter dynamometer wheel, and a complete process control system which provides automatic sequencing and control of the test dynamometer and receives, processes, displays and records all test data.

A more complete description of these two test systems can be found in references 4 and 5.

University of Michigan Facility

Static tire data at the University of Michigan were obtained primarily from tests conducted on its small scale static test machine. This machine consists of a rigid bearing plate mounted on ball bearings, a hinged dead-weight arm and yoke for applying vertical loads to the test tire mounted in the yoke, a screw drive and load transducer system for applying and measuring lateral and fore-and-aft loads to the bearing plate, and dial gages and variable transformers for measuring displacements. A more complete description of this apparatus is given in reference 6.

The slow-rolling quasi-static, yawed tests were conducted on a 30-inch diameter cast iron road wheel discussed in reference 2. This apparatus consists primarily of a driven roadwheel, a hinged arm equipped with a tire yoke, and transducers to monitor lateral force and self-aligning torque.

Dynamic data were obtained from tests conducted on the University of Michigan 40-inch diameter inside-outside road-

wheel. This apparatus consists of a driven cantilevered roadwheel with apparatus similar to that on the smaller wheel. All tests described in this report were obtained on the outside surface of this wheel.

RESULTS AND DISCUSSION

Since the participants in this test program used different equipment in making their measurements, it was necessary to convert most of the raw data to some common format. This conversion was done, and to some extent it masked individual differences in measuring techniques, as, for example, curved steel drums as opposed to flat concrete surfaces. However such a presentation does allow direct comparison of results between different test facilities.

Several pertinent tire mechanical properties were calculated in terms of parameters defined in reference 1 and these are presented, where possible, to illustrate any changes associated with the newer type VII tires.

STATIC TEST RESULTS

Pure Vertical Loading - The load-deflection curves presented in figure 1 for the 49x17 tire and in figure 2 for the 18x5.5 tire include the four vertical loading conditions. As is commonly observed, a hysteresis loop in the vertical load deflection curve is obtained but the load deflection relationship is nearly linear for increasing load except for relatively low values of the load.

While there is some variation in the data obtained between the participants as noted in figures 1 and 2, no consistent difference of any magnitude was observed between vertical load deflection data taken at different test facilities.

The scale model data seems to be within the same general range of variation as the full size data.

Vertical Spring Rate: Vertical spring rates were obtained for each of the test conditions defined in figures 1 and 2 by measuring the slope of the load-deflection curve extending from its maximum to a point midway between the loading and unloading portion of the curve, at one half the maximum tire deflection, as illustrated in figure 3. These vertical spring rates are summarized in figure 4. Again the single dashed lines represent spring rates calculated in the same fashion from the load-deflection curves predicted by the empirical formula of NASA TR R-64, equation (23).

Contact Patch: Dimensions of the contact patch were obtained for all static vertical loadings by inking or chalking foot prints of the tires at each of the prescribed test conditions. A summary of the measured contact patch lengths for both tire sizes is presented in figure 5. The measurements agree well among the three test facilities, and the contact patch lengths calculated from equation (5) in NASA TR R-64 are also given. These computed patch lengths seem to be in good agreement with the measurements.

In general, as is evidenced from figures 1-5, measurements representing vertical response of the tire under static loading seem to be in good agreement from both full size test facilities as well as from the scale model tire. In addition, formulas derived earlier from NASA TR R-64 seem to be in good agreement for all vertical stiffness characteristics with measurements made on these more modern Type VII aircraft tires.

Combined Vertical and Lateral Loadings - When a stationary vertically loaded tire is subjected to a lateral load perpendicular to the wheel plane the tire experiences a corresponding lateral deformation, a vertical sinking and a lateral shifting of the vertical force-resultant location. As the lateral load is cycled from zero to a maximum, back through zero to a minimum and returns to zero, a hysteretic load deflection loop is generated. Such loops are illustrated in figures 6 and 7 for the two test tires in question. Since it has been observed that the nature of these loops is dependent on the maximum amplitude of the applied lateral load, all test data were obtained at lateral loads equal to 30% of the vertical load so the comparisons between different test facilities could be made.

Again, figures 6 and 7 show that both full-scale sets of measurements and the model tire measurements seem to agree quite well.

Lateral Spring Rate: Because of runway roughness, friction effects, and data recording differences it was often necessary to smooth the raw data obtained from these lateral load deflection curves. Such smoothed data were used to determine lateral spring rates and hysteretic effects described as follows.

Lateral spring rates were measured for all test conditions by measuring the slope of the line joining the end points of the load-deflection loop. A summary of these lateral spring rates is shown in figure 8. Again there is reasonably good agreement between spring rates obtained from full scale and model tires, and once more the formulation described in equation (33) of TR R-64 agrees well with measurements.

Lateral Hysteresis: The static lateral hysteresis can be obtained from the lateral load-deflection curves of figures 6 and 7 which indicate the energy dissipated during the loading and unloading cycle. This energy loss is believed to be primarily due to hysteretic effects in the tire materials. A measure of this hysteretic loss is the ratio of the area of the hysteresis loop to the total energy input to the tire during the loading cycle, measured by the two triangular areas under the load-deflection curve. This ratio, denoted by η_y, is used to describe the lateral hysteresis ratio of the tires and is similar in concept to tan δ of a viscoelastic material. Curves of this damping ratio are plotted against vertical load in figure 9. Agreement seems to be good between the full scale and model tires for the 49x17 size, but for the 18x5.5 size the scale model version seems to exhibit somewhat more hysteresis than its full size counterparts.

Again, although not to the same degree as for vertical loads, measurements representing lateral response of the tires under static loading are similar from all three test facilities, including scale modeling.

Combined Vertical and Torsional Loadings - As the twisting moment is cycled a torque versus angle-of-twist curve is generated which produces a loop caused by hysteretic loss in the tire material. Such measurements on full size tires are difficult to make since equipment is not commonly available for producing a torque large enough for the high loads commonly encountered in aircraft tires. However, the University of Michigan scale model tires can be loaded in torsion with relatively small loads, and the results from tests on such scale tires are shown in figure 10.

Torsional Spring Rate: It is difficult to assess the validity of the data presented in figure 10 since there are no full size tests with which to compare. However, torsional spring rates can be obtained from the slope of the line joining the end points of load-deflection loops. The results from such measurements are given in figure 11. These data may be compared with values predicted by equations (44) in reference 1, and there is general agreement between the two.

Torsional Hysteresis: As was the case with static lateral deformation, torsional loss coefficients can be calculated from loops generated in load-deflection curves, such as those of figure 10. As was done in the lateral case, loss coefficients were obtained by using the ratio of the loop area to the triangular areas representing energy input to the tire during deformation. These loss coefficients are shown for the 49x17 tire in figure 12 as taken from scale model data and are of approximately the same magnitude as those found for the lateral tests. This similarity should be anticipated since twisting motion is essentially lateral motion of a non-uniform distribution.

Combined Vertical and Fore-and-Aft Loadings - When a stationary vertically loaded tire is subjected to a fore-and-aft load the tire experiences a corresponding fore-and-aft deformation, a vertical sinking and a fore-and-aft shifting of the vertical force resultant. As this fore-and-aft load is cycled back and forth, a load-deflection curve is generated forming a closed loop which is attributed to hysteretic characteristics of the

tire material. These fore-and-aft load tests are difficult to perform because they require the measurement of the relatively small deformation under large loads. Only the Flight Dynamics Laboratory has equipment at this time suitable for such measurements, and data from the 49x17 tire are presented in figure 13 and data from the 18x5.5 tire are presented in figure 14. Since fore-and-aft deflection curves are dependent on the maximum amplitude of the applied fore-and-aft force, all test data was taken at ± 15% of the vertical load carried by the tire.

It would seem logical to attempt to use small scale tire models for the generation of fore-and-aft stiffness characteristics since the loads involved should be considerably less than those needed for the full size tires. However, measurements on such models suffer from two difficulties:

(a) Full size tires may be expected to exhibit a certain amount of slip and realignment in the contact patch area, which may not apply to small scale models, particularly in the presence of the large loads induced in the full size tires.

(b) The model scaling laws for the small size tires are somewhat different for fore-and-aft motion than for the other types of loadings and displacements since fore-and-aft displacements of a tire are highly dependent upon carcass and tread material stiffness.

Because of the difficult nature of the measurements here some of the data were smoothed prior to being included in the plots shown in figures 13 and 14.

Fore-and-Aft Spring Rate: Fore-and-aft spring rates were measured for each test condition. These rates were again determined by measuring the slope of the line joining the end points of the fore-and-aft load deflection loop. A summary of these spring rates is shown in figure 15.

Fore-and-Aft Hysteresis: A loss coefficient can be measured for the fore-and-aft load deflection loops, similar in definition to the loss coefficients obtained for lateral and torsional loadings. This coefficient was computed from the ratio of the area under the loop to the area representing energy input to the tire during the loading cycle. Such data on loss coefficients is given in figure 16. Note that these coefficients do not vary significantly with vertical load and exhibit values of the same general magnitude as lateral and torsional hysteresis coefficients.

SLOW-ROLLING YAWED TEST RESULTS

The three mechanical tire characteristics reported in this section all occur when a tire is yawed with respect to its direction of motion and then slowly rolled straight ahead with the yaw angle ψ held constant. When rolling commences, the tire builds up a lateral force perpendicular to the wheel plane which exponentially approaches a steady-state value. The rapidity with which this force builds up is characteristic of the tire and is called the yawed rolling relaxation length when it is measured as a distance traversed by the axle. After steady state conditions are reached the lateral force and self-aligning torque, defined as the moment about the vertical steer axis of the wheel center, act on the axle and in turn on the vehicle. These quantities are also functions of the yaw angle of the tire.

Relaxation Length - It is common for tests of yawed rolling relaxation lengths of tires to produce results with considerable scatter and the data collected from this study proved to be no exception. Figures 17a and 17c illustrate composite plots of the results from the three test programs reported here. This is not unlike data reported from other sources.

String theory, reference 7, implies that for constant inflation pressure the major parameter affecting relaxation length is vertical load or tire deflection. Because of this, the relaxation lengths at different yaw angles but at the same load were averaged, and these values are plotted as a function of the load in summary plots given in figures 17b and 17d. They show that the three sets of tests, two full size and one scale model,

yield similar average values for the relaxation lengths for both tires, with some variation on the 18x5.5 tire. Predictions made from equation (64) in reference 1 are also given in these figures, and agree surprisingly well with the measurements reported.

One reason for the apparent wide scatter in relaxation lengths is found by examining the nature of such measurements. Figure 18 is a plot of side force versus distance traveled at fixed yawed angle. The force builds up from zero to a steady state value in a nearly exponential manner. Relaxation length is defined as the distance traveled for the side force to build to (1-1/e) of its steady state value. In figure 18 it can be seen that the determination of the steady state value requires a certain amount of judgment because of circumferential irregularities in the tire side force. Obviously this choice can influence the relaxation length considerably.

Steady State Side Force - Tire steady state side force increases with increasing yaw angle for fixed vertical load in a relatively linear fashion for the relatively small yaw angles specified in this test plan. This force will eventually approach asymptotically a maximum value controlled in part by the coefficient of friction between the tire and runway surface. Figures 19 and 20 show that the three different sets of tests produced comparable values for side force under most of the test conditions used. The scale model conversion factors used here are the same as used for the static vertical load-deflection data.

The interaction of side force and yaw angle on vertical load can be observed somewhat more clearly in carpet plots

conventionally used for displaying such data. Carpet plots for the side force on both test tires are given in figures 21 and 22. From these it is seen that the increase of side force with yaw angle is strong, as is expected, but also that for fixed yaw angle the side force remains relatively constant for increasing load except at angles above 6°. Care should be taken in comparing data between different laboratories since the results are dependent on the friction surfaces used.

The slope of the cornering force versus yaw angle curves at 0° yaw is defined as tire cornering power, and is a measure of tire lateral or steering stiffness. Data on this is presented in figure 23 for both tire sizes tested, and predictions from equations (83) in reference 1 are also given.

Self-Aligning Torque - The measurement of self-aligning torque against yaw angle is more difficult than the measurement of side force, since the quantities measured are smaller and can depend on tire force irregularities. Self-aligning torque data for the 49x17 and 18x5.5 tires are given in figures 24 and 25. In figure 24 it should be noted that the maximum self-aligning torque is reached at a yaw angle less than 9° on the full sized tires, while the scale tires exhibit increasing values of self-aligning torque up to the maximum yaw angle. The higher torque noted for the scaled tires is attributed to the higher friction coefficient available by virture of the lower tire contact pressures.

Carpet plots of self-aligning torque, yaw angle and vertical load can be constructed as done previously for side force values. These are shown for the two test tires in figures 26

and 27. In general these show that at fixed yaw angle the self-aligning torque increases with increasing tire load.

DYNAMIC TEST RESULTS

Pure Vertical Loading - A thorough study of the vertical load deflection characteristics of the two tire sizes used in this program was conducted at various surface speeds according to the test plan in Appendix B. Basically the test plan called for vertical load-deflection curves at 5, 50, 75, and 100 knots, with maximum vertical loads of 50%, 75%, 100%, and 125% of rated loads, all at rated inflation pressure. Typical curves from such tests are shown in figure 28. Again, as might be expected from quite different test facilities, the participants produced load-deflection curves having slightly different characteristics. For example, the NASA landing loads track produces load-deflection curves somewhat sensitive to runway roughness, which is to be expected. On the other hand, data taken on smooth cylindrical drums such as obtained from the Flight Dynamics Laboratory and from the University of Michigan scale model studies are smoother but less realistic since they include the effects of drum curvature.

Vertical spring rates were calculated for each of the forward speed test conditions in the same manner as were the static spring rates. Summaries of these spring rates are given in figures 29 and 30. In general there appears to be little influence of speed on vertical spring rate of a free rolling tire.

It has been observed in other test programs, (see 7.2.2 of reference 8), that the hysteresis loop in the vertical load-deflection curve of a rolling tire is much smaller, or even vanishes altogether, as compared with the size of the hysteresis

in a stationary tire under a vertical load. This negligible hysteresis implies that the effective damping of the vertical motion produced by the rolling tire is negligible when compared with the damping experienced by the stationary tire. This phenomenon is illustrated in figure 31 where various load-deflection curves have been plotted for the University of Michigan scale model tire under a variety of speeds. Their data merely confirm a phenomenon which has been observed in other test programs.

Yawed Rolling Side Force - When a wheel is yawed with respect to its direction of motion and then rolled forward with a yaw angle held constant a side force perpendicular to the wheel plane is generated. This side force comes from the elastic deformation of the tire carcass caused by friction forces in the contact patch. These forces were measured by each of the three participants in this test program under a variety of test conditions. Summaries of these results are given in figures 32 and 33. While there is some scatter in the data, in general a conclusion seems to be that there is little influence of speed on side force for either of these tires up to a speed of 100 knots.

The interaction of side force, speed, and yaw angle at a fixed load may be seen more clearly from carpet plots such as those presented in figures 34 and 35. From these it is clear that side force depends primarily upon yaw angle as would be expected.

Table 2 shows the results of computations of cornering power using data from slow rolling tests, and the formulation for cornering power, equation (83) reference 1. It is compared with measured data taken at 50 knots to determine if slow speed mechanical properties can be used to calculate cornering power at higher velocities. Note that agreement is not particularly bad.

Figure 36 is a plot of data taken from the last column of Table 2, illustrating cornering power versus vertical load at a speed of 50 knots. This figure is similar to figure 23 and shows that the calculated values of cornering power at 50 knots do not agree quite as well with the experiment as those values done under slow rolling conditions.

Self-Aligning Torque Under Yawed Rolling - When a tire is yawed with respect to its direction of motion by an angle and then rolled straight ahead with the yaw angle held constant, a self-aligning torque is generated by the interaction of the tire and the contact surface. This torque may be visualized as a moment about a vertical axis through the wheel center. Values for this self-aligning torque were measured by each of the facilities involved in this program and for the various test conditions described in the original test plan.

Data for the variation of self-aligning torque with speed for various yaw angles is presented in figures 37 and 38. As previously discussed, this type of measurement is difficult to carry out, even under slow rolling conditions. Under dynamic

conditions it is doubly difficult since self-aligning torque is quite sensitive to surface irregularities and tire construction. For that reason it is difficult to achieve good correlation between measurements made at different locations, and it is also difficult to assess the value of scale modeling here. The only general trend that can be drawn from this data is that there is a slight decrease in self-aligning torque as the speed of the tire increases.

A somewhat more comprehensive illustration of self-aligning torque versus speed and yaw angle at fixed vertical load is given in figures 39 and 40. These semi-carpet plots illustrate somewhat more clearly the slightly decreasing nature of self-aligning torque with speed. They also clearly illustrate the non-linear relationship between self-aligning torque and yaw angle for constant speed and vertical load.

Overall there seems to be considerable variations between values of self-aligning torque measured under runway and drum conditions, again possibly due to two reasons:

(a). The influence of runway or drum surface friction effects on self-aligning torque. Obviously a concrete runway and a steel drum present widely different friction limits to the tire contact patch.

(b). The curvature effect of the drum on self-aligning torque can be significant.

Overall it appears that while correlation is difficult to obtain between drum and runway tests, speed does not significantly affect the maximum value of self-aligning torque obtained, although the angle at which the maximum occurs is not the same for each test facility.

CONCLUDING REMARKS

There were several objectives to this study, but the major ones are as follows: a) Determine the relationship between tire mechanical properties obtained statically, quasi-statically and dynamically, b) Examine differences in measured tire properties between data taken on runway surfaces and on dynamometer drums, c) Evaluate the role of scale modeling in determining mechanical properties of aircraft tires, and d) Explore the application of empirical formulas derived in TR R-64 to more modern Type VII aircraft tires.

As has been observed before, it was found in the series of tests that the hysteresis characteristics of a rolling tire were negligible compared to the hysteresis found in the stationary tire, both under conditions of vertical oscillation.

Most of the effects measured in this study showed little or no change with speed up to about 100 knots. For example, vertical spring rate of the tires did not change significantly nor did side forces generated due to rolling at a yaw angle. However there seems to be less consistency to self-aligning torque data. In some cases it appeared to be rather independent of speed, while in other cases it showed some variation with speed, usually decreasing as the speed became higher. The nature of this particular relationship is dependent on the magnitude of the yaw angle.

The level of agreement between test facilities was good for static mechanical properties, since both facilities used flat surfaces for such measurements. Measurements made dynamically showed less agreement, probably because the curvature effects

associated with the steel dynamometer drums may have caused some differences in properties, particularly self-aligning torque. Generally agreement was good for side force and self-aligning torque for small yaw angles, but measurements tended to differ at larger yaw angles as curvature effects became more pronounced.

Scale modeling of tire mechanical properties has generally proved to be satisfactory for obtaining large quantities of data at low cost. For example, static vertical load-deflection curves from model tires agree well with full size tire data, and lead consequently to good agreement for spring rates and contact patch lengths. Similarily lateral load-deflection characteristics agree well between scale models and the full size tires, although hysteresis effects are not quite as closely modeled as the stiffness properties.

Scale modeling does not seem to be adequate for fore-and-aft stiffness measurements since the scaling laws involving translation from small models to full size tires are quite different for this property than for the other properties. Fore-and-aft characteristics depend almost entirely on the elastic stiffness of the tire carcass, while for vertical and lateral properties the inflation characteristics are dominant.

Scale modeling of both slow rolling and dynamic effects seems also to be quite good. Side force and self-aligning torque both seem to agree well at relatively small yaw angles but not at larger yaw angles. Similarily, speed effects seem to agree quite well between model and full size tires.

In summary it appears that scale modeling of aircraft tire mechanical properties is warranted, provided that care is taken to use it judiciously in those areas where it has proven to be successful.

Finally, it is encouraging to note the good agreement between the formulations developed in NASA TR R-64 some years ago to the tire mechanical properties measured on these more modern Type VII aircraft tires. Load-deflection curves and vertical spring rates are well represented, as are contact patch lengths, lateral spring rates, and relaxation lengths. Predictions of fore-and-aft spring rates, slow rolling cornering power and cornering power at high speeds can not be confirmed as well because of variations in measured data. However, due to the relatively speed insensitive nature of mechanical properties measured here, it may be concluded that the data from TR R-64 probably apply equally well to dynamic tire characteristics as to slow speed characteristics. This is one of the major conclusions of this work.

REFERENCES

1. Smiley, Robert F. and Walter B. Horne, "Mechanical Properties of Pneumatic Tires With Special References to Modern Aircraft Tires", NASA TR R-64, National Aeronautics and Space Administration, Washington D.C., 1960.

2. Clark, S.K., R. N. Dodge, J. I. Lackey, and G. H. Nybakken, "The Structural Modeling of Aircraft Tires", AIAA Paper No. 71-346, AIAA, N.Y., 1971.

3. Tanner, John A., "Fore-and-Aft Elastic Response of 34x9.9, Type VII, 14 Ply-Rating Aircraft Tires of Bias-Ply, Bias-Belted, and Radial Design", ANSA TN D-7449, National Aeronautics and Space Administration, Washington D.C., 1974.

4. Hampton, James R., "Aircraft Tire Mechanical Property Testing", Paper presented at 4th Symposium on Nondestructive Testing of Tires, 23-25 May 1978, Sponsored by Army Materials and Mechanics Research Center.

5. "Air Force Flight Dynamics Laboratory Landing Gear Test Facility Wright-Patterson Air Force Base", Brochure prepared by the Mechanical Branch Air Force Flight Dynamics Laboratory 1977.

6. Dodge, R. N., R. B. Larson, S. K. Clark, and G. H. Nybakken, "Testing Techniques for Determining Static Mechanical Properties of Pneumatic Tires", NASA CR-2412, National Aeronautics and Space Administration, Washington D.C., June 1974.

7. Von Schlippe, B., and Dietrich, R., "Zur Mechanik of Luftreifens" (The Mechanics of Pneumatic Tires.) Junkers Flugzeug-und Motorenwerke, A-G. (Desau). (Translation available from ASTIA as ATI 105296)

8. Clark, S. K., "Mechanics of Pneumatic Tires", National Bureau of Standards Monograph 122, National Bureau of Standards, Washington, D.C., 1971.

Appendix A

The basic concept used in modeling mechanical properties of aircraft tires is shown in figure A-1. After considerable experimentation it has been verified that most tire elastic stiffnesses are linearly proportional to inflation pressure. This conclusion holds for vertical stiffness, lateral stiffness, fore-and-aft stiffness and torsional stiffness.

Notice in figure A-1 that the intercept is not zero at zero inflation pressure, but rather some positive value. This observation gives rise to the concept that a typical tire stiffness value may be expressed analytically as shown in equation (A-1),

$$K = C_1 Eh + C_2 p_o D \qquad (A\text{-}1)$$

where K represents a typical tire spring rate, the product "Eh" represents tire membrane stiffness, which for the same cord angle between model and prototype may be expressed approximately as the number of plies times the end count times the cord modulus. p_o is the inflation pressure and D is the tire diameter, used here as a characteristic length. C_1 and C_2 are constants which must be determined from experiment. In equation (A-1), the influence of the tire carcass is expressed by the product $C_1 Eh$. The influence of the inflation pressure in the tire is given by the term $C_2 p_o D$. In the formulation C_1 and C_2 are constants for each tire and for each different stiffness property under consideration.

In view of the fact that equation (A-1) represents the spring rate, then the load carried by the tire may be represented in equation (A-2) as derived directly from equation (A-1) where F is equal to a typical tire force.

$$\left(\frac{F}{D}\right) = [C_1 Eh + C_2 p_o D] \left(\frac{\delta}{D}\right) \qquad \text{(A-2)}$$

In Eq. (A-2), the tire diameter D has been inserted in the denominator of each side of the equation, so as to retain a dimensionless tire deflection $(\frac{\delta}{D})$.

Practically we know that a non-linear load deflection curve is formed when either a model tire or a full size tire is cyclically loaded. If such a curve could be reduced to dimensionless form then it should be the same for both model and prototype. Alternately if one could determine the dimensionless load deflection curve for the mode, then it could be used to predict the full size load deflection curve. This process uses Eq. (A-2) as its basis, since it is a dimensionless load-deflection relation.

We may achieve this by reducing the load-deflection loop on the model to dimensionless form and then reevaluating it back up to the true dimensions of the full size tire. This may be done in the three steps illustrated in figure (A-2)., where the variables used are the dimensionless force and the dimensionless deflection as given by Eq. (A-3).

$$\pi = \frac{F/D}{C_1 Eh + C_2 p_o D} = g\left(\frac{\delta}{D}\right) \qquad \text{(A-3)}$$

where g is the general functional form and $\frac{\delta}{D}$ is a dimensionless variable.

In figure (A-2a) the model force-deflection curve is shown as originally taken on the model tire. This may be reduced to a dimensionless form by scale change as given by figure (A-2b), using the variables as given in Eq. (A-3). These may then be

expanded to the full size tire by the relations between the diameter of the full size tire and model, and between the products Eh and p_0D of the full size tire and model. This is illustrated in Figure (A-2c). In practice this is nothing more than a scale change of the original load deflection curve taken on the model tire. This concept is simply that if one reduces the load deflection curve of either the model tire or the full size tire to a dimensionless form, then those two curves should be identical if scale modeling has been done properly.

It is necessary to devise a means for determining the constants C_1 and C_2 which appear in Eqs. (A-1), (A-2), and (A-3). This may be done by constructing the scale model of the tire and measuring the appropriate spring rate as a function of inflation pressure as shown in figure (A-1). By taking a series of measured spring rates at different inflation pressures, this curve can be produced for any one of the tire stiffness properties. For example, figure (A-3) shows actual data for the 49x17 model tire for the vertical spring rate as a function of inflation pressure for three different model tires. One can see the excellent linearity obtained from this data.

In figure (A-3) it is seen that the three different scale models have a very linear relationship between vertical spring rate and inflation pressure, so that the constant C_1 may be determined from the intercept of the line with the ordinate, while the constant C_2 is determined from the slope of the line.

From figure (A-3) and Table 1 one can calculate the coefficients required to convert model static vertical load deflection data to full size data for the 49x17 tire. First,

the end count and ply thickness were the same for the full size tires and models used in this study. Thus the "Eh" was directly proportional to the number of plies. Therefore:

$$K_z = C_1Eh + C_2Dp_o$$

where $C_1Eh = 28.22$ and $C_2D = 5.457$ but "Eh" = 2 and D = 4,

thus: $C_1 = \frac{28.22}{2} = 14.11$ and $C_2 = \frac{5.457}{4} = 1.364$

Referring to figure (A-2b) and (A-2c):

$$F_p = D_pQ[C_1Eh + C_2Dp_o]_p, \quad Q = \frac{F_m}{D_m[C_1Eh + C_2Dp_o]_m}$$

where subscript m refers to the model and p refers to the full size. Substituting:

$$F_p = \{\frac{[C_1Eh + C_2Dp_o]}{[C_1Eh + C_2Dp_o]_m}p\} F_m$$

Using data from Table 1 and assuming C_1Eh and C_2D are the same for model and prototype:

$$F_p = \{\frac{48}{4} \frac{[14.11(26) + 1.364(170)(48)]}{[28.22 + 5.457(50)]}\}F_m$$

$$F_p = 458\ F_m$$

This implies that to convert a vertical force on the 49x17 model tire to full size, the model value must be multiplied by 458. Similar coefficients were obtained for the other static elastic properties of each tire size.

The deflection coefficient was simply the scale factor:

$$\delta_p = \frac{48}{4}\delta_m = 12\delta_m \text{ for 49x17}$$

Table A-1 presents a complete tabulation of all conversion factors used in this report.

Table A-1 - Conversion Factors Used in Converting UM Model Data to Full Size Data - Dimensionless

TIRE	p_o Full Size	p_o Model	F_z	F_y	F_x	M_z	δ_z	δ_y	δ_x
18x5.5	1482 kPa (215 psi)	103.4 kPa (15 psi)	99.2	120	-	-	4	4	4
		344.8 kPa (50 psi)	51.6	53.5	-	-	4	4	4
49x17	1172 kPa (170 psi)	137.9 kPa (20 psi)	1005	1005	557	5880	12	12	12
		344.8 kPa (50 psi)	458	458	119	4077	12	12	12

F_z = vertical load

F_y = lateral load

F_x = fore-aft load

M_z = self aligning torque

δ_z = vertical deflection

δ_y = lateral deflection

δ_x = fore-aft deflection

Appendix B

The details of the test plan used to produce the data in this report are listed below:

I. Static Mechanical Properties (each loading at 4 tire locations, 90° apart)

A. Vertical Load

1. Vertical load deflection as per SAE AIR 1380, where the vertical loads are to be 50, 75, 100 and 125 percent of the tire rated load; the inflation pressure prior to loading is to be maintained at the rated value.

2. Contact patch lengths measured under each of the vertical loads.

B. Lateral Load (Maximum lateral loads limited to ±30% of the vertical loads

1. Lateral load-deflection under each vertical load as per SAE AIR 1380

2. Lateral hysteresis for all tests in B-1.

3. Center of pressure shift as per SAE AIR 1380 for all tests in B-1.

C. Torsional Load (Maximum torsional loading limited to ±80% of linearity)

1. Torsional load-deflection curves for all vertical loads.

2. Torsional hysteresis for all tests in C-1.

D. Fore-and-aft Load (maximum fore-and-aft loads limited to ±15% of the vertical load.

1. Fore-and-aft load deflection curves for all vertical loads.

2. Fore-and-aft relaxation length for all tests in D-1.

3. Fore-and-aft hysteresis measurements for all tests in D-1.

4. Fore-and-aft center of pressure shift for all tests in D-1.

II. Quasi-Static Slow-Rolling Yawed Mechanical Properties (All tests at rated inflation pressure).

A. Cornering Force - Fully developed cornering force at slip angels of 1,3,6, and 9 degrees at the four vertical loadings.

B. Self-Aligning Torque - Fully developed self-aligning torque at slip angles of 1,3,6, and 9 degrees at the four vertical loadings.

C. Lateral Relaxation Length - As determined by transient yawed rolling tests under the four test vertical loads and slip angles of 1,3,6, and 9 degrees.

D. Lateral Center of Pressure Shift - as per SAE AIR 1380 for all tests in II-A.

III. Dynamic Mechanical Properties (All tests at rated inflation pressure).

A. Vertical Load

1. Load-deflection curves up to the four test vertical loadings at speeds of 5, 50, 75, and 100 knots.

2. Hysteresis loss for all tests in A-1.

B. Cornering Force - Cornering force versus slip angle at 5, 50, 75, and 100 knots, at the four test vertical loadings for slip angles of 1,3,6, and 9 degrees.

C. Self-Aligning Torque - Self-aligning torque versus slip angle at 5,50,75, and 100 knots at the four test vertical loadings for slip angles of 1,3,6 and 9 degrees.

TABLE 1 - GEOMETRIC PROPERTIES OF THE TEST TIRES

Geometric Property	49x17		18x5.5	
	Full Size	Model	Full Size	Model
Ply Rating	26	2	14	4
Max. Outside Dia.	125.17 cm (49.28 in.)	10.16 cm (4.00 in.)	46.23 cm (18.20 in.)	11.43 cm (4.50 in.)
Min. Outside Dia.	119.84 cm (47.18 in.)	-	43.18 cm (17.00 in.)	-
Max. Width	43.76 cm (17.23 in.)	3.61 cm (1.42 in.)	14.94 cm (5.88 in.)	3.43 cm (1.35 in.)
Min. Width	39.45 cm (15.53 in.)	-	13.16 cm (5.18 in.)	-
Shoulder Diameter	109.22 cm (43.00 in.)	-	41.15 cm (16.20 in.)	-
Shoulder Width	36.83 cm (14.50 in.)	-	12.70 cm (5.00 in.)	-
Weight	907 N (204 lbs)	-	69 N (15.50 lbs)	-
Maximum Load	176.1 kN (39600 lbs)	378 N (85 lbs)	27.6 kN (6200 lbs)	506 N (113.7 lbs.)
Rated Inflation (unload)	1172 kPa (170 psi)	345 kPa (50 psi)	1482 kPa (215 psi)	345 kPa (50 psi)
Rated Inflation (load)	1220 kPa (177 psi)	-	1544 kPa (224 psi)	-
Aspect Ratio	0.84	-	0.87	-
Loaded Radius at Rated Conditions	51.31 cm (20.20 in.)	-	19.05 cm (7.50 in.)	-
Flange Diameter	56.69 cm (23.50 in.)	4.98 cm (1.96 in.)	24.76 cm (9.75 in.)	6.25 cm (2.46 in.)
Rim Diameter	50.80 cm (20.00 in.)	-	20.32 cm (8.00 in.)	-

Table 2 - Measured and Calculated Values of Cornering Power

$$N = \frac{\pi}{180} (Ly + h)k_\lambda \text{ kN/deg (lb/deg)}$$

Tire and Facility	F_z kN (lb)	$\frac{dF}{d\psi}$, ψ=0 N/deg Measured N (lb/deg)	Ly cm (in)	h cm (in)	k_λ N/cm (lb/in)	Calculated N kN/deg (lb/deg)	Measured N 50 knots kN/deg (lb/deg)
49x17 26 PR p_o = 1172 kPa (170 psi) NASA	200.2 (45000)	11100 (2500)	58.4 (23.0)	27.99 (11.02)	8835 (5045)	13.33 (2996)	11.68 (2625)
	176.1 (39600)	11100 (2500)	66.0 (26.0)	26.42 (10.40)	9110 (5202)	14.70 (3305)	14.22 (3196)
	132.1 (29700)	9880 (2222)	55.6 (21.9)	23.39 (9.21)	9519 (5436)	13.13 (2952)	12.93 (2908)
	88.1 (19800)	10500 (2352)	51.3 (20.2)	19.86 (7.82)	10582 (6043)	13.14 (2955)	12.15 (2732)
FDL	220.2 (49500)	8150 (1833)	59.7 (23.5)	30.43 (11.98)	6584 (3760)	10.35 (2328)	7.17 (1612)
	176.1 (39600)	8900 (2000)	62.2 (24.5)	2731 (10.75)	6975 (3983)	10.90 (2450)	7.53 (1693)
	132.1 (29700)	9200 (2069)	61.5 (24.2)	24.00 (9.45)	7343 (4193)	10.96 (2463)	7.38 (1660)
	88.1 (19800)	9880 (2222)	54.6 (21.5)	19.94 (7.85)	7646 (4366)	9.95 (2237)	5.82 (1308)

Table 2 - Measured and Calculated Values of Cornering Power

$$N = \frac{\pi}{180} (Ly + h)k_{\lambda} \text{ kN/deg (lb/deg)}$$

Tire and Facility	F_z kN (lb)	$\frac{dF}{d\psi}$, ψ=0 Measured N N/deg (lb/deg)	Ly cm (in)	h cm (in)	k_{λ} N/cm (lb/in)	Calculated N kN/deg (lb/deg)	Measured N 50 knots kN/deg (lb/deg)
UM	221.5 (49800)	10400 (2333)	57.2 (22.5)	31.55 (12.42)	6355 (3629)	9.84 (2212)	-
	170.8 (38400)	11100 (2500)	53.3 (21.0)	28.50 (11.22)	7260 (4146)	10.69 (2403)	8.93 (2007)
	127.2 (28600)	11600 (2609)	42.7 (16.8)	2393 (9.42)	8619 (4922)	10.02 (2252)	10.31 (2319)
	86.3 (19400)	11700 (2631)	30.2 (11.9)	20.12 (7.92)	9807 (5600)	8.62 (1937)	7.54 (1695)
18x5.5 14PR p_o = 1482 kPa (215 psi) NASA	34.5 (7750)	1454 (327)	15.5 (6.1)	10.01 (3.94)	4164 (2378)	1.85 (417)	-
	27.6 (6200)	1481 (333)	9.6 (3.8)	9.27 (3.65)	4254 (2429)	1.40 (316)	-
	20.7 (4650)	1632 (367)	11.2 (4.4)	8.30 (3.27)	4662 (2662)	1.58 (356)	-
	13.8 (3100)	1690 (380)	7.9 (3.1)	7.06 (2.78)	4536 (2590)	1.18 (266)	-

Table 2 - Measured and Calculated Values of Cornering Power

$$N = \frac{\pi}{180} (Ly + h)k_{\lambda} \text{ kN/deg (lb/deg)}$$

Tire and Facility	F_z kN (lb)	$\frac{dF}{d\psi}$, ψ=0 N/deg Measured N (lb/deg)	Ly cm (in)	h cm (in)	k_{λ} N/cm (lb/in)	Calculated N kN/deg (lb/deg)	Measured N 50 knots kN/deg (lb/deg)
FDL	34.5 (7750)	1601 (360)	39.6 (15.6)	10.03 (3.95)	3269 (1867)	2.83 (637)	-
	27.6 (6200)	1512 (340)	36.8 (14.5)	9.40 (3.70)	3380 (1930)	2.73 (613)	-
	20.7 (4650)	1512 (340)	31.0 (12.2)	8.00 (3.15)	3515 (2007)	2.39 (538)	-
	13.8 (3100)	1156 (260)	22.9 (9.0)	6.60 (2.60)	3818 (2180)	1.96 (441)	-
UM	34.5 (7750)	1619 (364)	20.8 (8.2)	10.41 (4.10)	3889 (2221)	2.21 (477)	-
	27.6 (6200)	1779 (400)	18.0 (7.1)	9.04 (3.56)	4371 (2496)	2.06 (464)	-
	20.7 (4650)	1690 (380)	15.7 (6.2)	7.52 (2.96)	4805 (2744)	1.95 (439)	-
	13.8 (3100)	1468 (330)	13.7 (5.4)	6.05 (2.38)	5380 (3072)	1.85 (417)	-

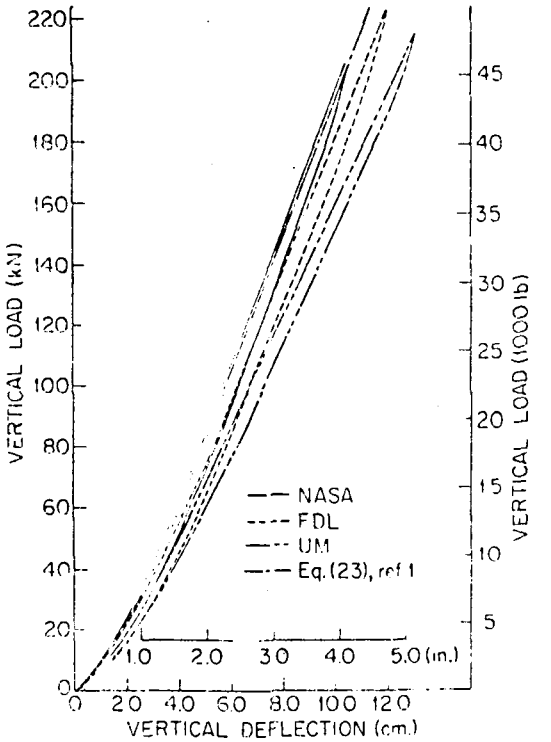

(a) $(F_Z)_{max}$ = 125% Rated Load

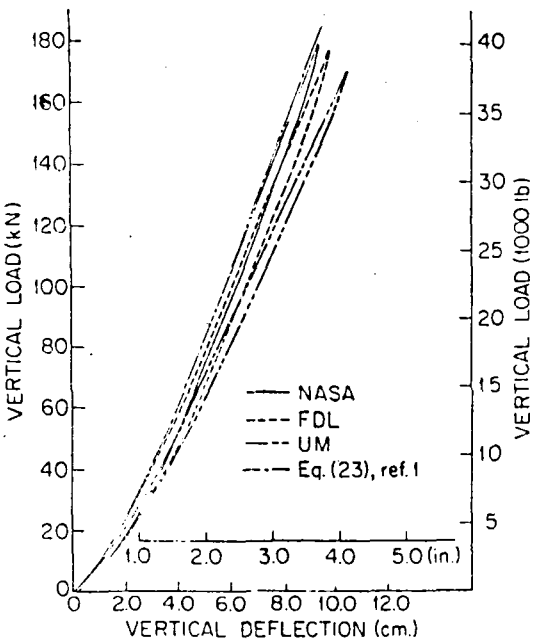

(b) $(F_Z)_{max}$ = 100% Rated Load

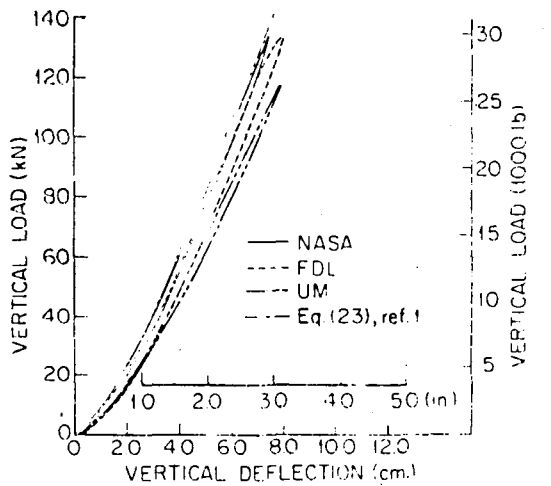

(c) $(F_Z)_{max}$ = 75% Rated Load

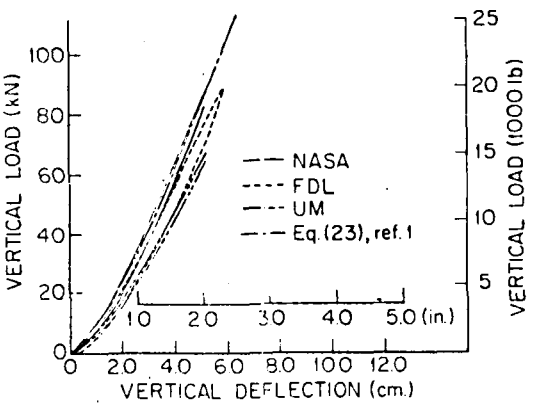

(d) $(F_Z)_{max}$ = 50% Rated Load

Figure 1 - Composite Static Vertical Load-Deflection Curves (49x17, 26 PR, Type VII Tire; Inflation Pressure=1172 kPa (170 psi); Rated Load=176.1 kN (39600 lb))

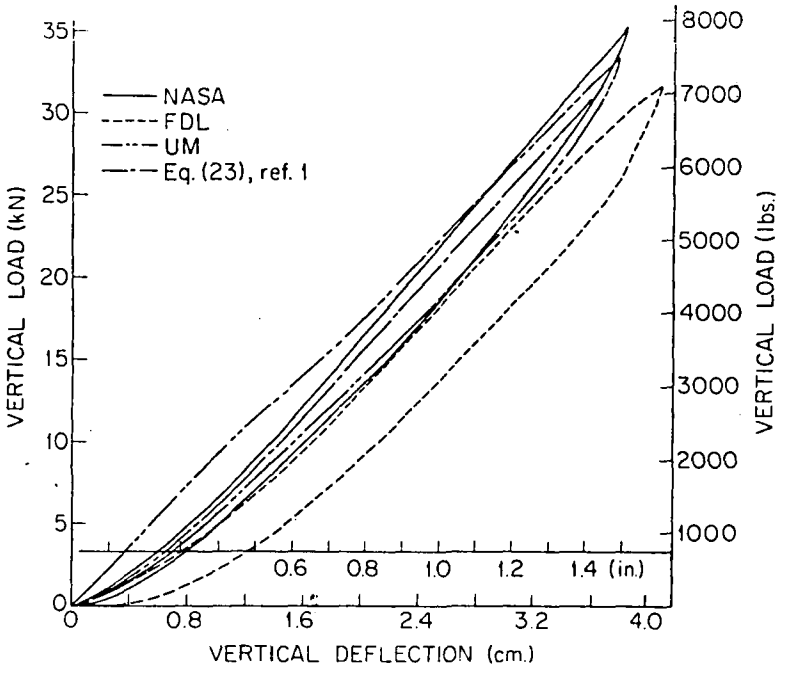

(a) $(F_z)_{max}$ = 125% Rated Load

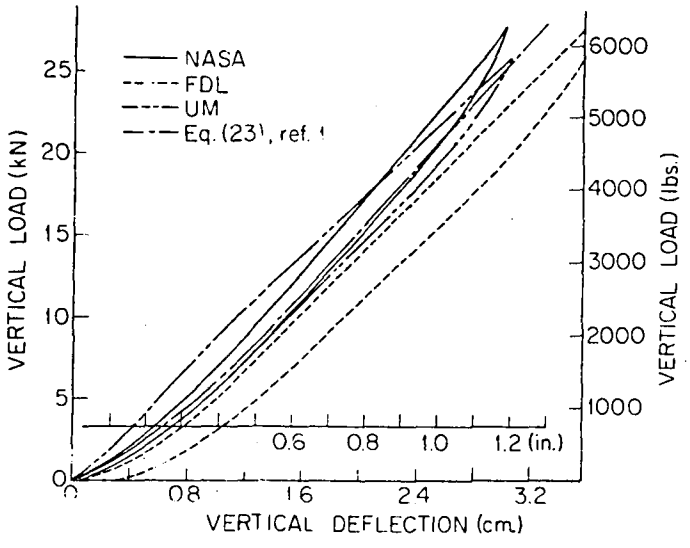

(b) $(F_z)_{max}$ = 100% Rated Load

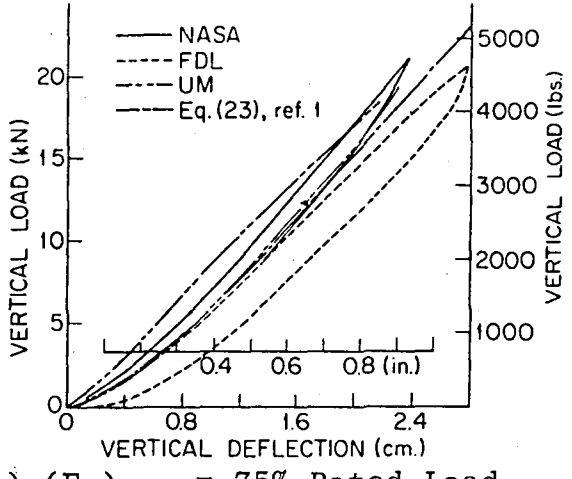

(c) $(F_z)_{max}$ = 75% Rated Load

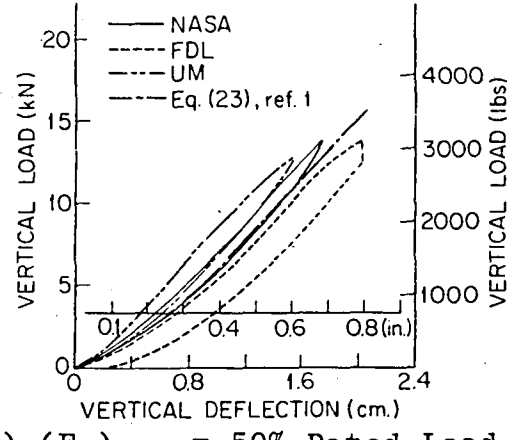

(d) $(F_z)_{max}$ = 50% Rated Load

Figure 2 - Composite Static Vertical Load-Deflection Curves. (18X5.5, 14 PR, Type VII Tire; Inflation Pressure=1482 kPa (215 psi); Rated Load=27.6 kN (6200 lb))

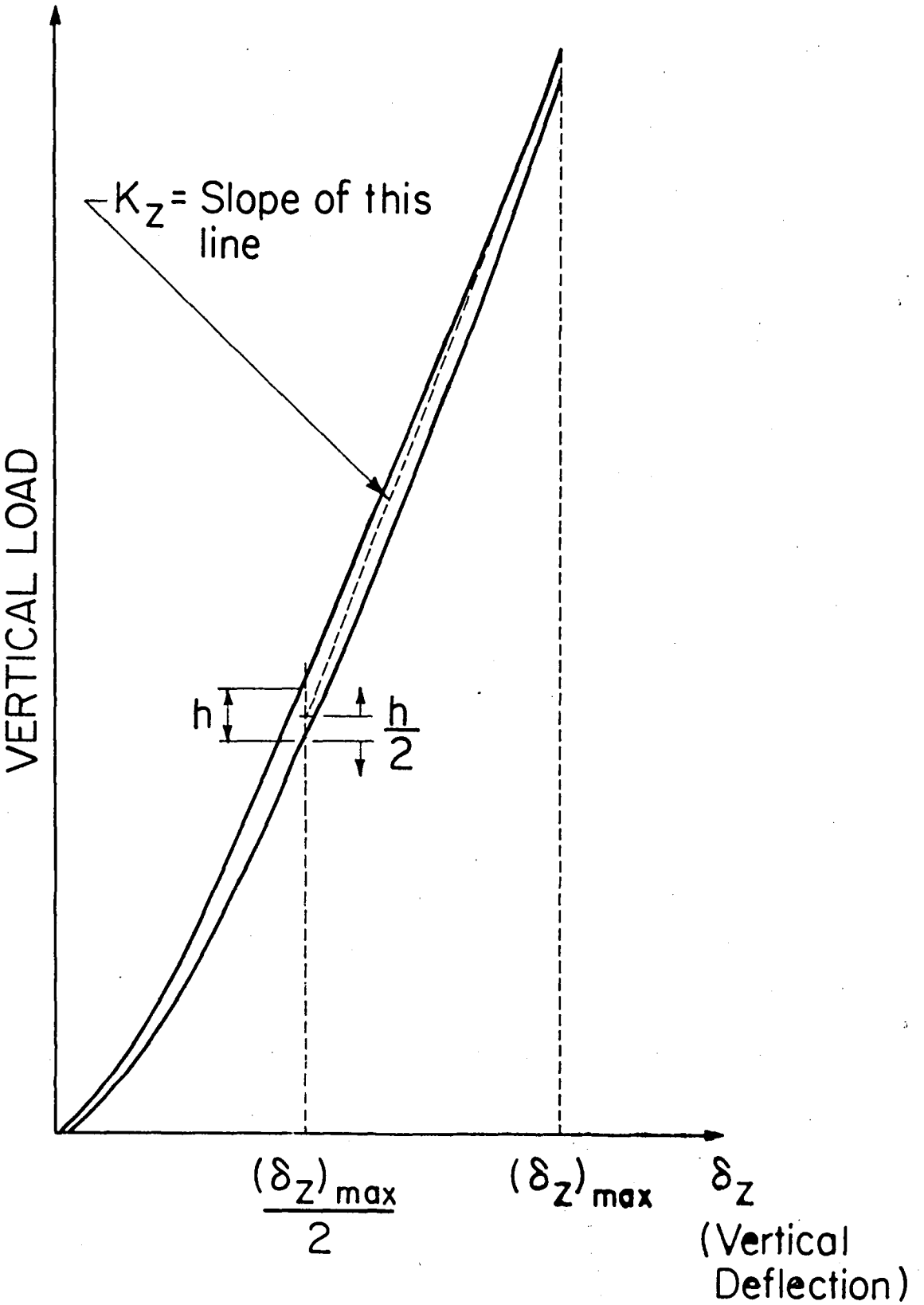

Figure 3 - Graphical illustration of determination of k_z

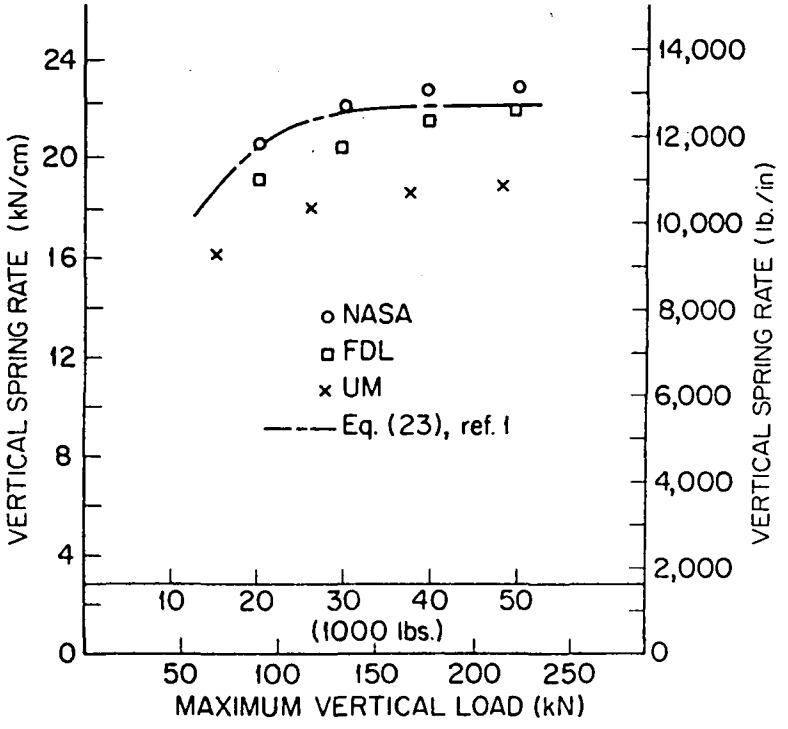

(a) 49 x 17 P_o = 1172 kPa (170 psi)

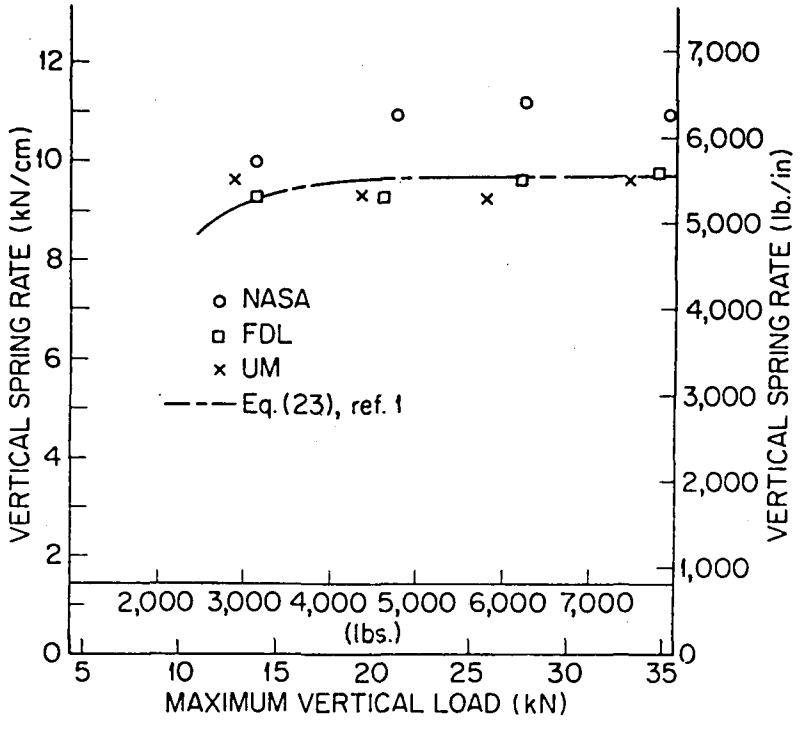

(b) 18 x 5.5 P_o = 1482 kPa (215 psi)

Figure 4 - Static Vertical Spring Rate vs Maximum Vertical Load

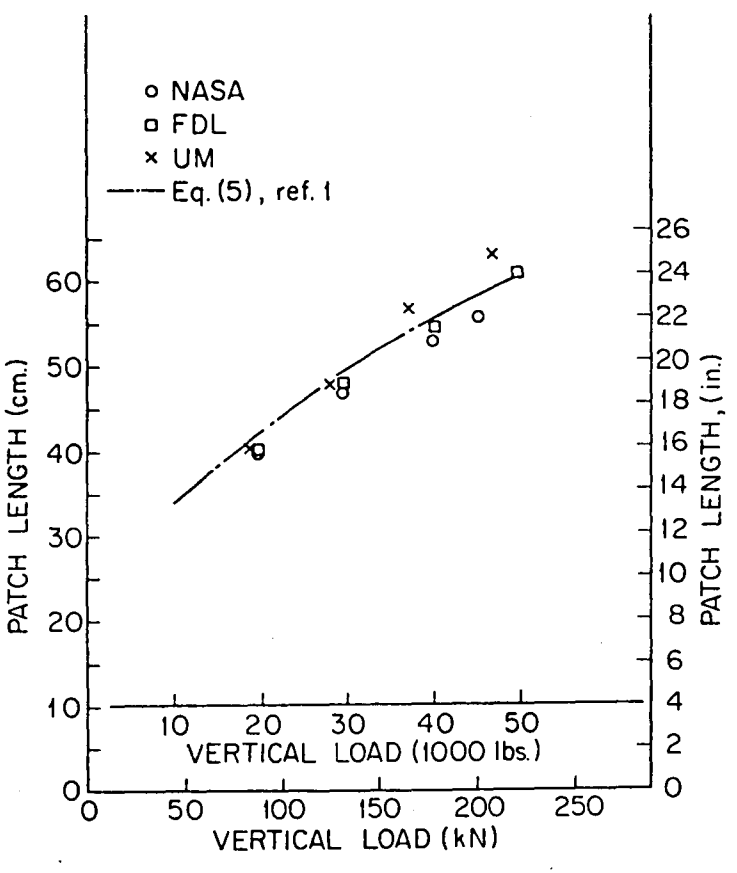

(a) 49 x 17 P_o = 1172 kPa (170 psi)

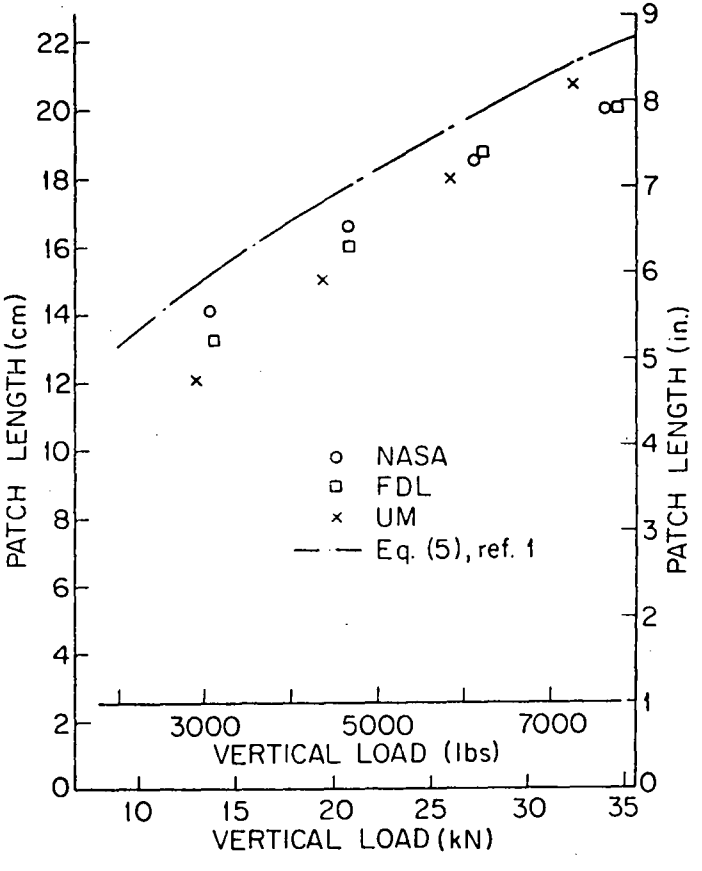

(b) 18 x 5.5 P_o = 1482 kPa (215 psi)

Figure 5 - Patch Length vs Vertical Load

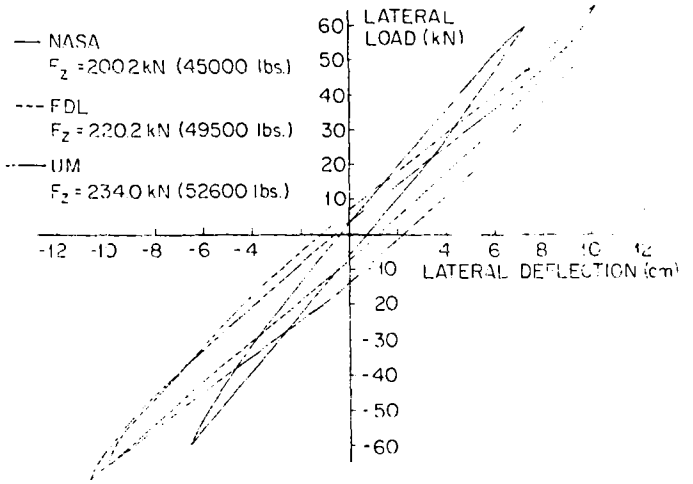

(a) $F_z \simeq$ 222.4 kN (50000 lbs.)

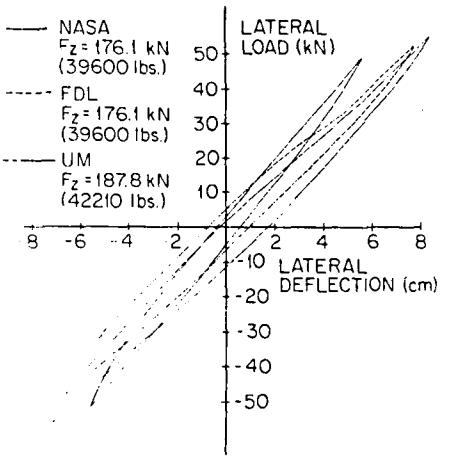

(b) $F_z \simeq$ 177.9 kN (40000 lbs.)

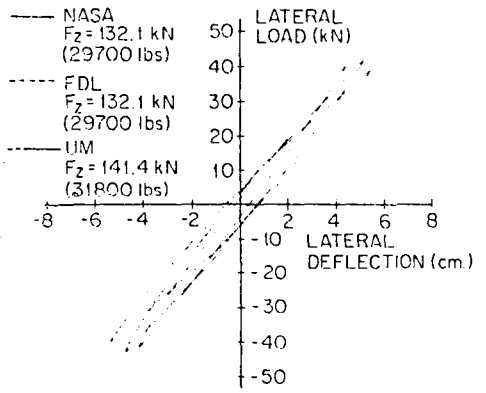

(c) $F_z \simeq$ 133.4 kN (30000 lbs.)

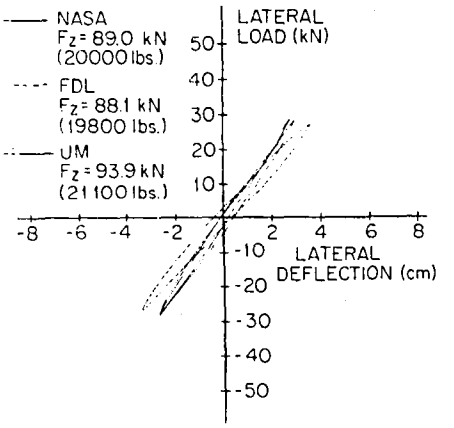

(d) $F_z \simeq$ 89.0 kN (20000 lbs.)

Figure 6 - Composite Static Lateral Load-Deflection Curves (49x17, 26 PR Tire; Inflation Pressure=1172 kPa (170 psi); Maximum Lateral Load ≃ ± 30% of Vertical Load).

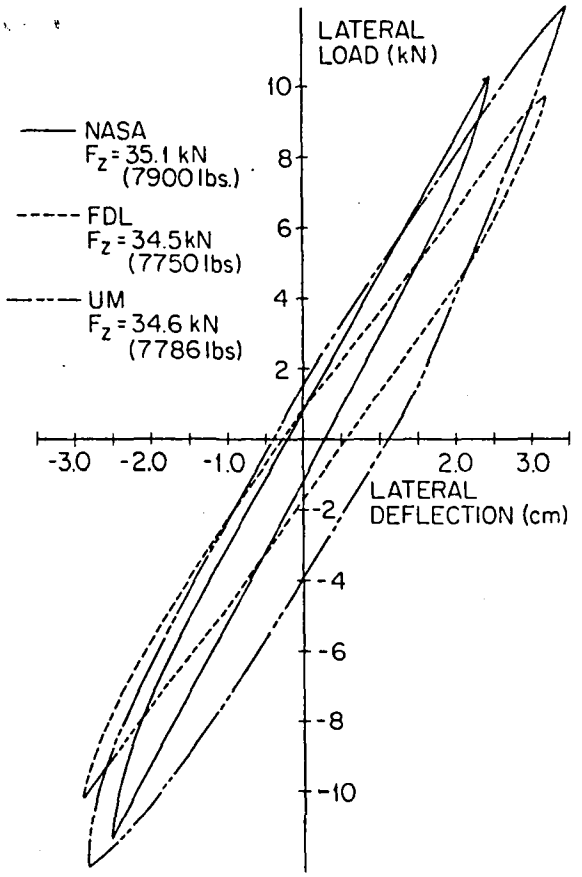

(a) $F_z \simeq$ 34.2 kN (7700 lbs.)

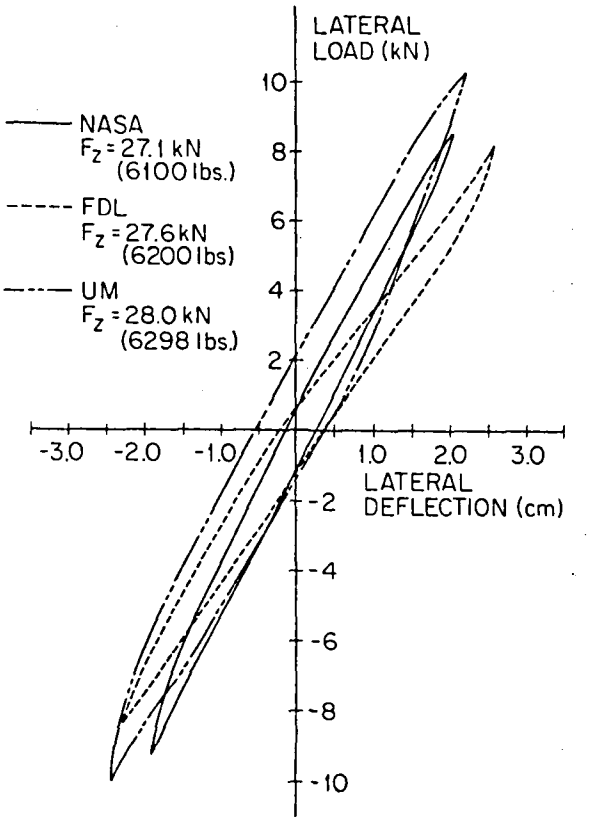

(b) $F_z \simeq$ 27.6 kN (6200 lbs.)

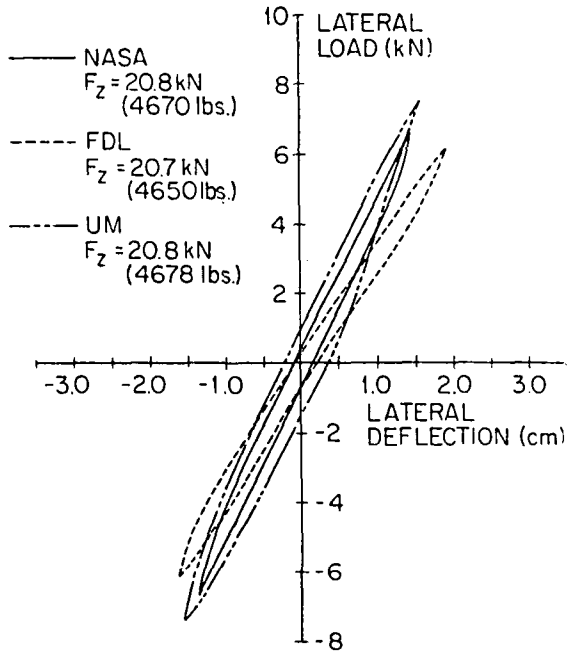

(c) $F_z \simeq$ 20.5 kN (4600 lbs.)

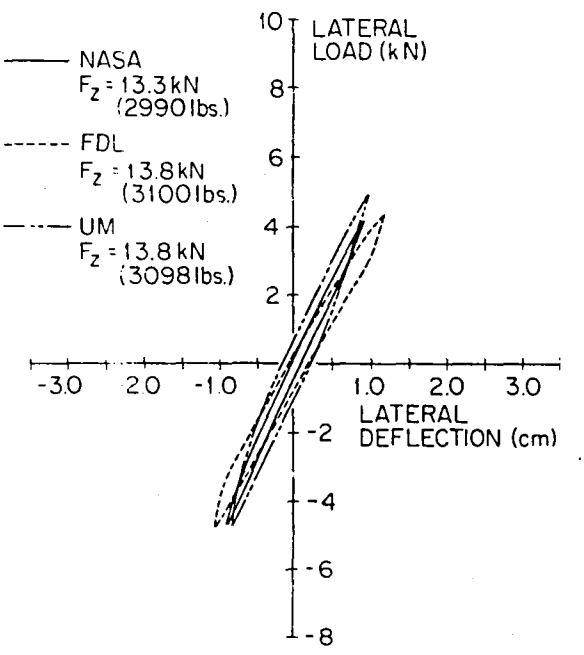

(d) $F_z \simeq$ 13.8 kN (3100 lbs.)

Figure 7 - Composite Static Lateral Load Deflection Curves (18x5.5, 14 PR Tire; Inflation Pressure=1482 kPa (215 psi); Maximum Lateral Load ≃ ± 30% of Vertical Load))

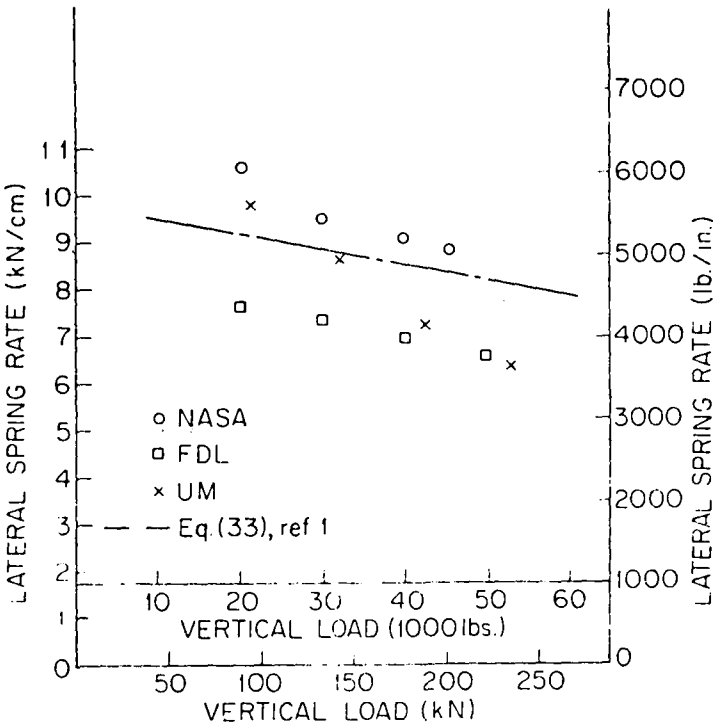

(a) 49x17 26 PR P_o=1172 kPa (170 psi)

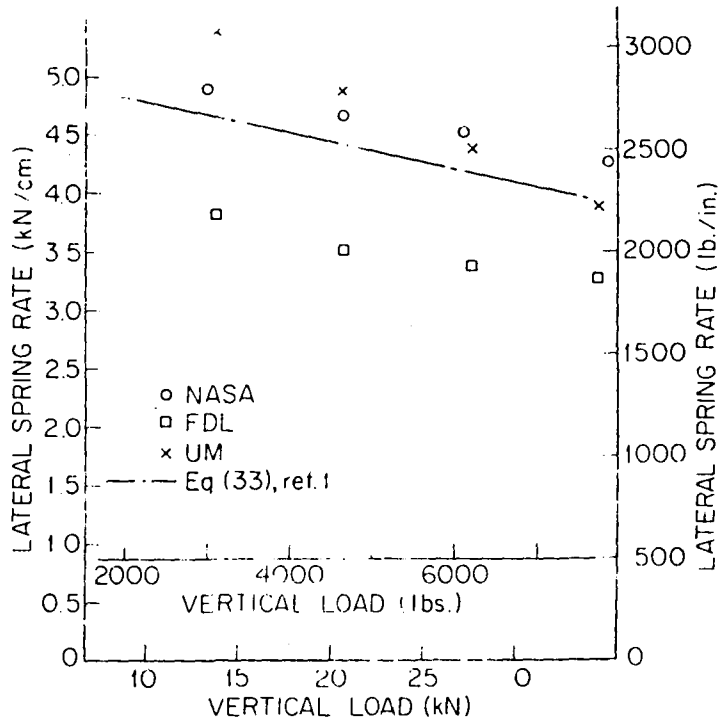

(b) 18x5.5 14 PR P_o=1482 kPa (215 psi)

Figure 8 - Static Lateral Spring Rate vs Vertical Load

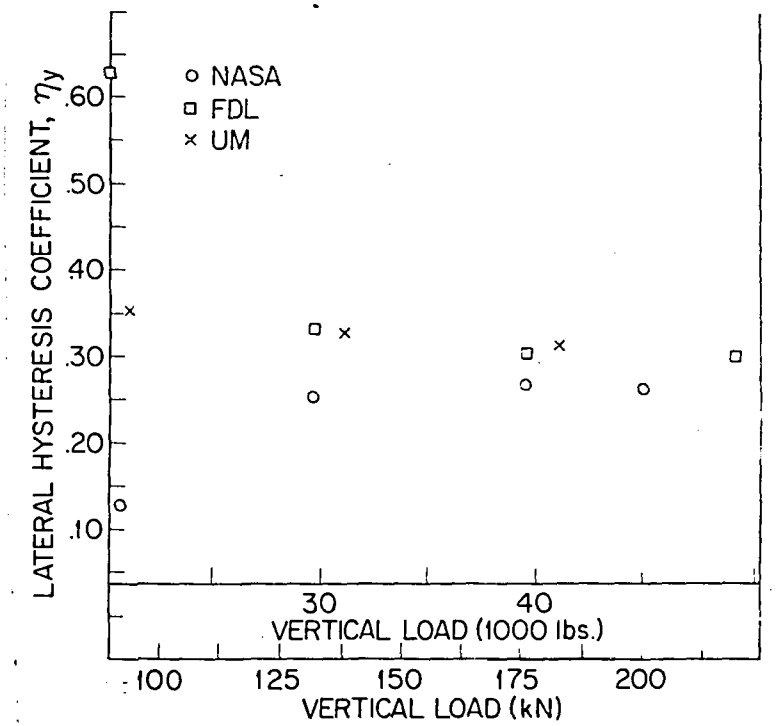

(a) 49 x 17 26 PR P_o = 1172 kPa (170 psi)

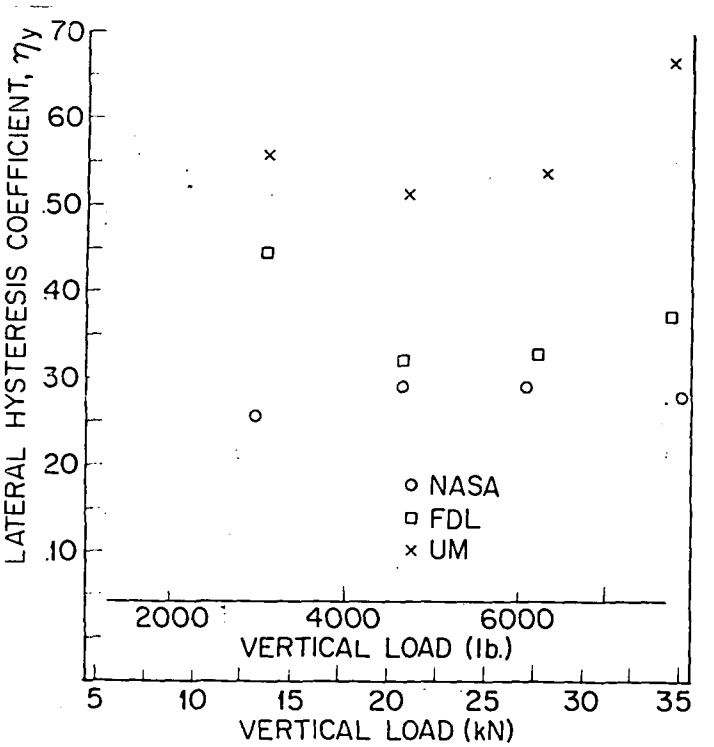

(b) 18 x 5.5 14 PR P_o = 1482 kPa (215 psi)

Figure 9 - Static Lateral Hysteresis Coefficient vs Vertical Load

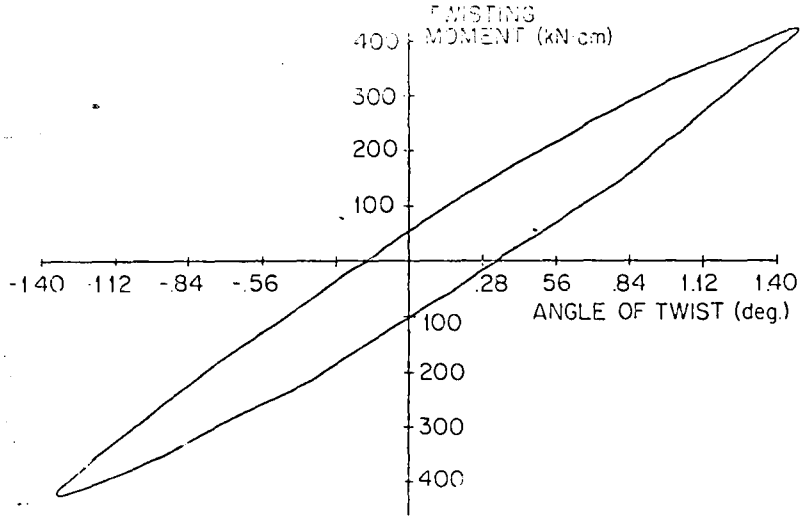

(a) F_z=228.0 kN (51250 lbs.)

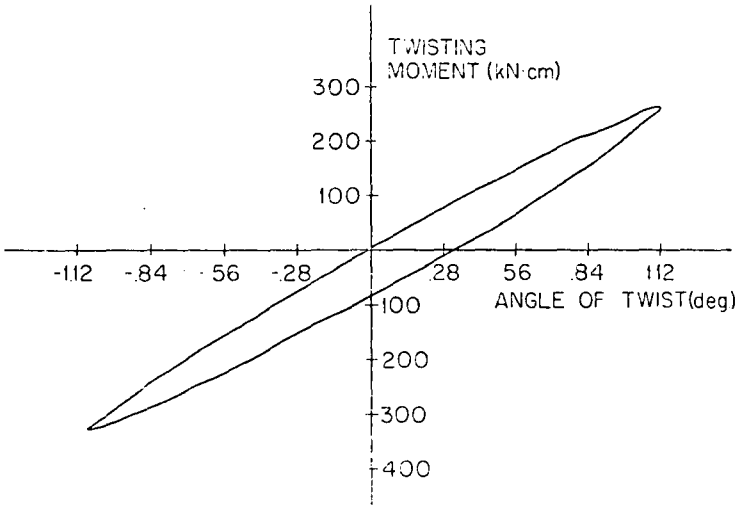

(b) F_z=182.4 kN (41000 lbs.)

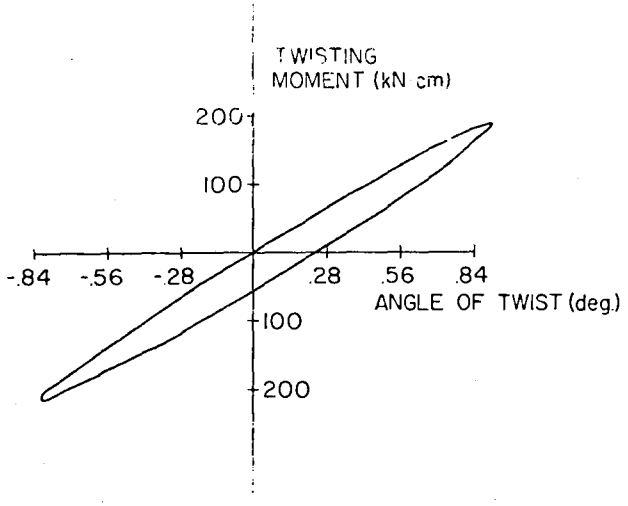

(c) F_z=137.9 kN (31000 lbs.)

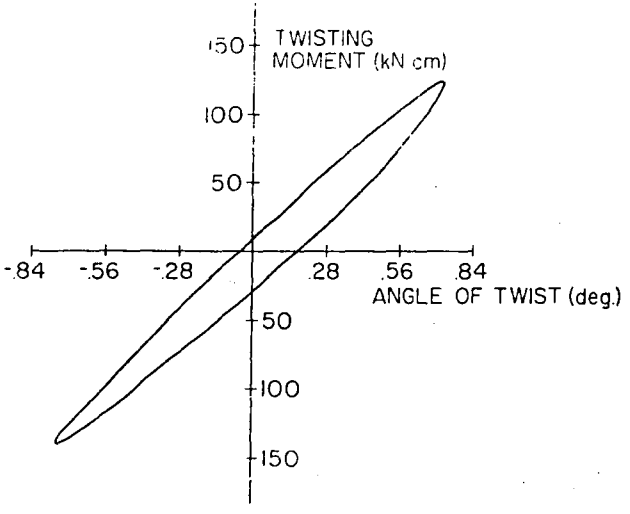

(d) F_z=91.2 kN (20500 lbs.)

Figure 10-Static Twisting Moment About Vertical Axis vs Angle of Twist - UM Model to Full Size 49x17, 26 PR Tire; P_o=1172 kPa (170 psi)

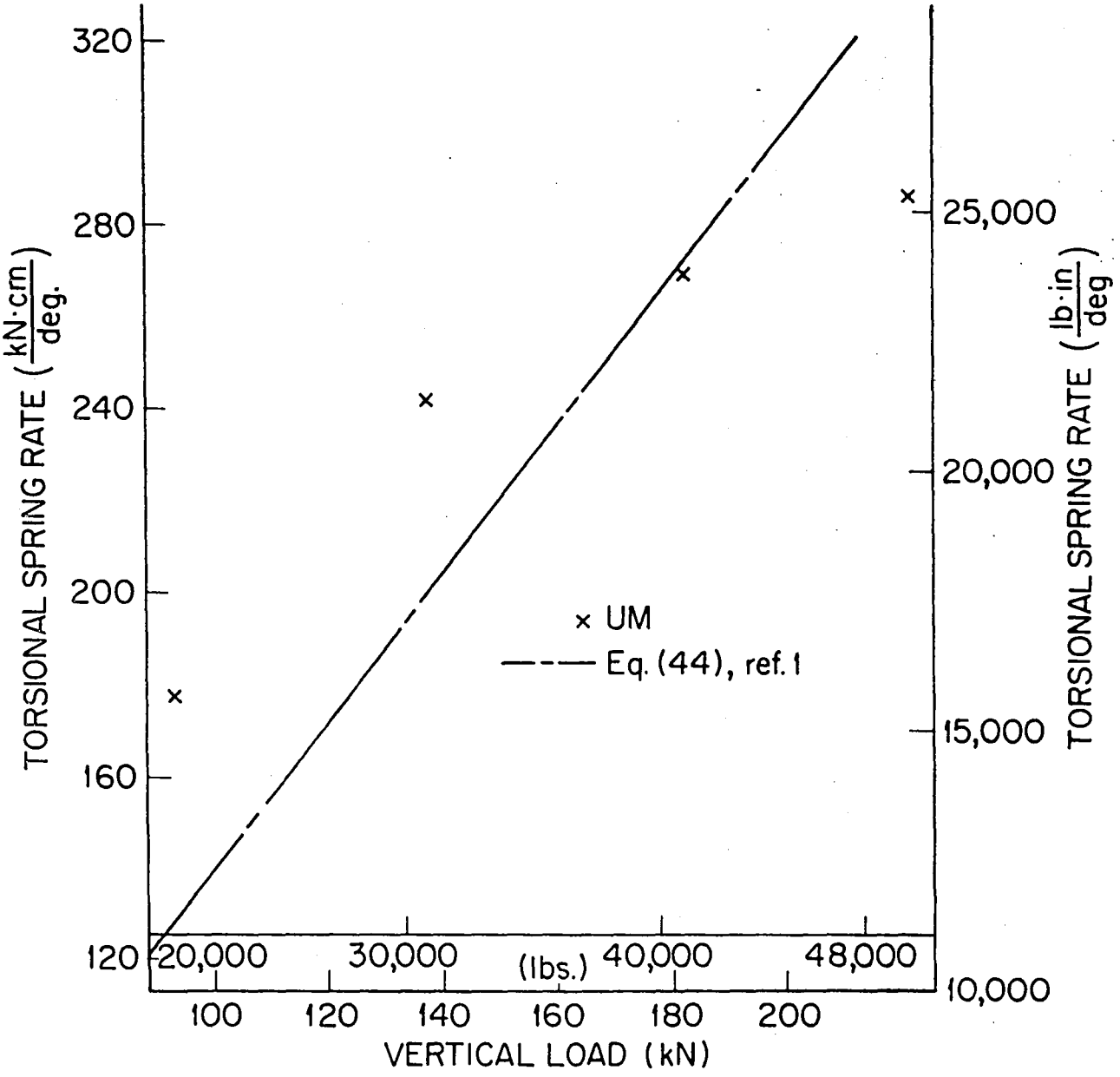

Fig. 11 - Static Torsional Spring Rate vs Vertical Load UM Model to Full Size 49 x 17, 26 PR Tire; P_o=1172 kPa (170 psi)

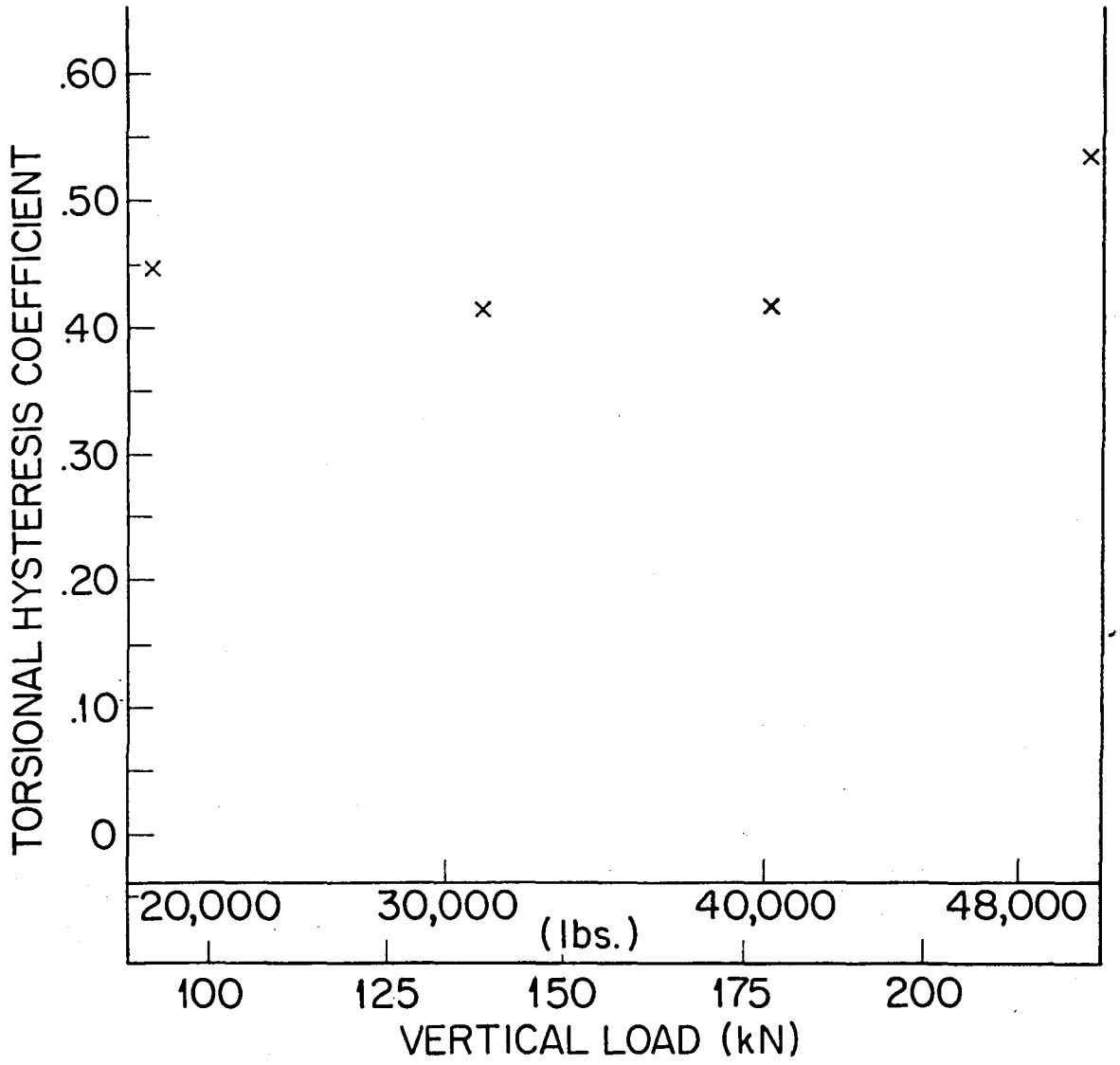

Fig. 12 - Static Torsional Hysteresis Coefficient vs Vertical Load UM Model to Full Size 49 x 17, 26 PR Tire; P_o=1172 kPa (170 psi)

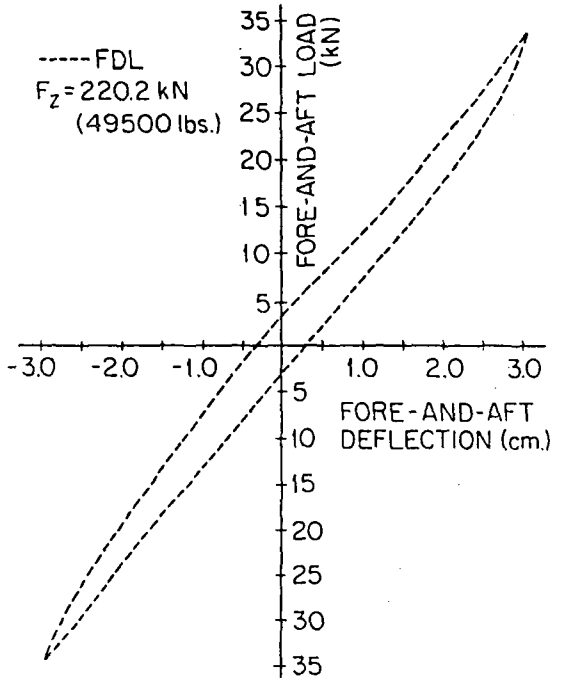

(a)

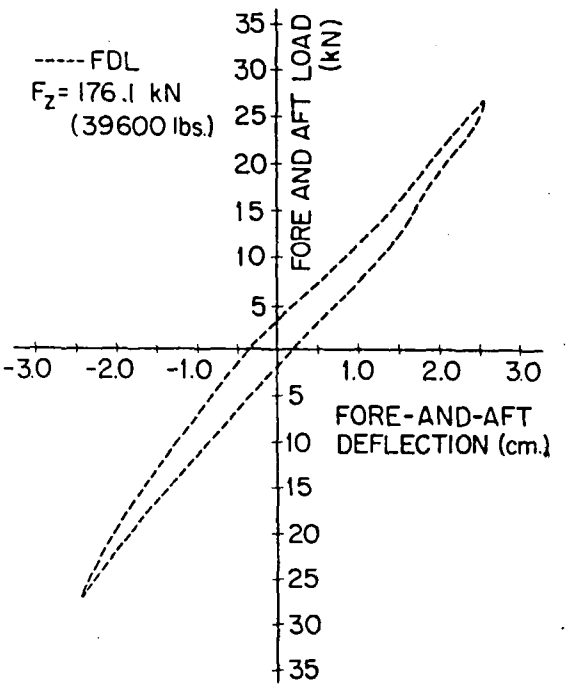

(b)

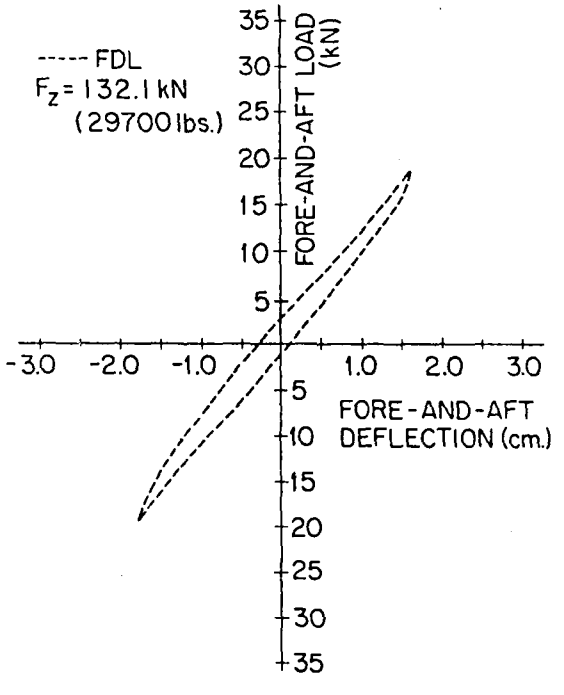

(c)

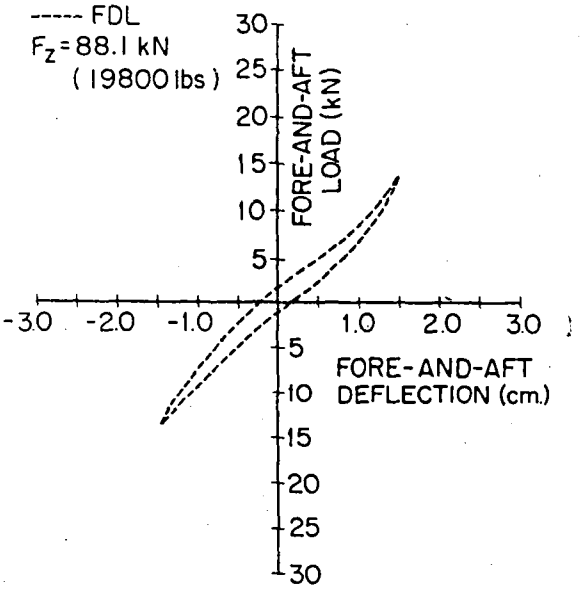

(d)

Figure 13 - Composite Static Fore-and-Aft Load-Deflection Curves (49x17, 26 PR Tire; Inflation Pressure=1172 kPa (170 psi); Maximum Fore-and-Aft Load ≈ ± 15% of Vertical Load)

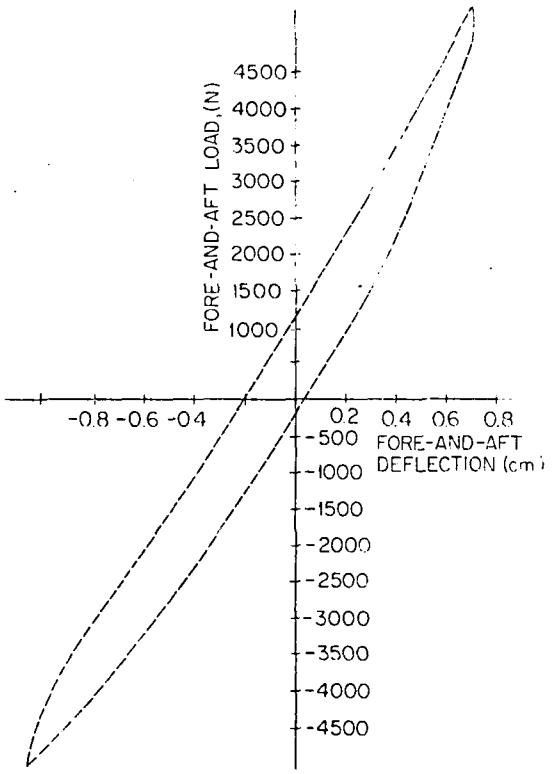

(a) F_Z=34.5 kN (7750 lbs.)

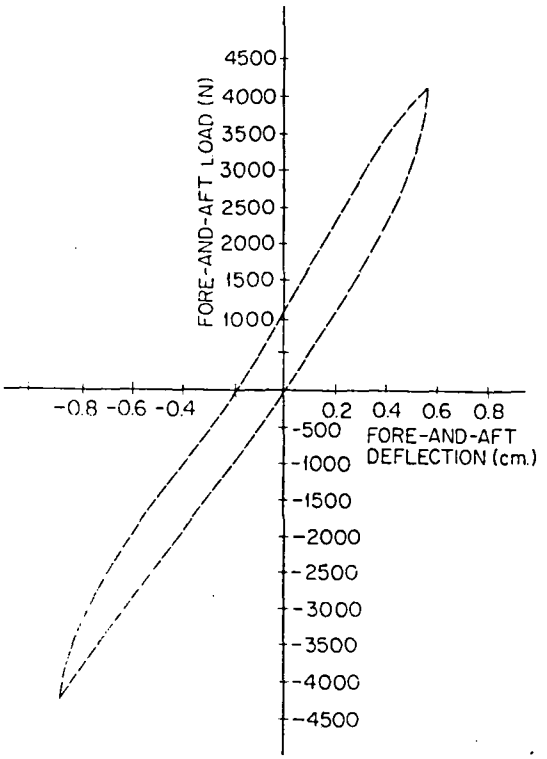

(b) F_Z=27.6 kN (6200 lbs.)

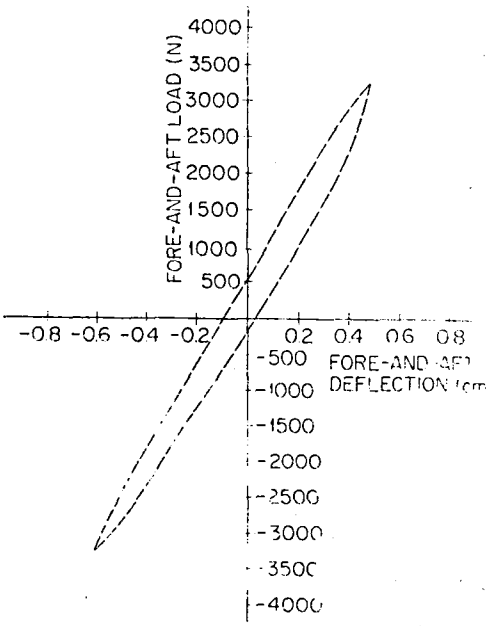

(c) F_Z=20.7 kN (4650 lbs.)

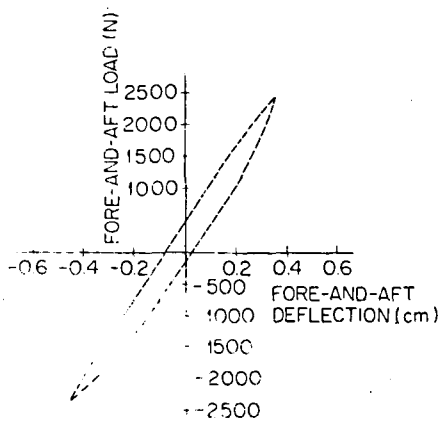

(d) F_Z=13.8 kN (3100 lbs.)

Figure 14 - Composite Static Fore-and-Aft Load-Deflection Curves (18x5.5, 14 PR Tire; Inflation Pressure=1482 kPa (215 psi); Maximum Fore-and-Aft Load ≈ ± 15% Vertical Load)

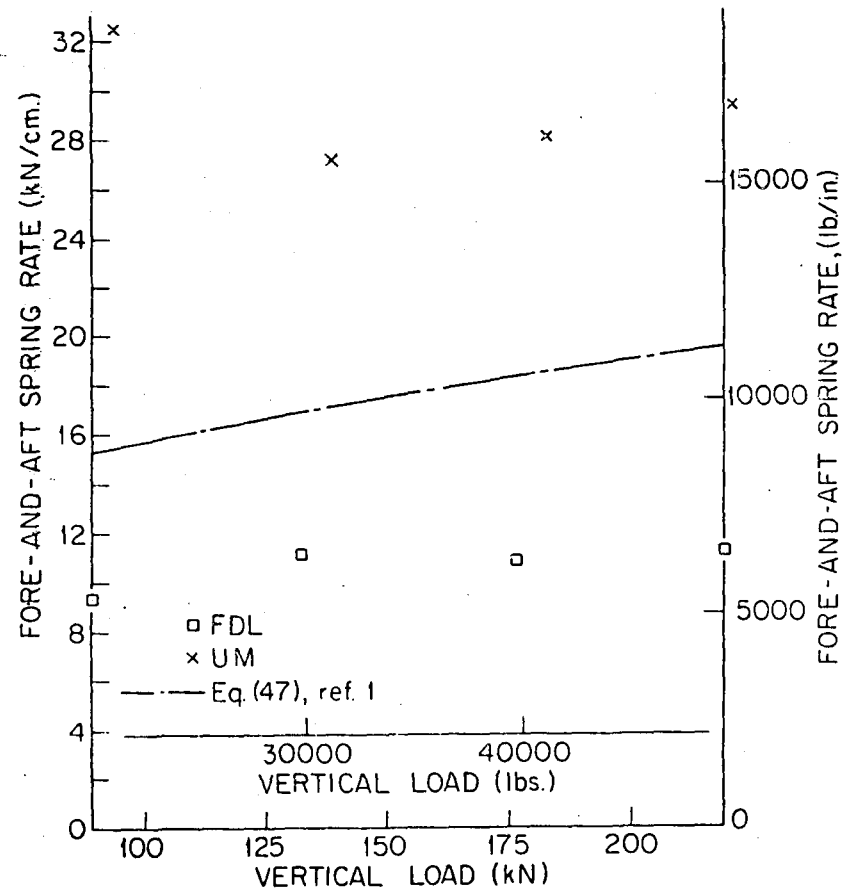

(a) 49 x 17

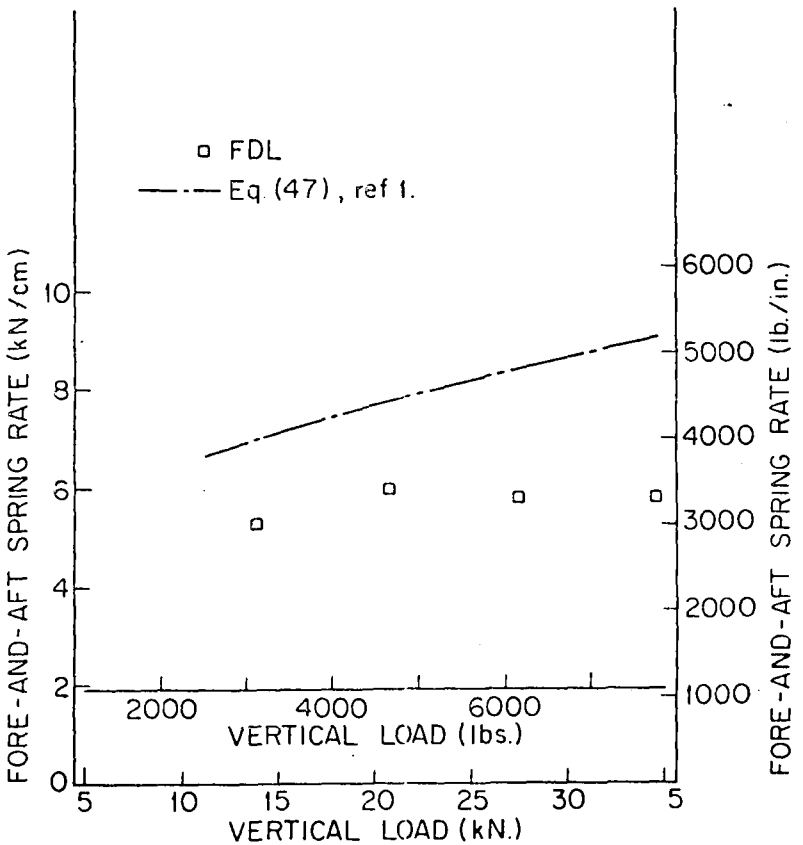

(b) 18 x 5.5

Figure 15 - Static Fore-and-Aft Spring Rate vs Vertical Load.

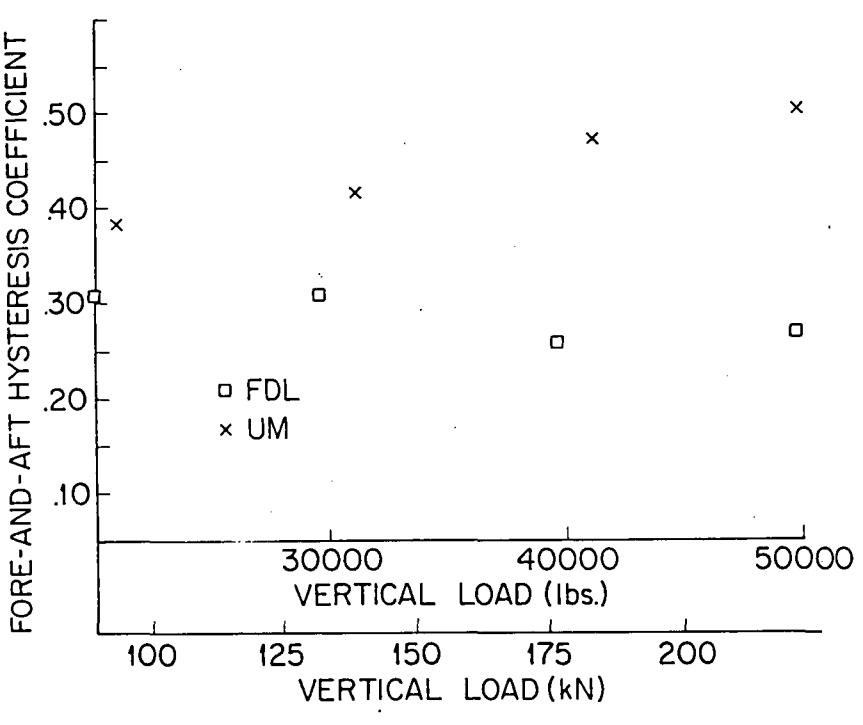

(a) 49 x 17, 26 PR Tire; P_o = 1172 kPa (170 psi)

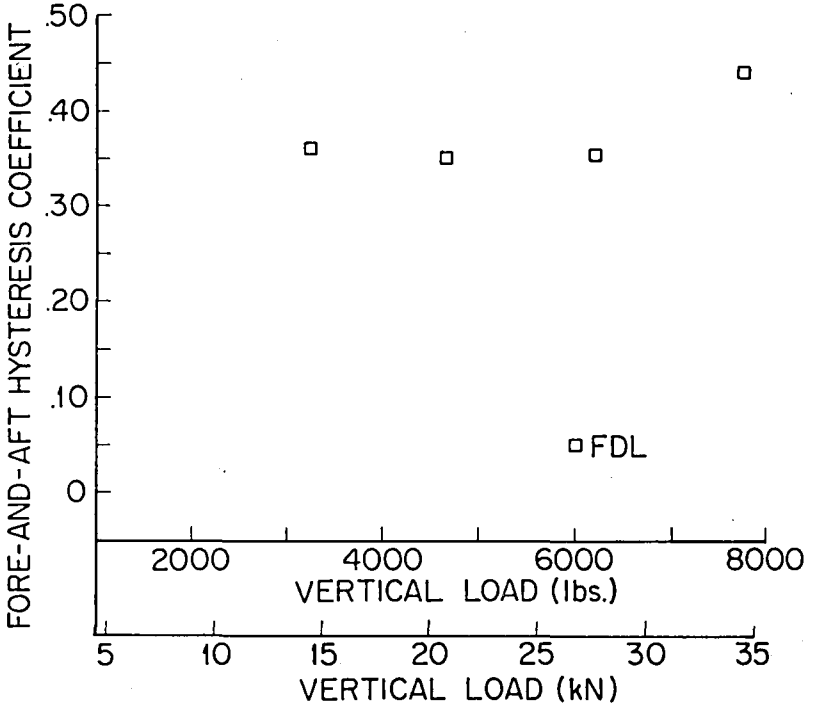

(b) 18 x 5.5, 14 PR Tire; P_o = 1482 kPa (215 psi)

Figure 16 - Static Fore-and-Aft Hysteresis Coefficient vs Vertical Load

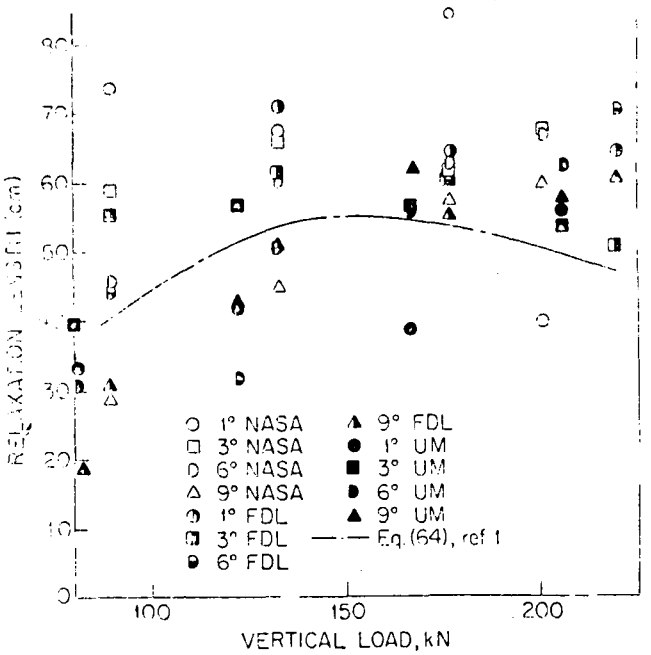

(a) 49 x 17, 26 PR Tire; P_o=1172 kPa (170 psi)=

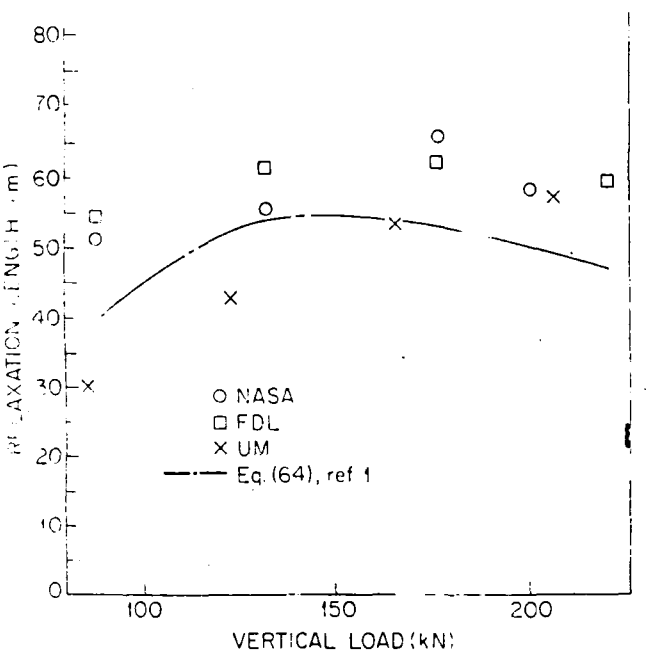

(b) 49 x 17, 26 PR Tire; Average Values P_o=1172 kPa (170 psi)

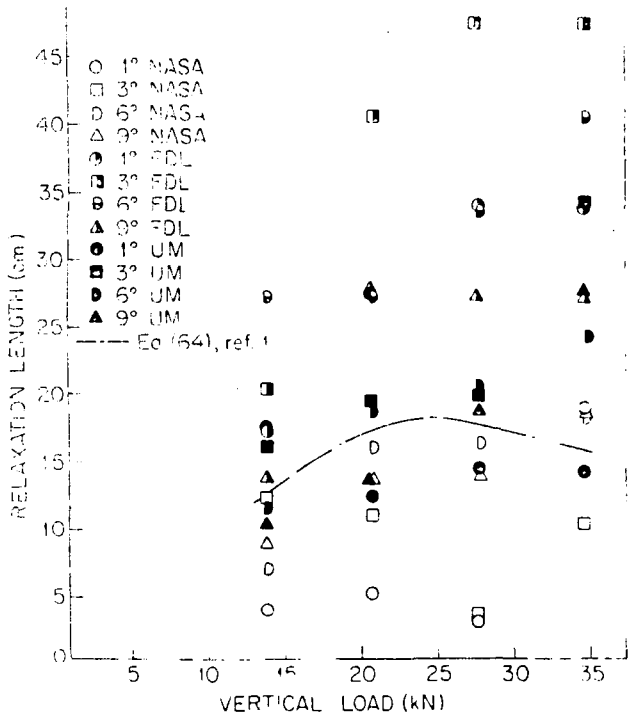

(c) 18 x 5.5, 14 PR Tire; P_o=1482 kPa (215 psi)

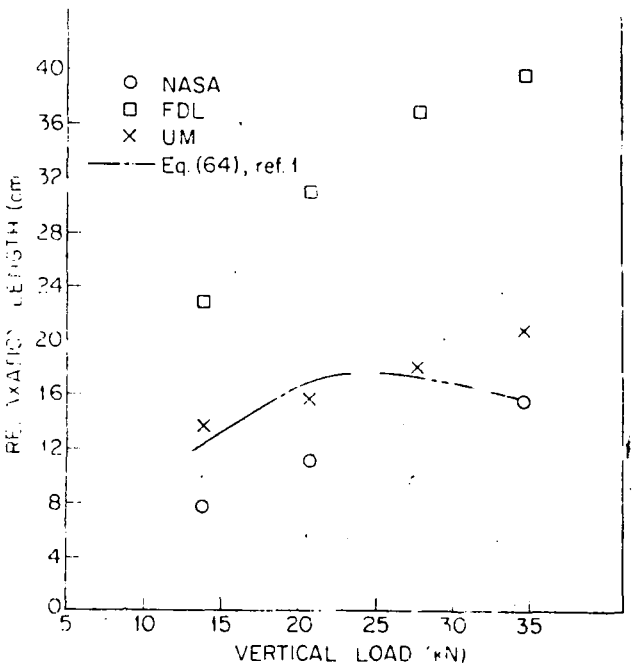

(d) 18 x 5.5, 14 PR Tire; Average Values P_o=1482 kPa (215 psi)

Figure 17 - Yawed-Rolling Relaxation Length vs Vertical Load

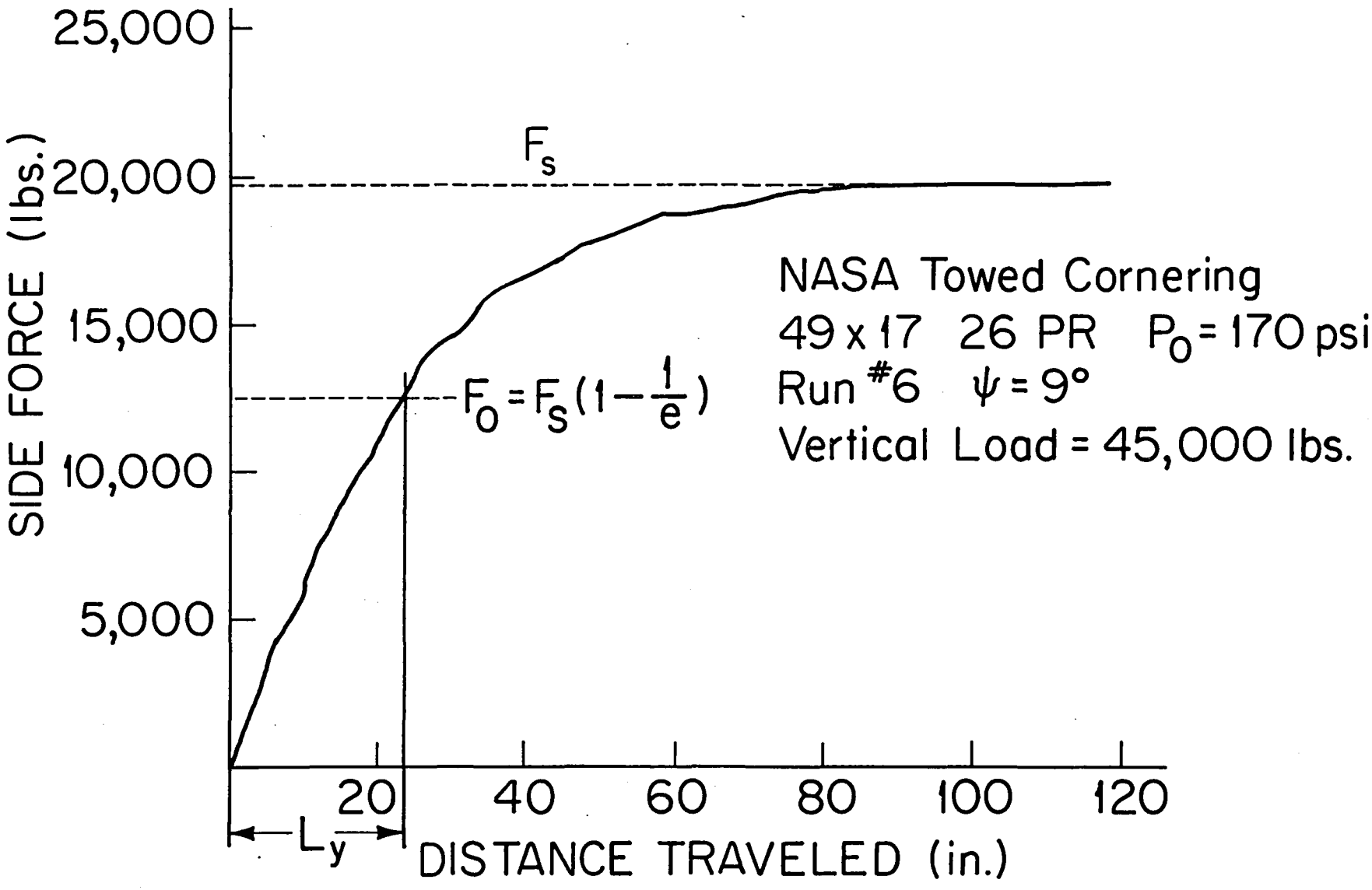

Figure 18 - Illustration of Determining Yawed-Rolling Relaxation Length, L_y

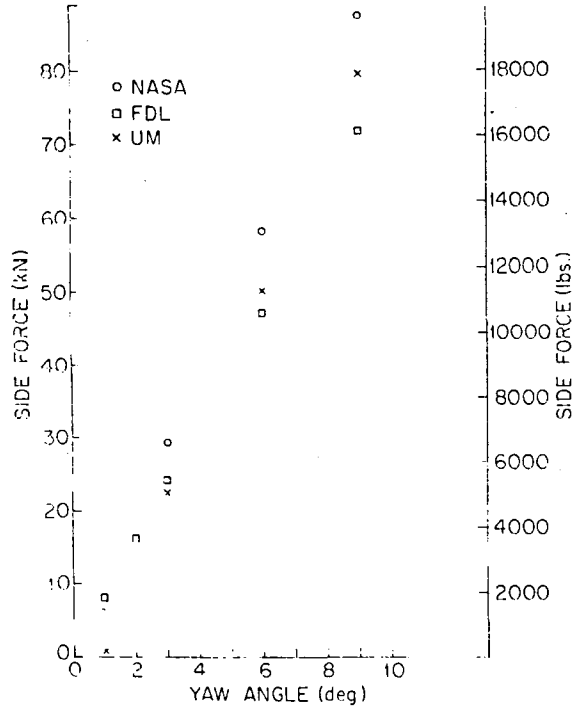

(a) $F_Z \simeq 218.0$ kN (49000 lbs.)

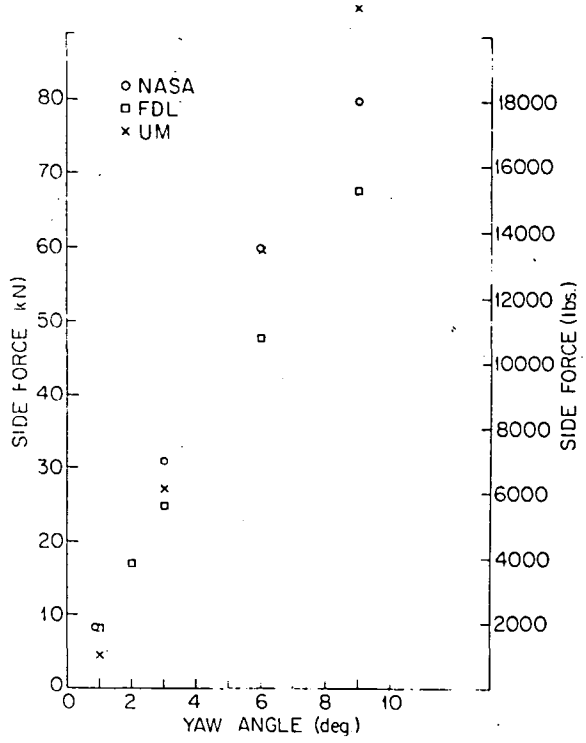

(b) $F_Z \simeq 173.5$ kN (39000 lbs.)

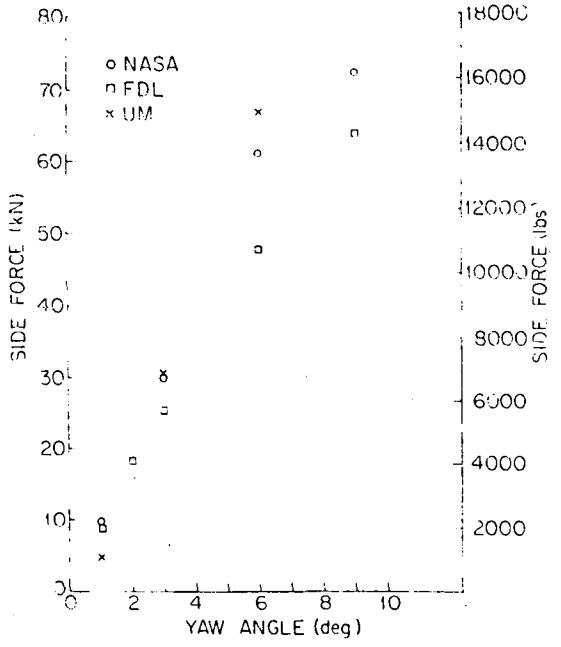

(c) $F_Z \simeq 133.4$ kN (30000 lbs.)

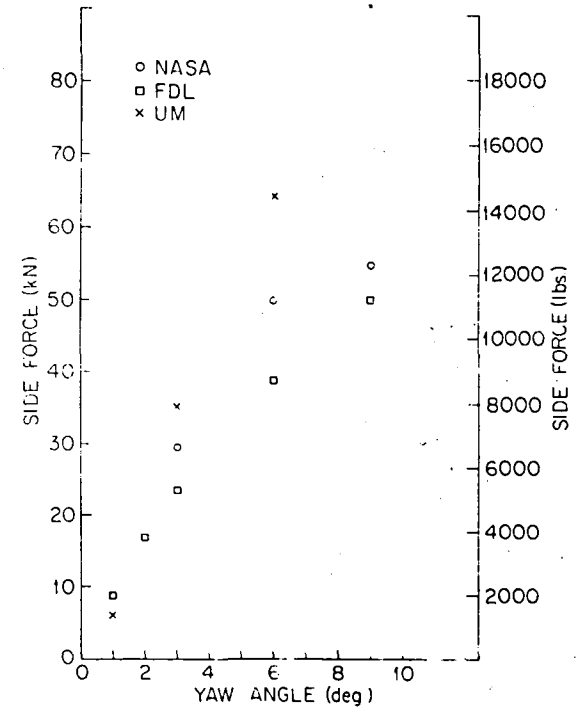

(d) $F_Z \simeq 89.0$ kN (20000 lbs.)

Figure 19 - Slow-Rolling Side Force vs Yaw Angle (49x17, 26 PR Tire; P_o=1172 kPa (170 psi))

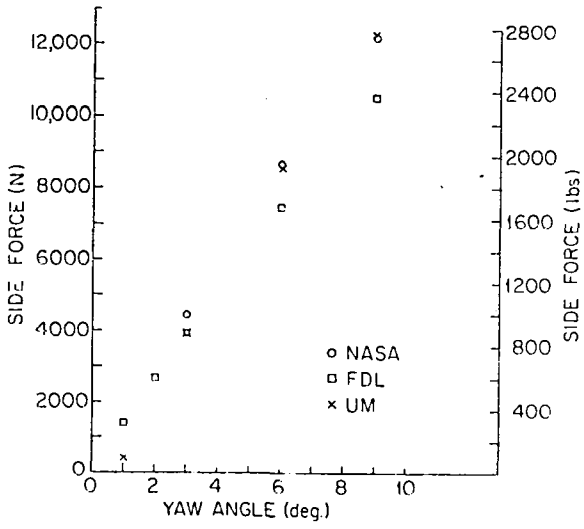

(a) $F_Z \simeq$ 34.5 kN (7750 lbs.)

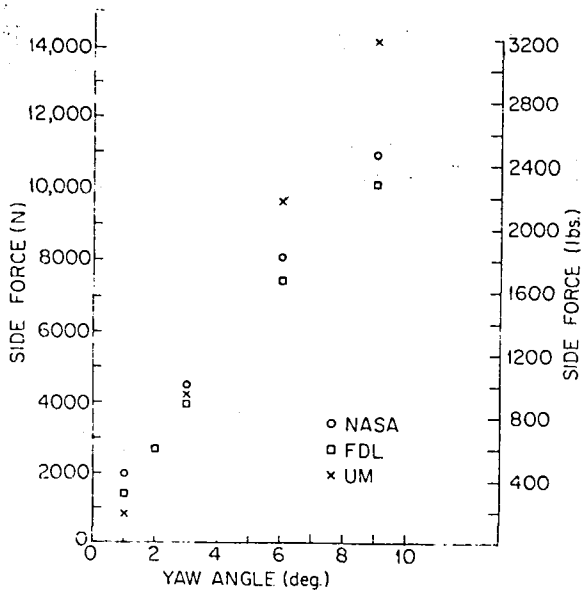

(b) $F_Z \simeq$ 27.6 kN (6200 lbs.)

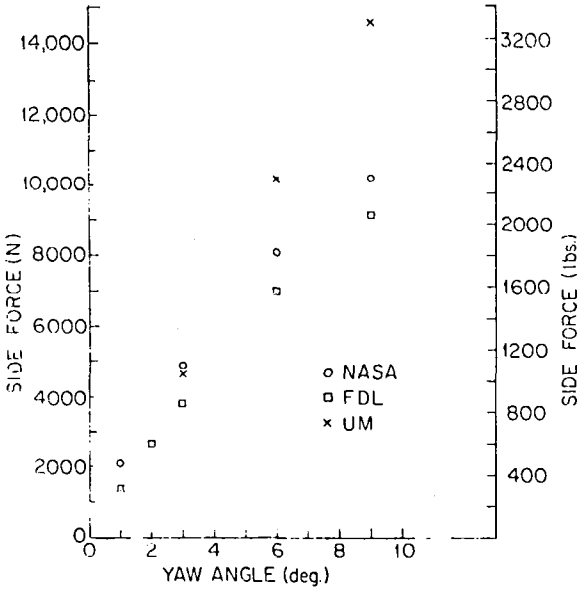

(c) $F_Z \simeq$ 20.7 kN (4650 lbs.)

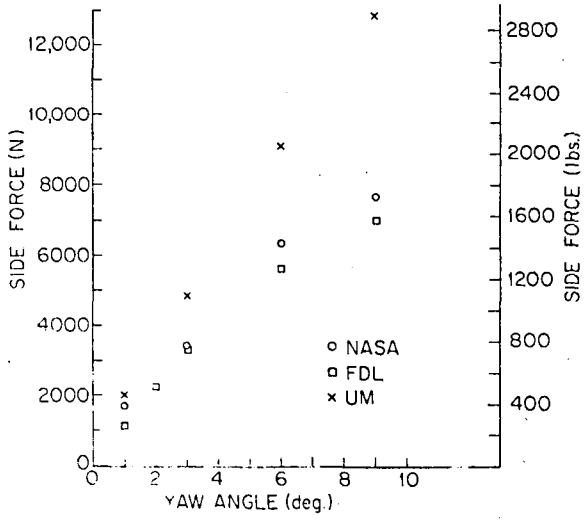

(d) $F_Z \simeq$ 13.8 kN (3100 lbs.)

Figure 20 - Slow-Rolling Side Force vs Yaw Angle (18x5.5, 14 PR Tire; P_o=1482 kPa (215 psi))

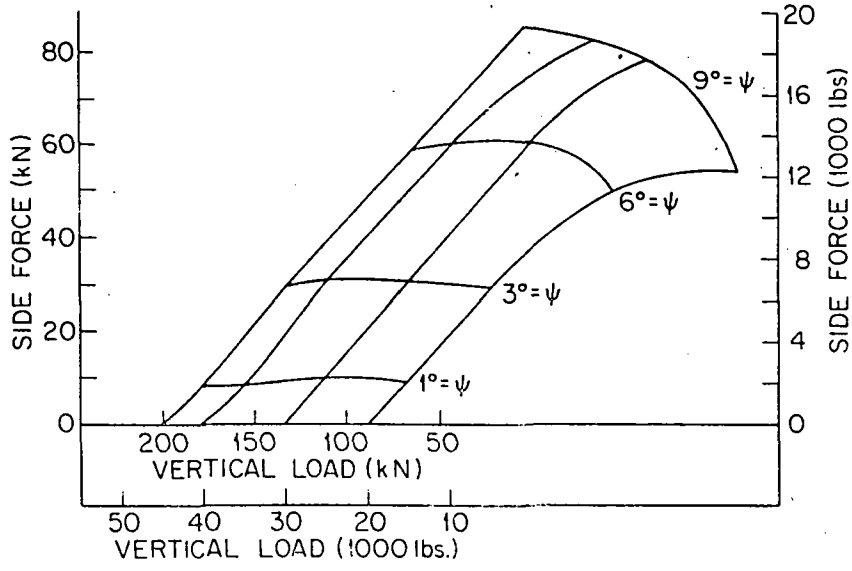

(a) NASA

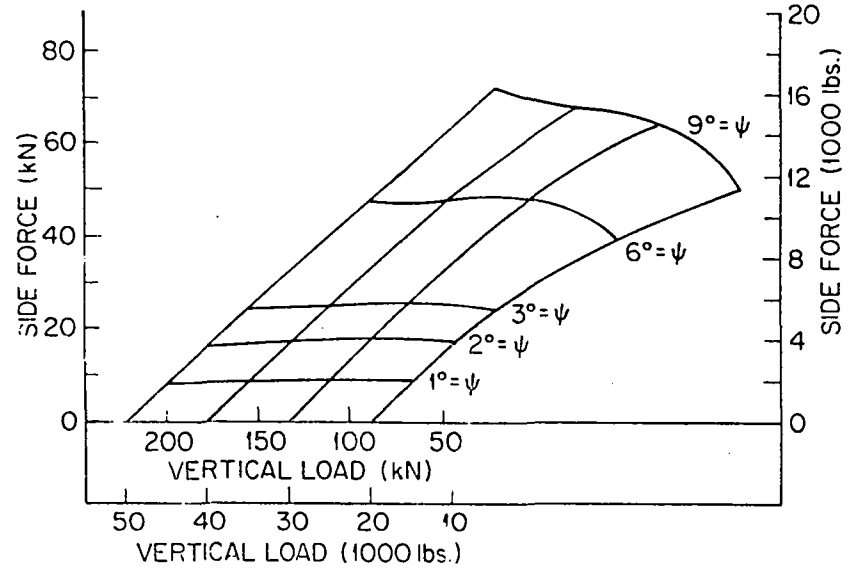

(b) FDL

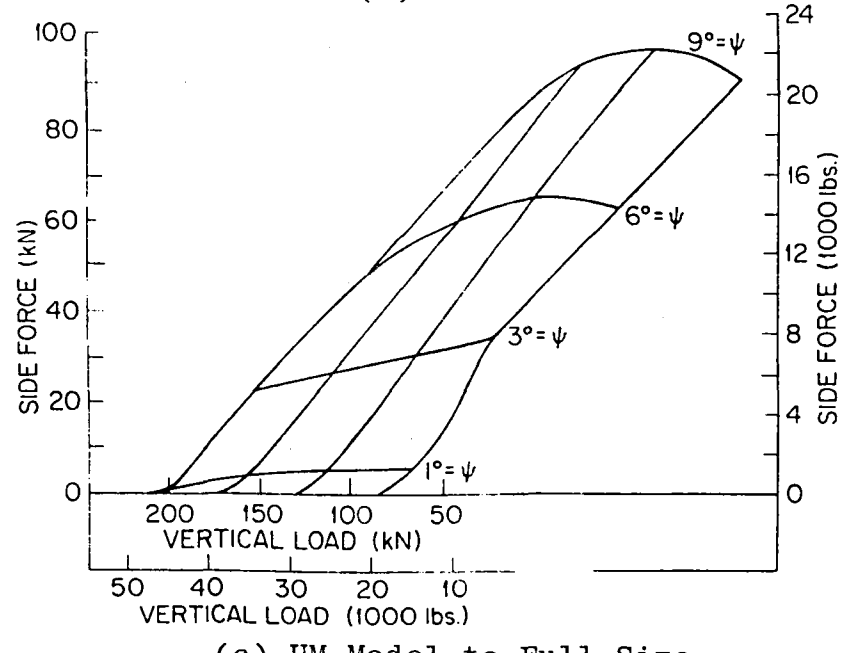

(c) UM Model to Full Size

Figure 21 - Slow Rolling Side Force vs Vertical Load and Yaw Angle, ψ
(49x17, 26 PR Tire; P_o = 1172 kPa (170 psi))

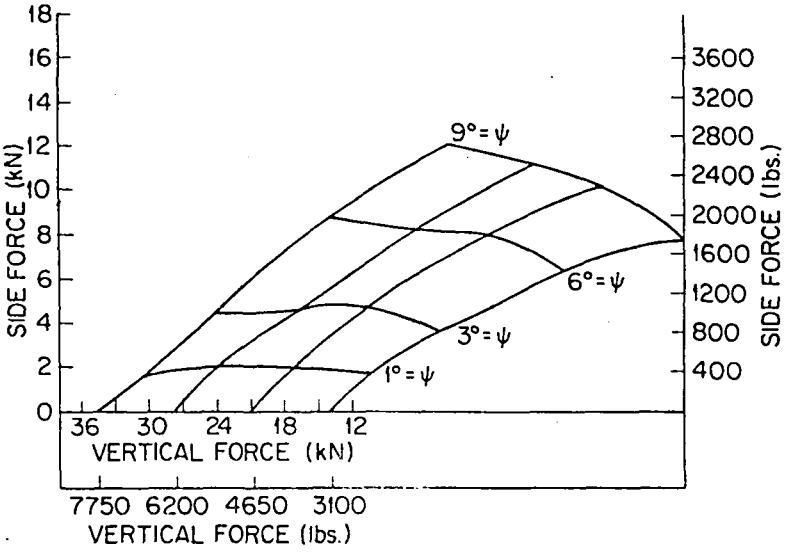

(a) NASA

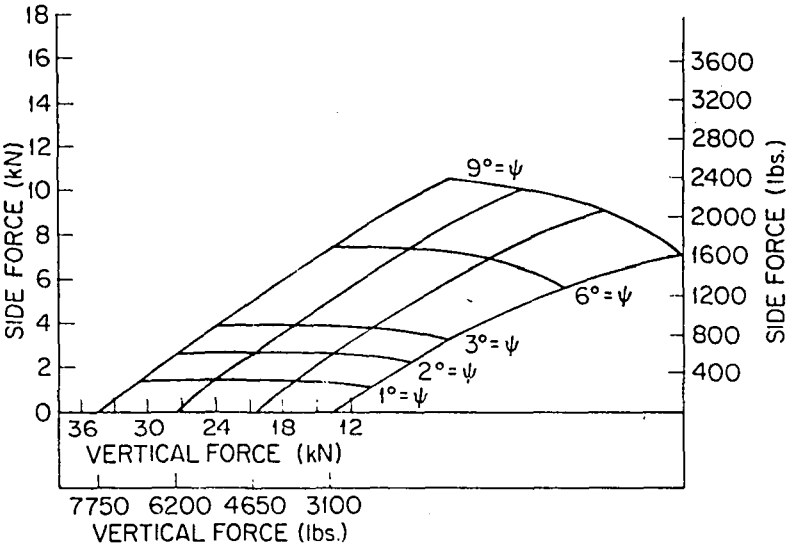

(b) FDL

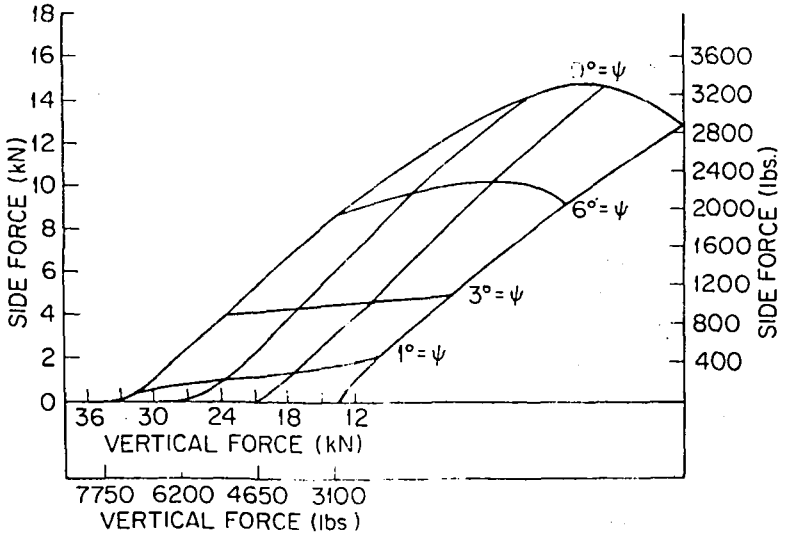

(c) UM Model to Full Size

Figure 22 - Slow-Rolling Side Force vs Vertical Load and Yaw Angle, ψ (18x5.5, 14 PR Tire; P_o=1482 kPa (215 psi))

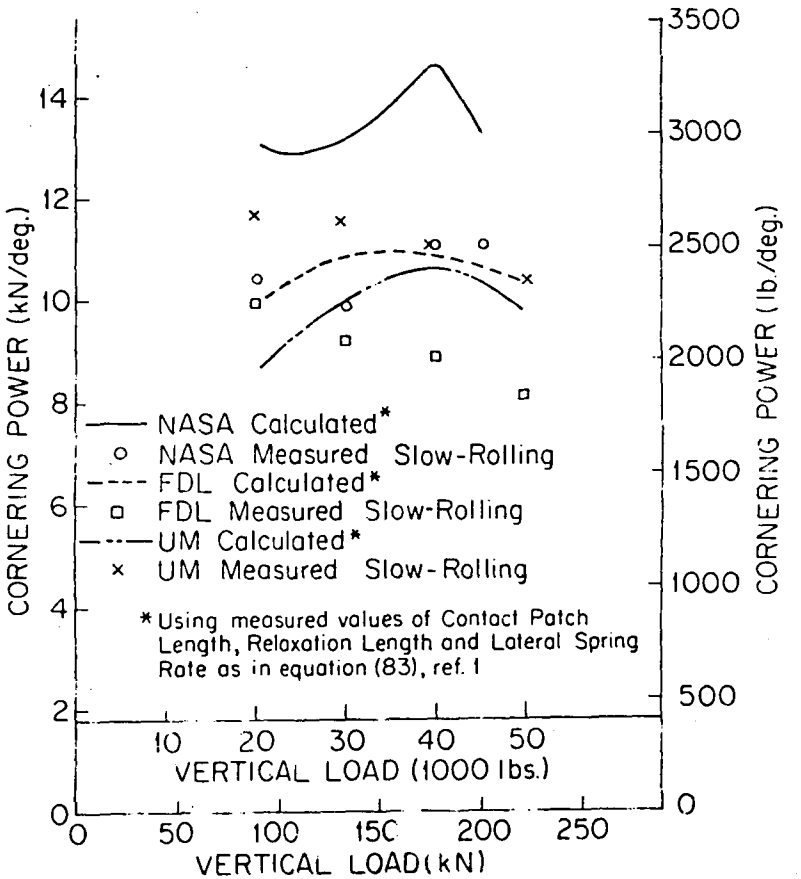

(a) 49 x 17 26 PR P_o = 1172 kPa (170 psi)

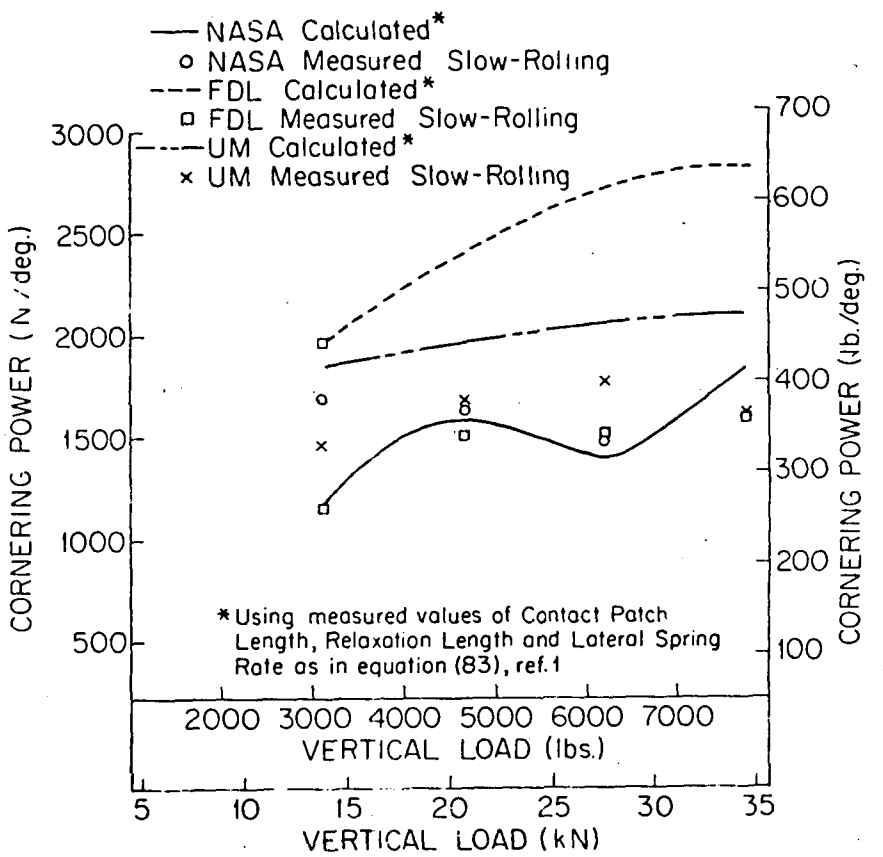

(b) 18 x 5.5 14 PR P_o = 1482 kPa (215 psi)

Figure 23 - Cornering Power vs Vertical Load Slow-Rolling - Comparison of Measured Values and Those Calculated From Eq. (83), ref. 1.

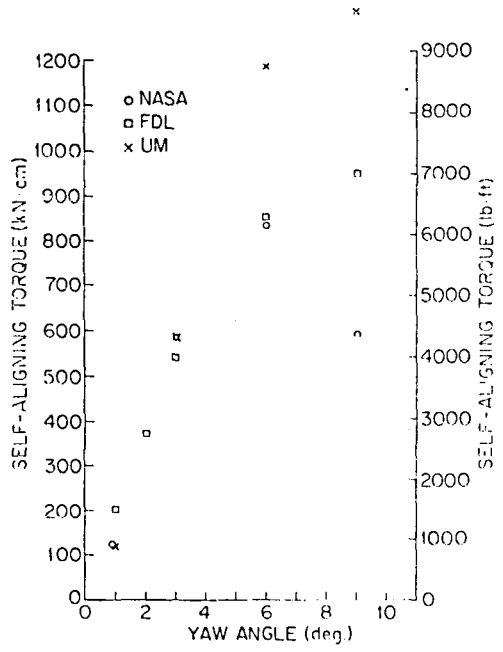

(a) $F_Z \simeq$ 218.0 kN (49000 lbs.)

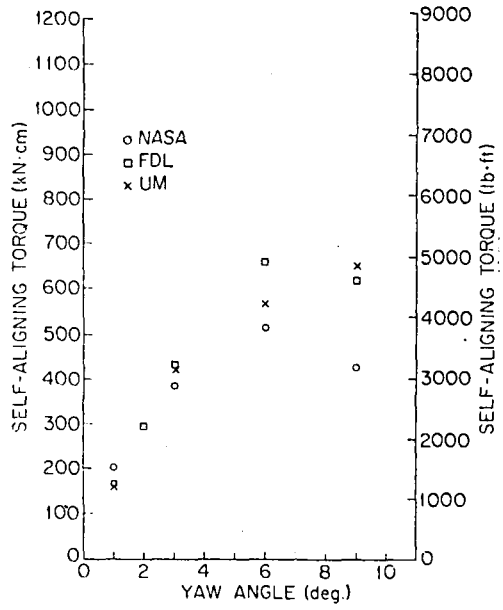

(b) $F_Z \simeq$ 173.5 kN (39000 lbs.)

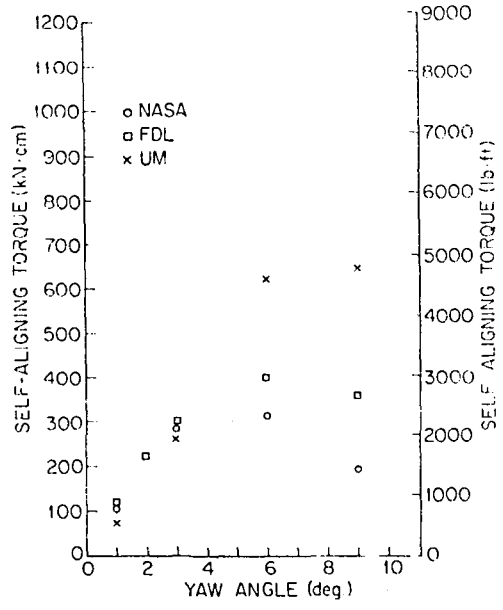

(c) $F_Z \simeq$ 129.0 kN (29000 lbs.)

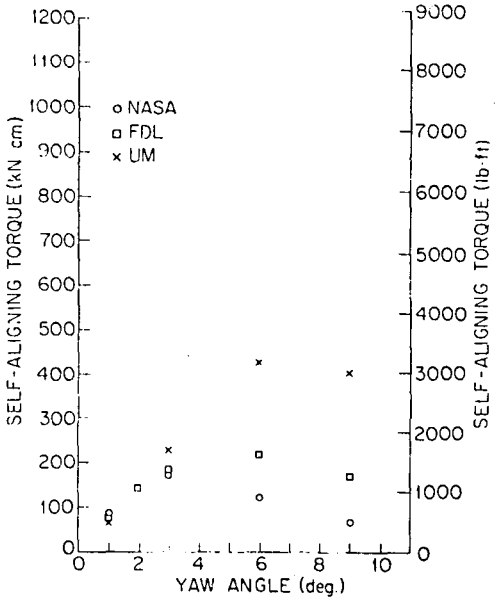

(d) $F_Z \simeq$ 89.0 kN (20000 lbs.)

Figure 24 - Slow-Rolling Self-Aligning Torque vs Yaw Angle (49x17, 26 PR Tire; $P_o \simeq$ 1172 kPa (170 psi))

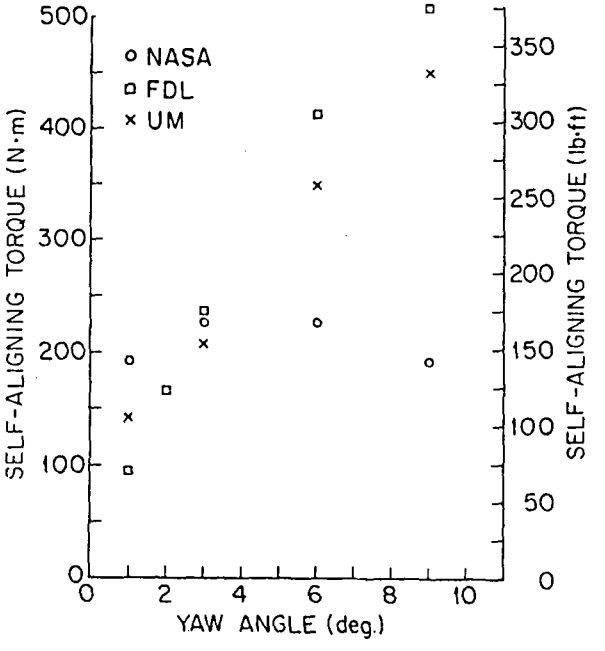

(a) $F_Z \simeq$ 34.5 kN (7750 lbs.)

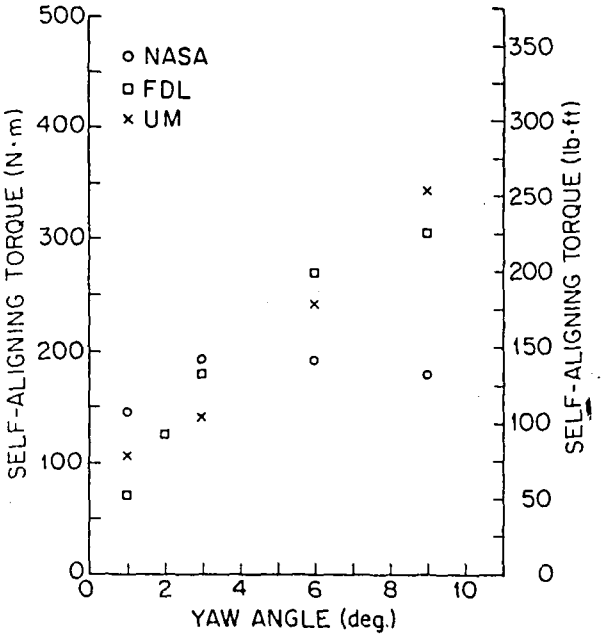

(b) $F_Z \simeq$ 27.6 kN (6200 lbs.)

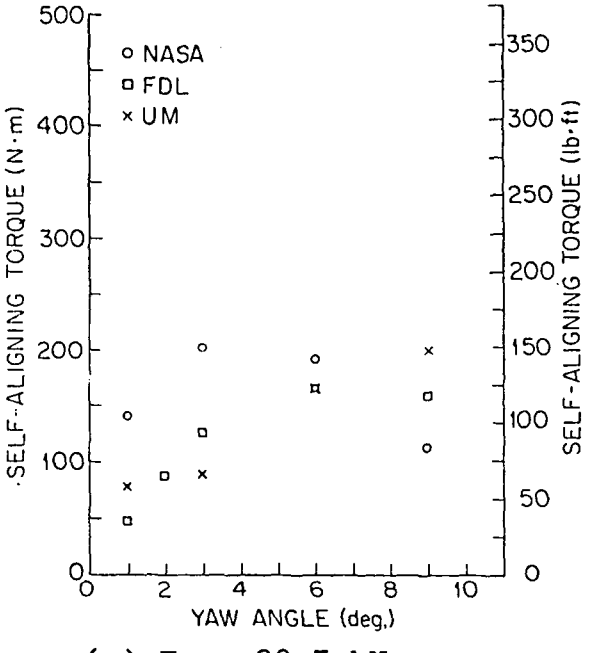

(c) $F_Z \simeq$ 20.7 kN (4650 lbs.)

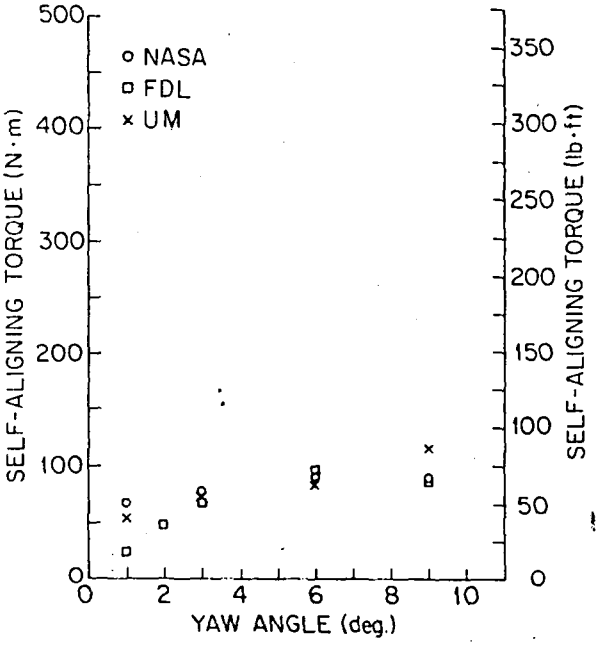

(d) $F_Z \simeq$ 13.8 kN (3100 lbs.)

Figure 25 - Slow-Rolling Self-Aligning Torque vs Yaw Angle (18x5.5, 14 PR Tire; $P_O \simeq$ 1482 kPa (215 psi))

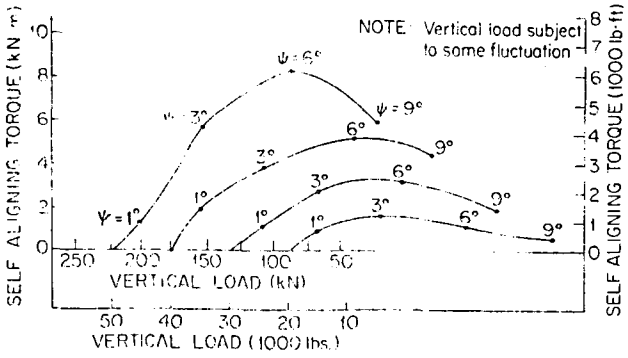

(a) NASA

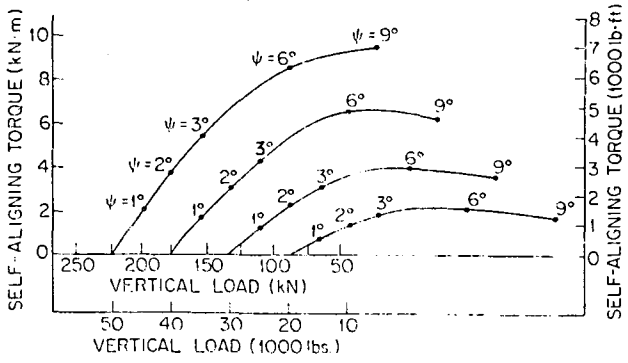

(b) FDL

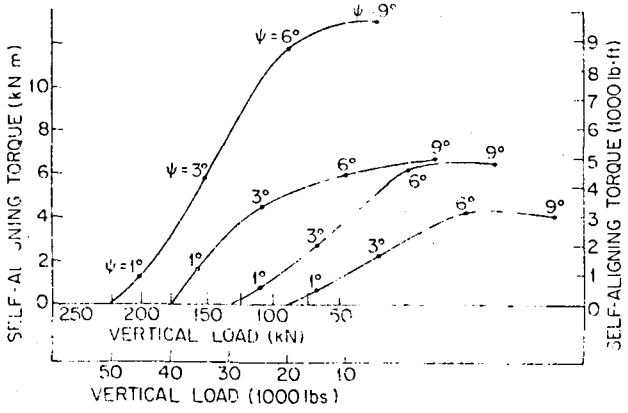

(c) UM Model to Full Size

Figure 26 - Slow-Rolling Self-Aligning Torque vs Vertical Load and Yaw Angle, ψ (49x17, 26 PR Tire; $P_o \approx 1172$ kPa (170 psi))

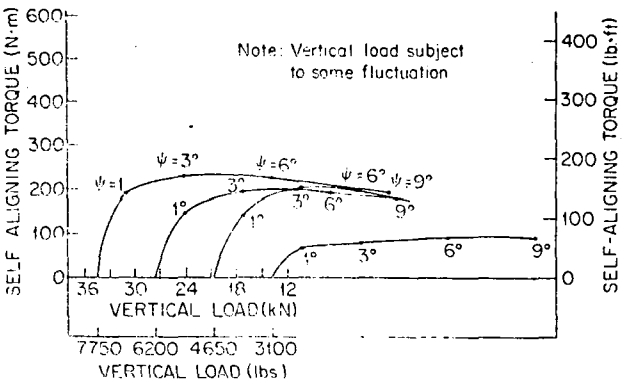

(a) NASA

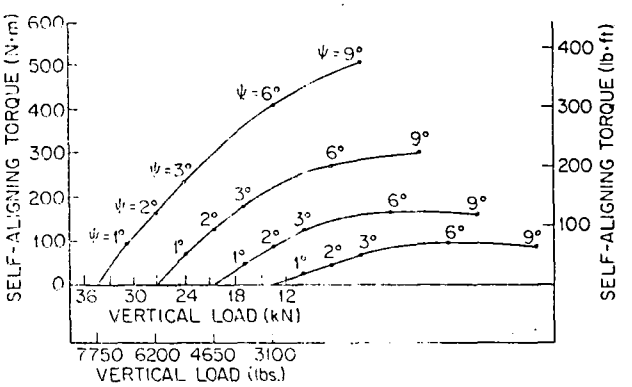

(b) FDL

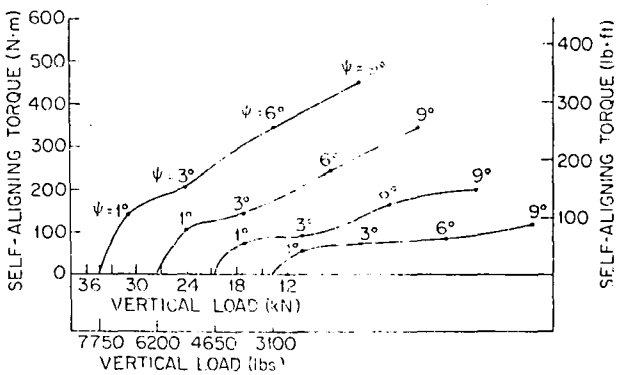

(c) UM Model to Full Size

Figure 27 - Slow-Rolling Self-Aligning Torque vs Vertical Load and Yaw Angle, ψ (18 x 5.5,14 PR Tire; $P_o \approx 1482$ kPa (215 psi))

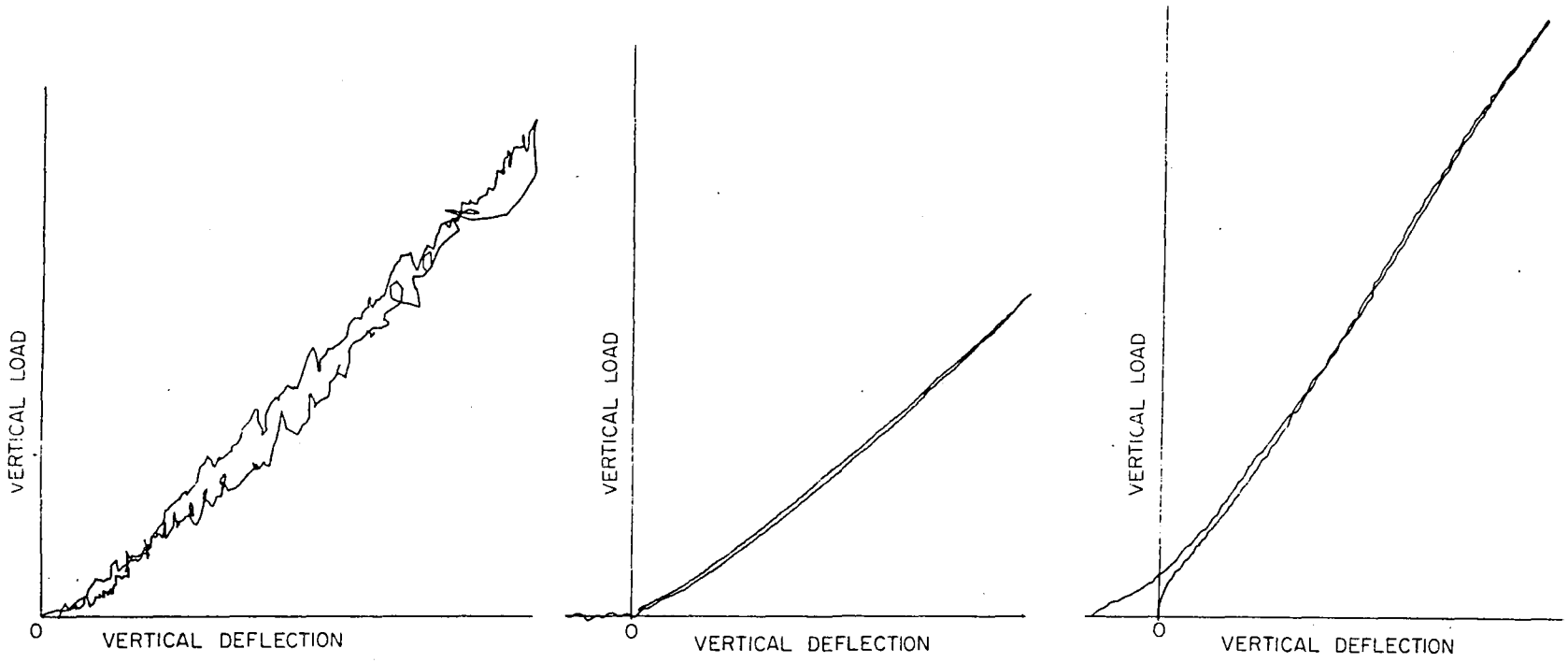

(a) NASA;49 x 17, 26 PR Tire v=50 knots

(b) FDL; 49 x 17, 26 PR Tire v=50 knots

(c) UM Model; 49 x 17, 26 PR Tire v=50 knots

Figure 28 - Typical Vertical Load-Deflection Curves at Non-Zero Speeds

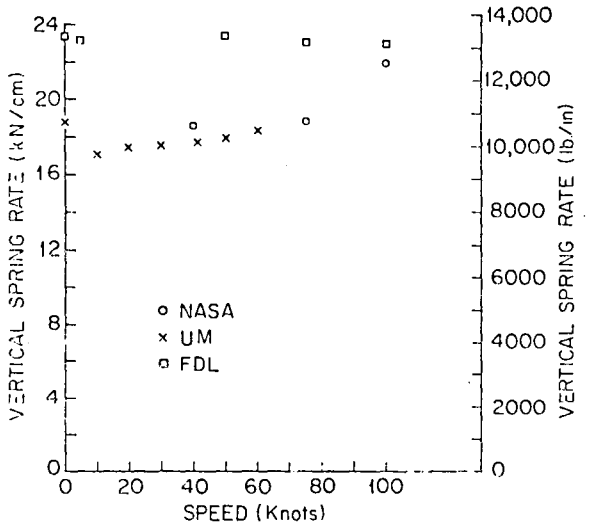

(a) $F_Z \simeq 222.4$ kN (50000 lbs.)

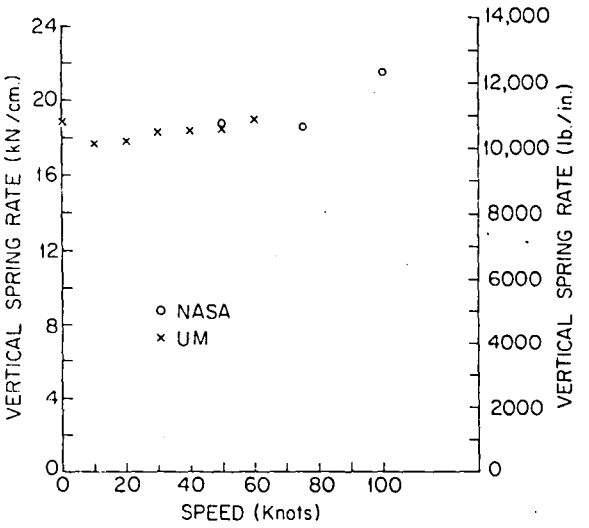

(b) $F_Z \simeq 177.9$ kN (40000 lbs.)

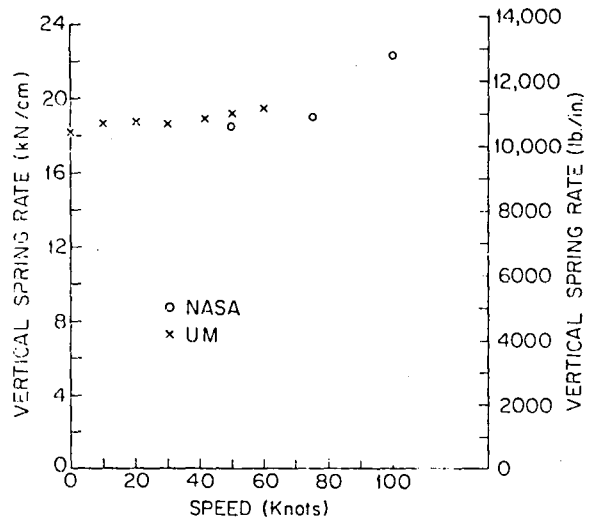

(c) $F_Z \simeq 133.4$ kN (30000 lbs.)

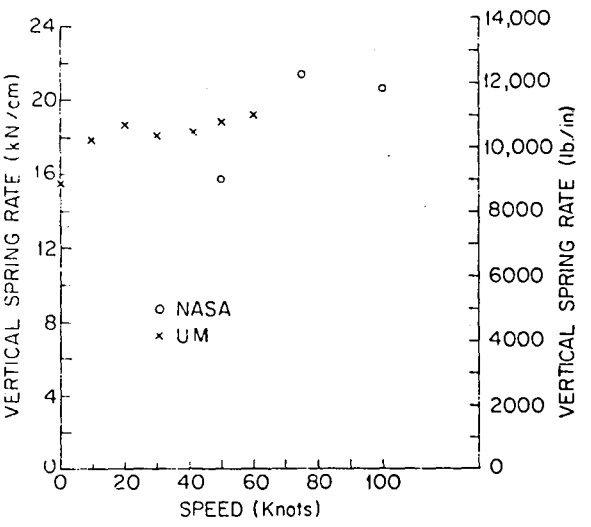

(d) $F_Z \simeq 89.0$ kN (20000 lbs.)

Figure 29 - Vertical Spring Rate vs Speed (49x17, 26 PR Tire; P_o=1172 kPa (170 psi))

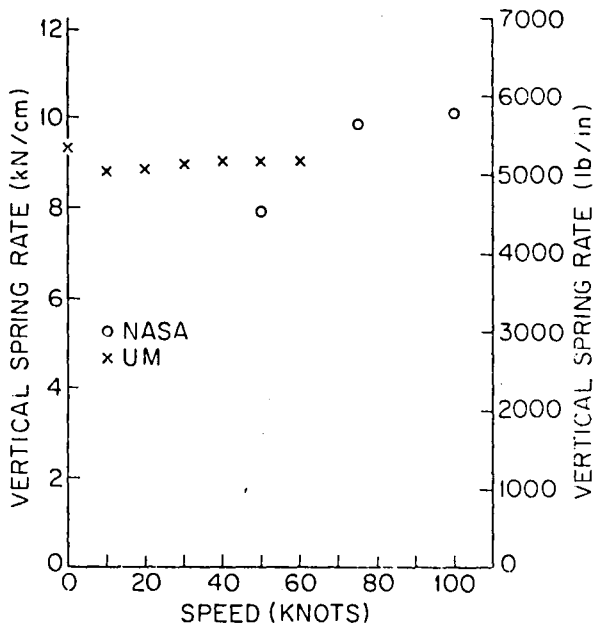

(a) $F_Z \simeq 34.5$ kN (7750 lbs.)

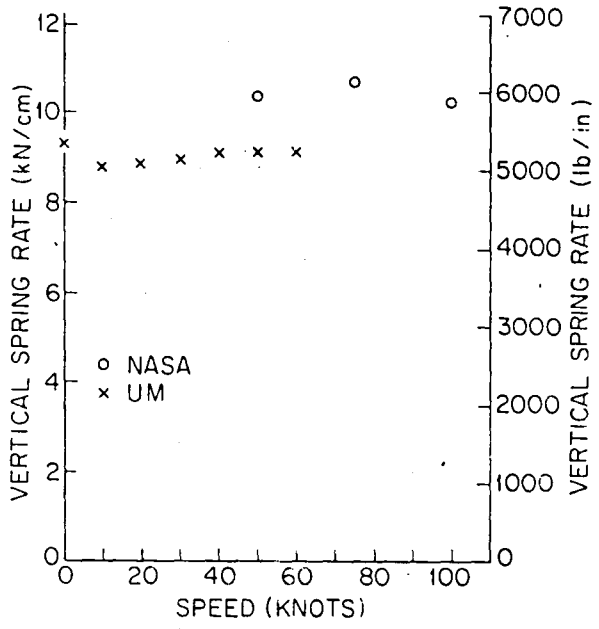

$F_Z \simeq 27.6$ (6200 lbs.)

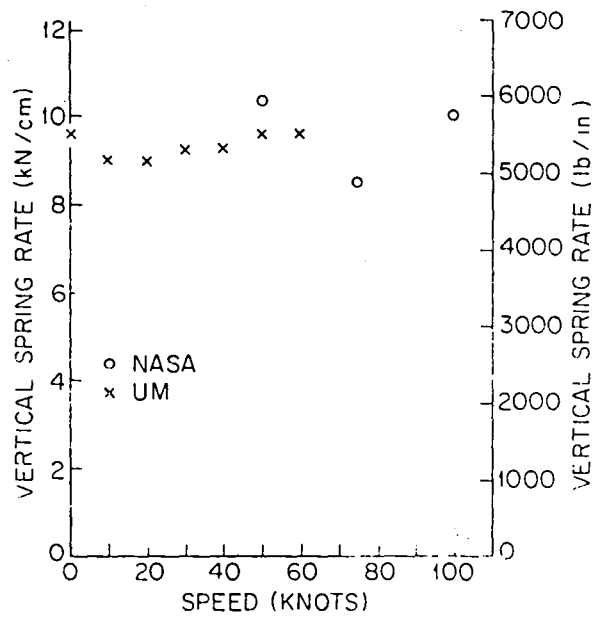

(c) $F_Z \simeq 20.7$ kN (4650 lbs.)

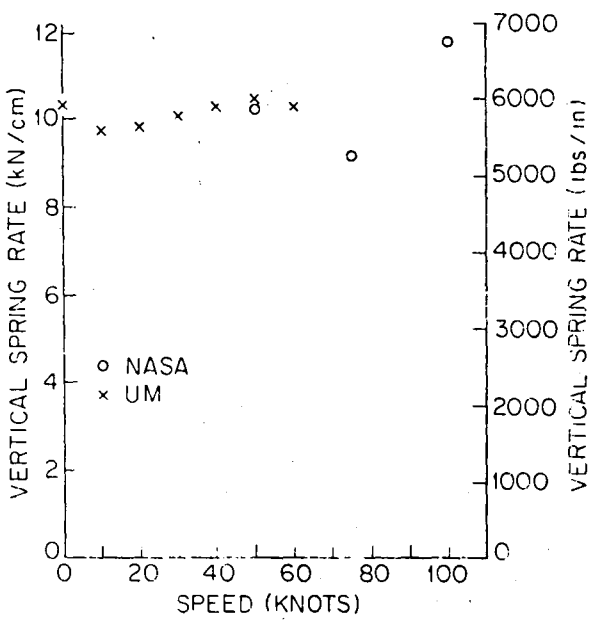

(d) $F_Z \simeq 13.8$ kN (3100 lbs.)

Figure 30 - Vertical Spring Rate vs Speed (18x5.5, 14 PR Tire; P_o=1482 kPa (215 psi))

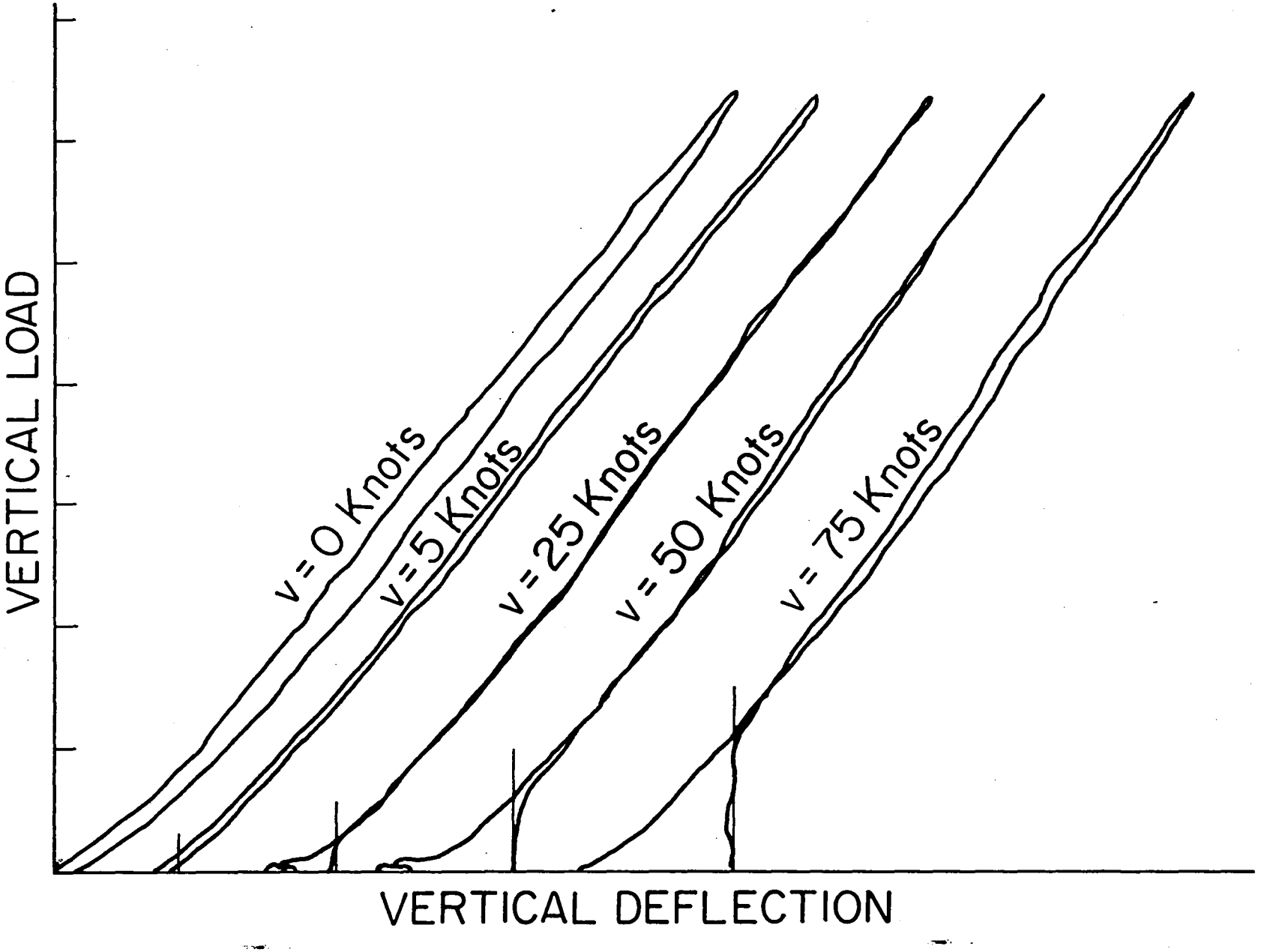

Figure 31 - Vertical Hysteresis Loops at Various Speeds UM Model 49 x 17 26 PR

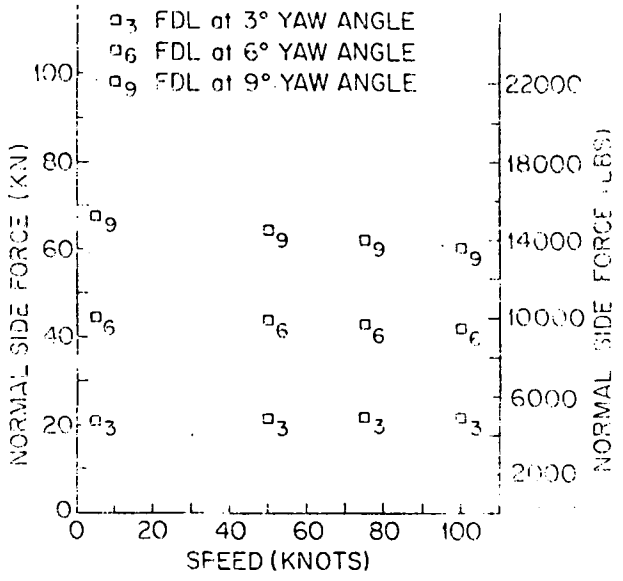

(a) $F_Z \simeq 222.4$ kN (50000 lbs.)

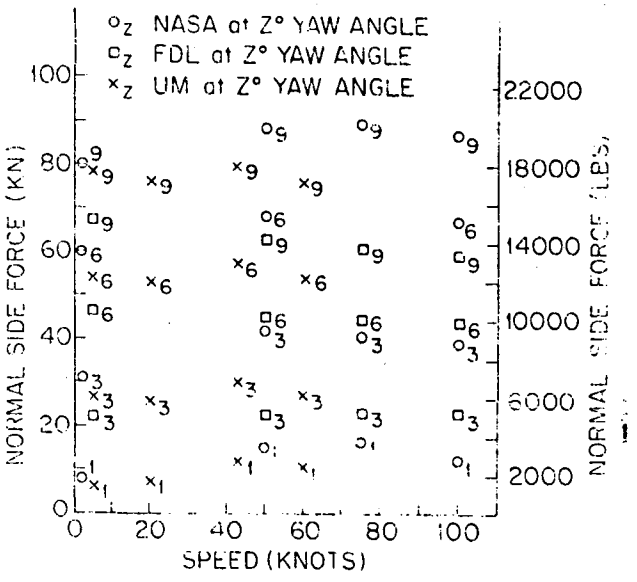

(b) $F_Z \simeq 177.9$ kN (40000 lbs.)

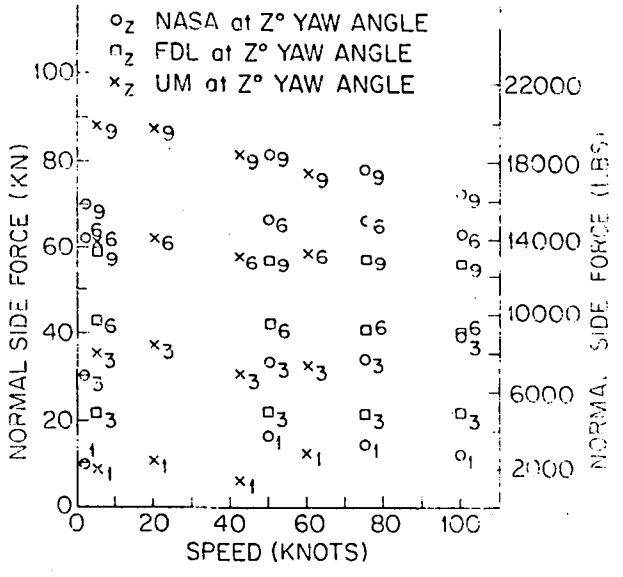

(c) $F_Z \simeq 133.4$ kN (30000 lbs)

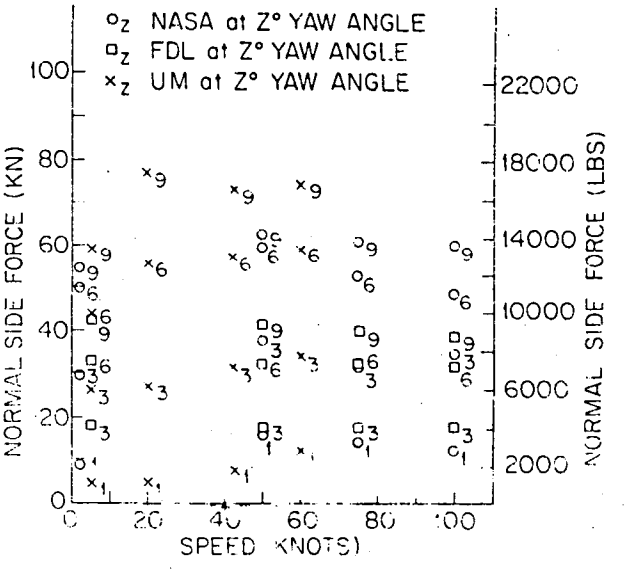

(d) $F_Z \simeq 89.0$ kN (20000 lbs.)

Figure 32 - Side Force vs Speed at Various Yaw Angles (49x17, 26 PR Tire; P_o=1172 kPa (170 psi))

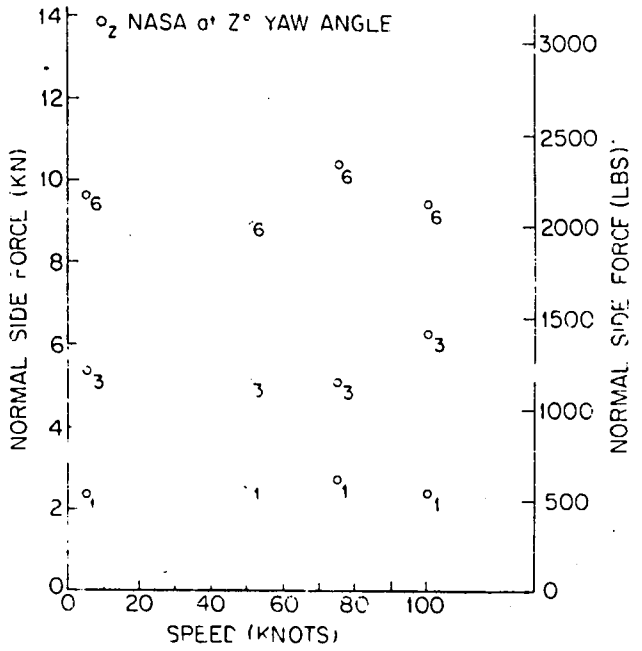

(a) $F_Z \simeq 34.5$ kN (7750 lbs.)

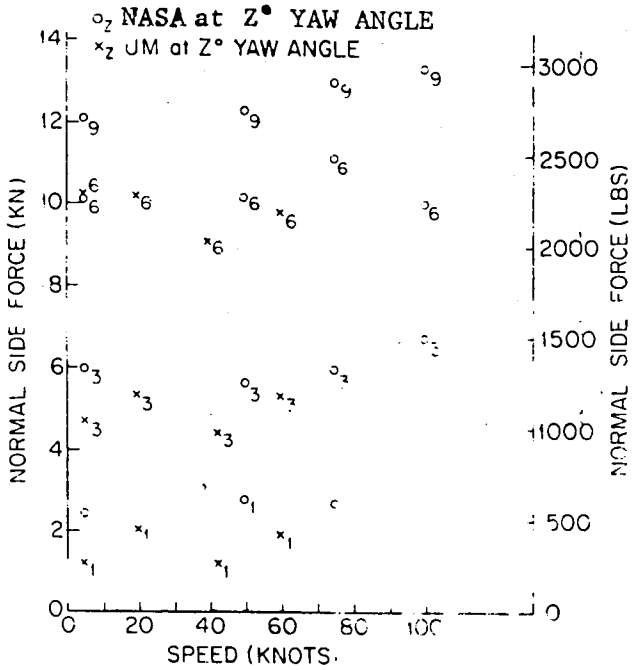

(b) $F_Z \simeq 27.6$ kN (6200 lbs.)

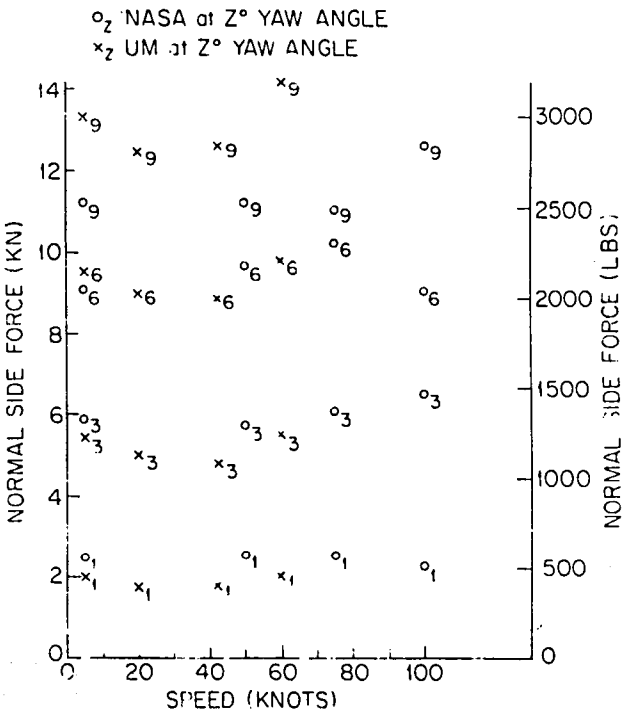

(c) $F_Z \simeq 20.7$ kN (4650 lbs.)

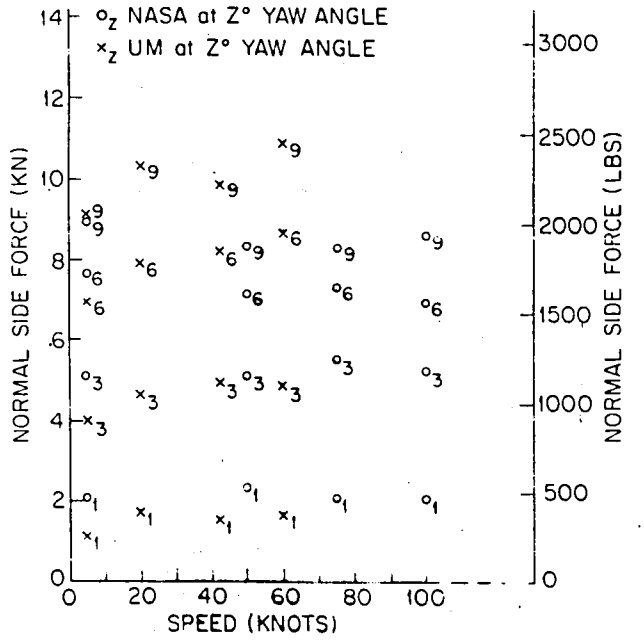

(d) $F_Z \simeq 13.8$ kN (3100 lbs.)

Figure 33 - Normal Side Force vs Speed at Various Yaw Angles (18x5.5, 14 PR Tire; P_o=1482 kPa (215 psi))

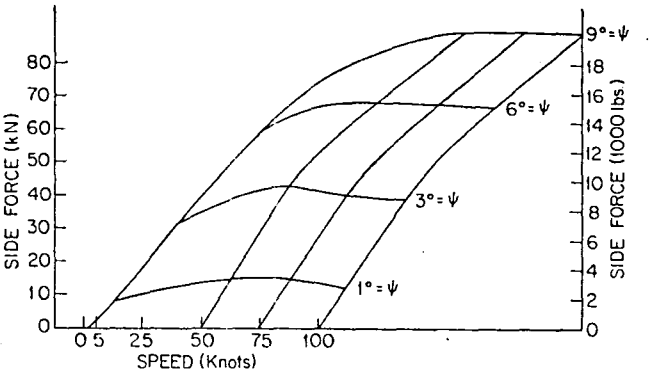

(a) NASA

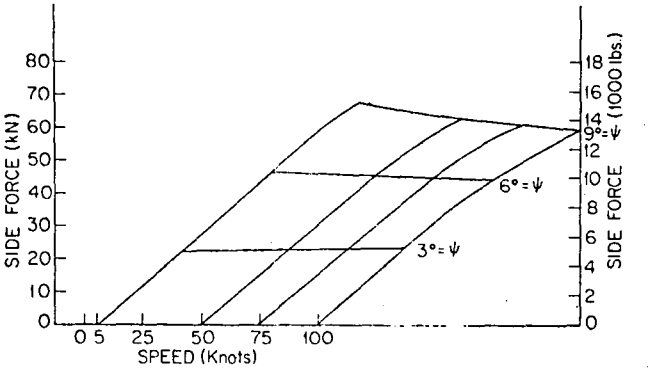

(b) FDL

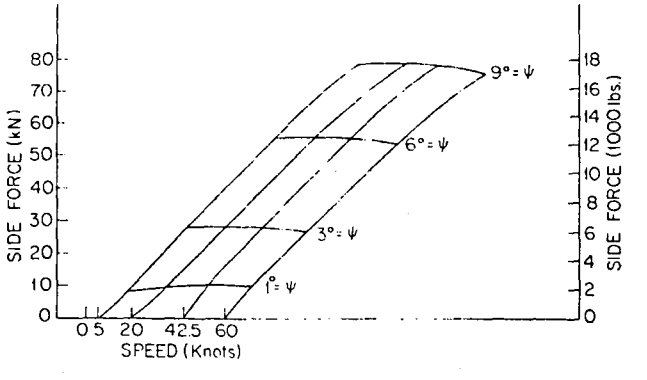

(c) UM Model to Full Size

Figure 34 - Side Force vs Speed and Yaw Angle (49x17, 26 PR Tire; Vertical Load = 177.9 kN (40000 lbs.); P_o=1172 kPa (170 psi))

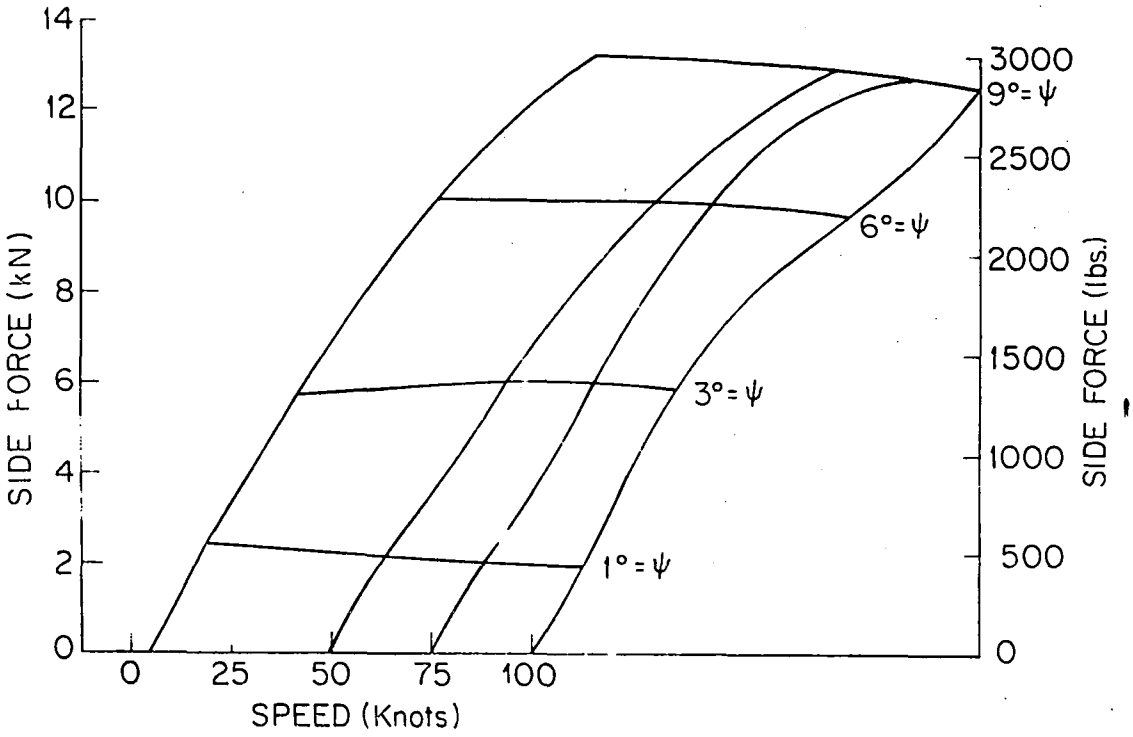

(a) NASA

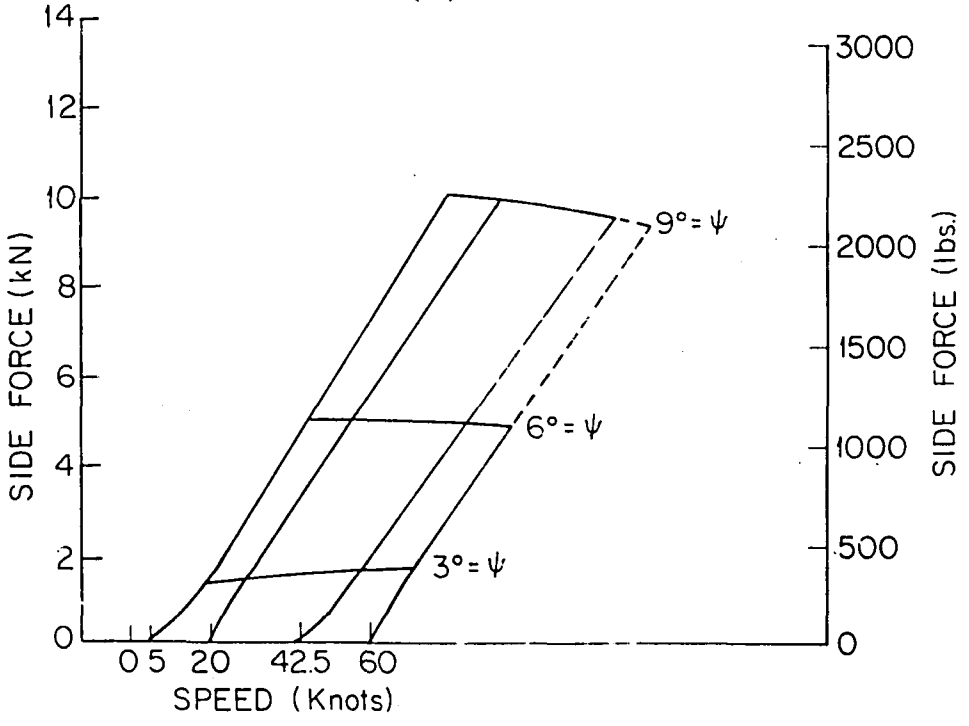

(b) UM Model to Full Size

Figure 35 - Side Force vs Speed and Yaw Angle (18x5.5, 14 PR Tire; Vertical Load ≈ 27.6 kN (6200 lbs.); P_o=1482 kPa (215 psi))

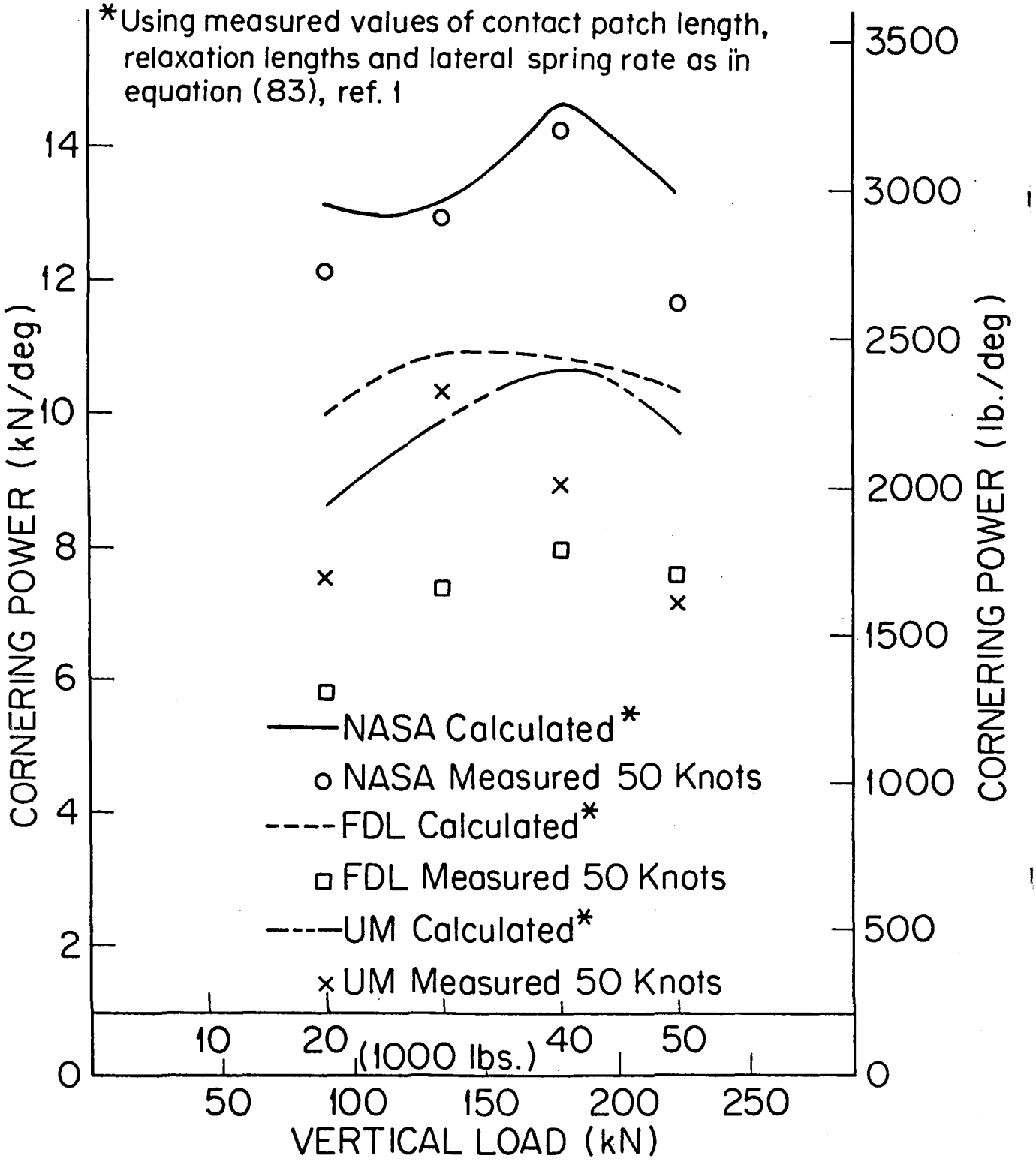

Figure 36 - Cornering Power vs Vertical Load

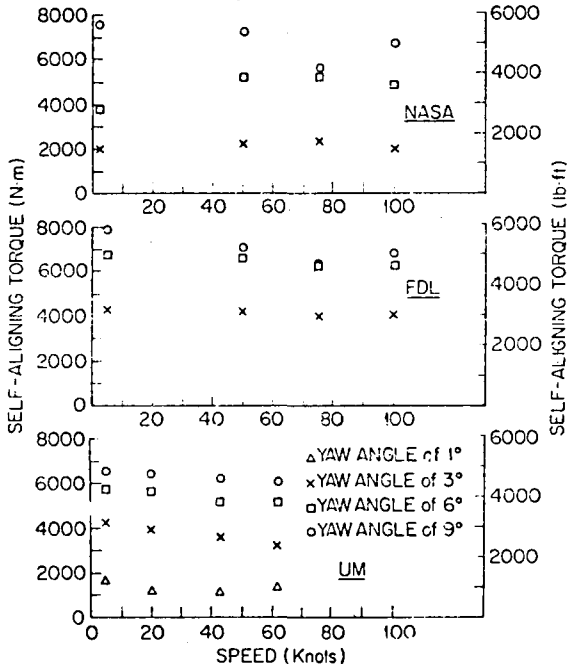

(a) $F_z \simeq$ 177.9 kN (40000 lbs.)

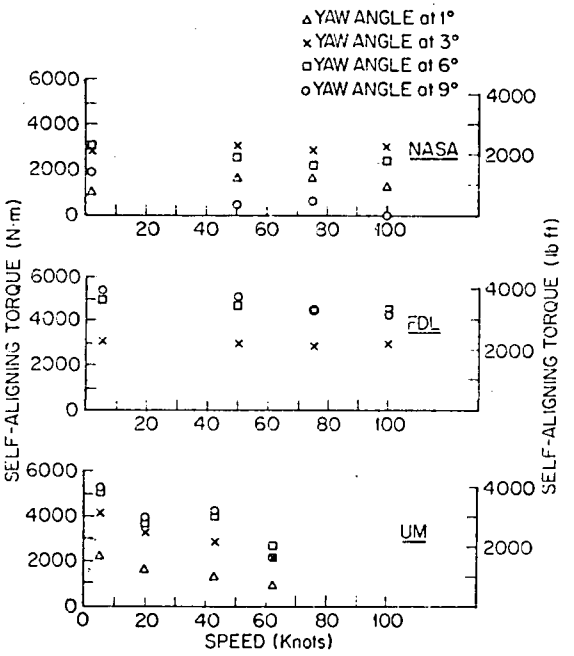

(b) $F_z \simeq$ 133.4 kN (30000 lbs.)

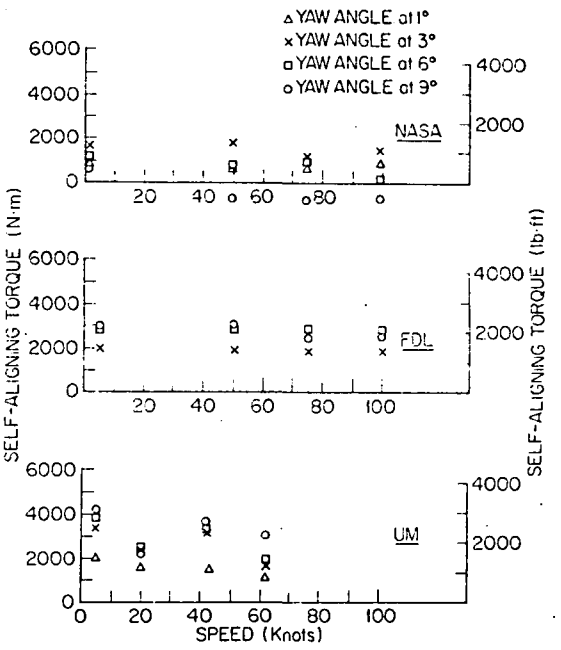

(c) $F_z \simeq$ 89.0 kN (20000 lbs.)

NOTE: NASA vertical load subject to some fluctuation

Figure 37 - Self-Aligning Torque vs Speed at Several Yaw Angles (49x17, 26 PR Tire; P_o=1172 kPa (170 psi))

Figure 37

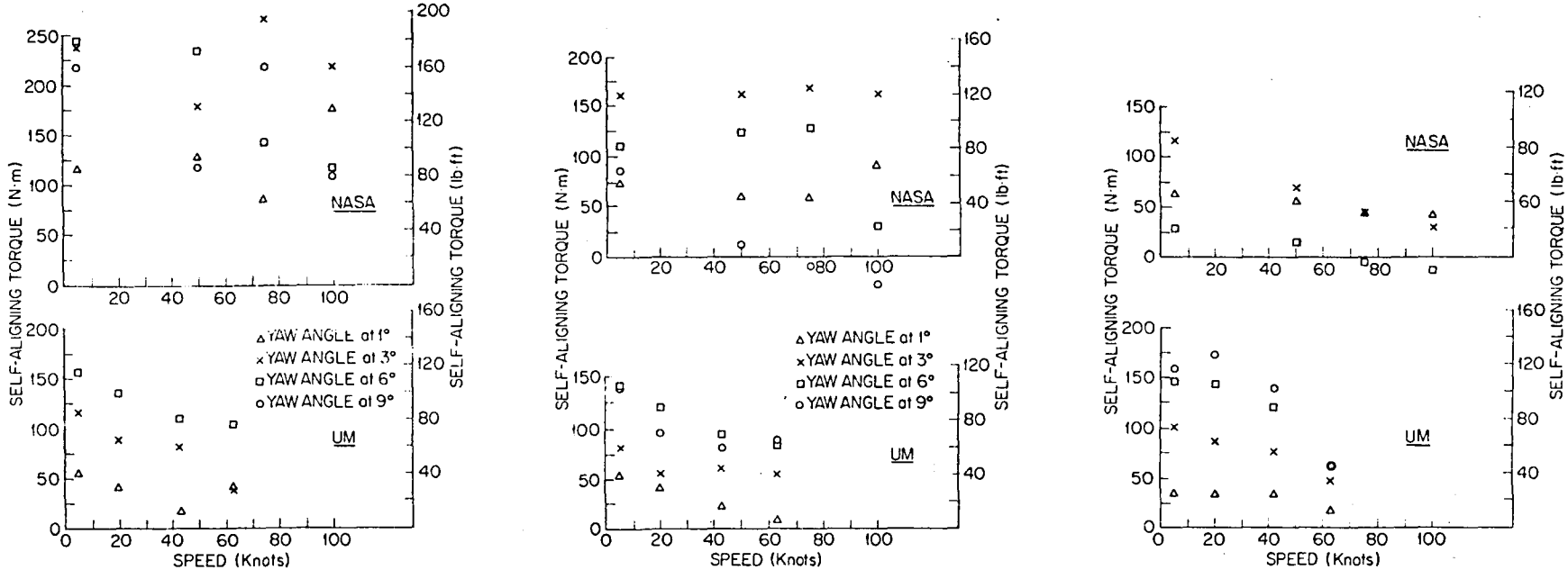

(a) $F_Z \simeq 27.6$ kN (6200 lbs.)

(b) $F_Z \simeq 20.7$ kN (4650 lbs.)

(c) $F_Z \simeq 13.8$ kN (3100 lbs.)

Figure 38 - Self-Aligning Torque vs Speed at Several Yaw Angles. (18x5.5, 14 PR Tire; P_o=1482 kPa (215 psi))

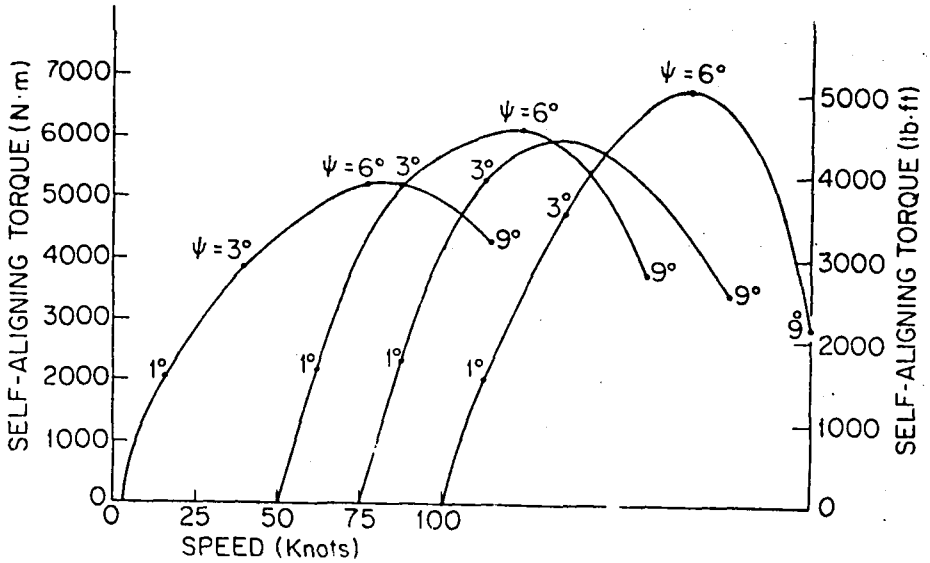

(a) NASA

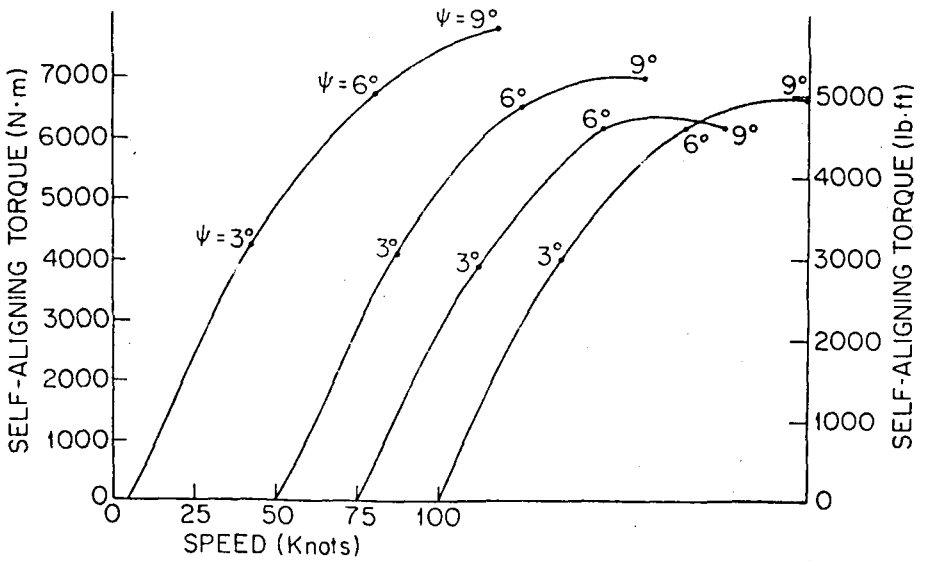

(b) FDL

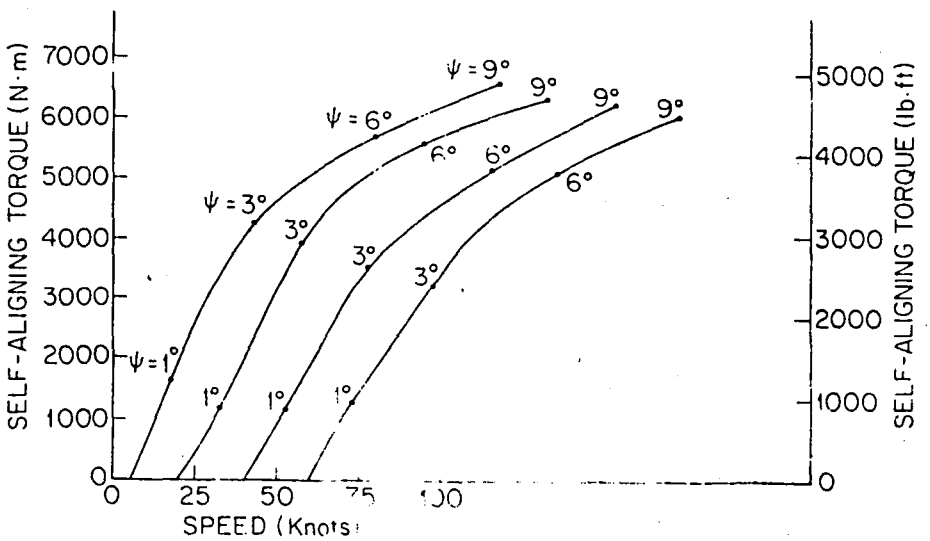

(c) UM Model to Full Size

Figure 39 - Self-Aligning Torque vs Speed, Yaw Angle (49x17, 26 PR Tire; Vertical Load = 177.9 kN (40000 lbs.); P_o=1172 kPa (170 psi))

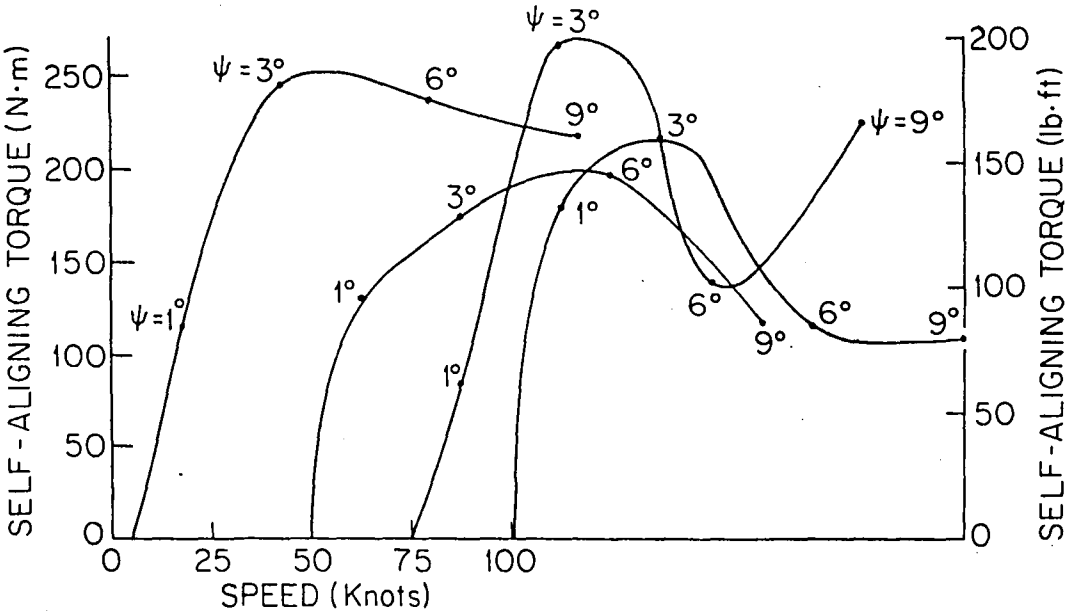

(a) NASA

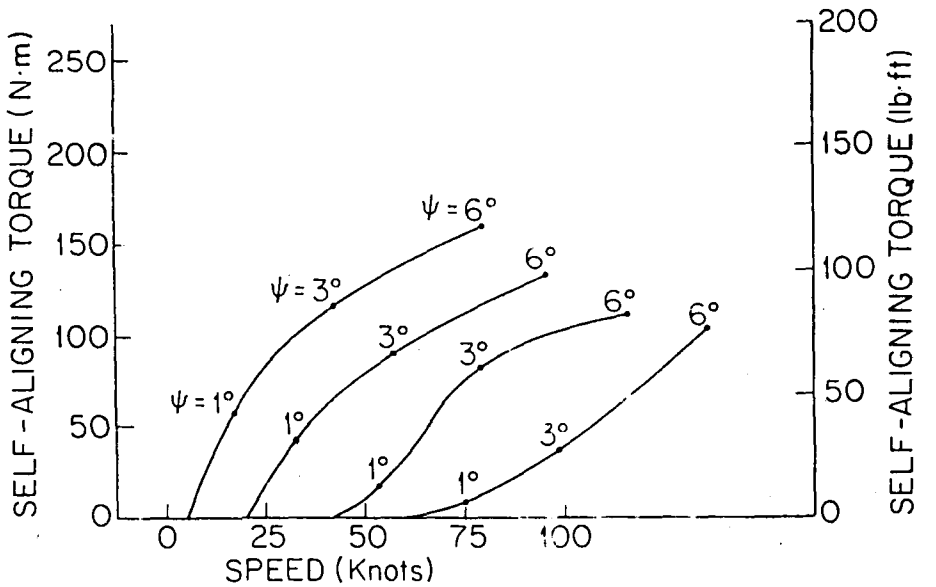

(b) UM Model to Full Size

Figure 40 - Self-Aligning Torque vs Speed, Yaw Angle. (18x5.5, 14 PR Tire; Vertical Load ≈ 27.6 kN (6200 lbs); P_o=1482 kPa (215 psi))

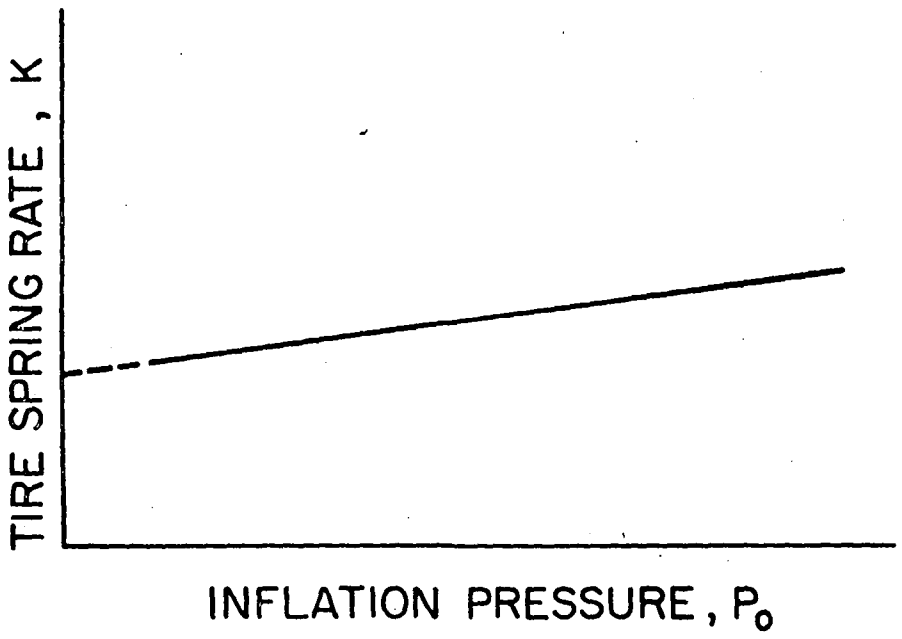

Figure A-1. Tire spring rate vs inflation pressure

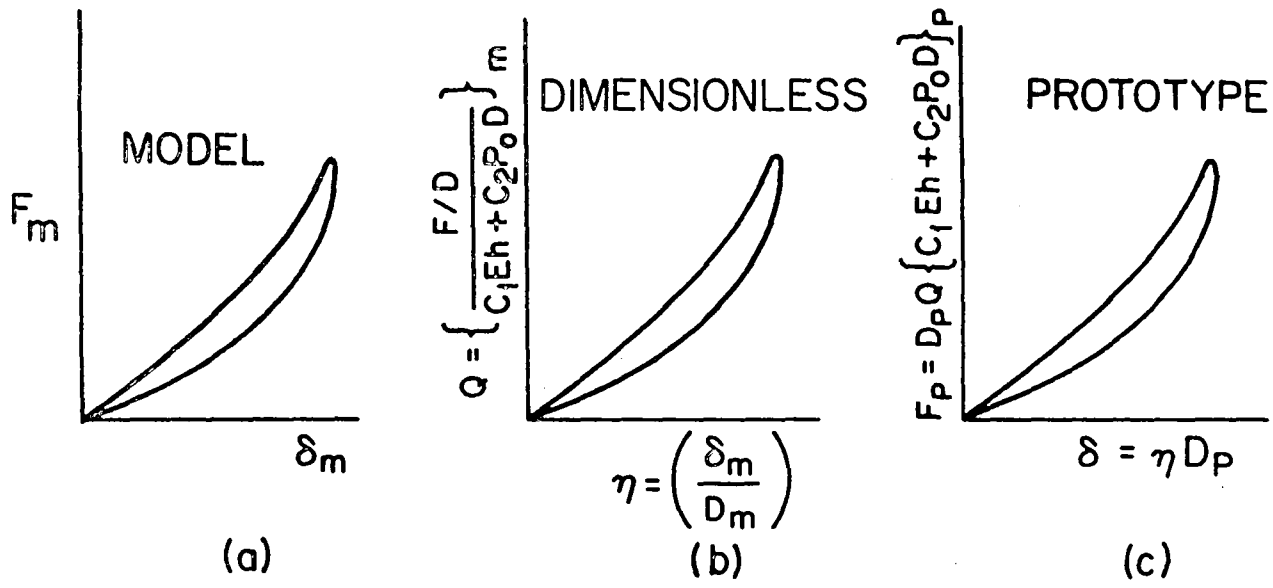

Figures A-2. Typical load-deflection curves.

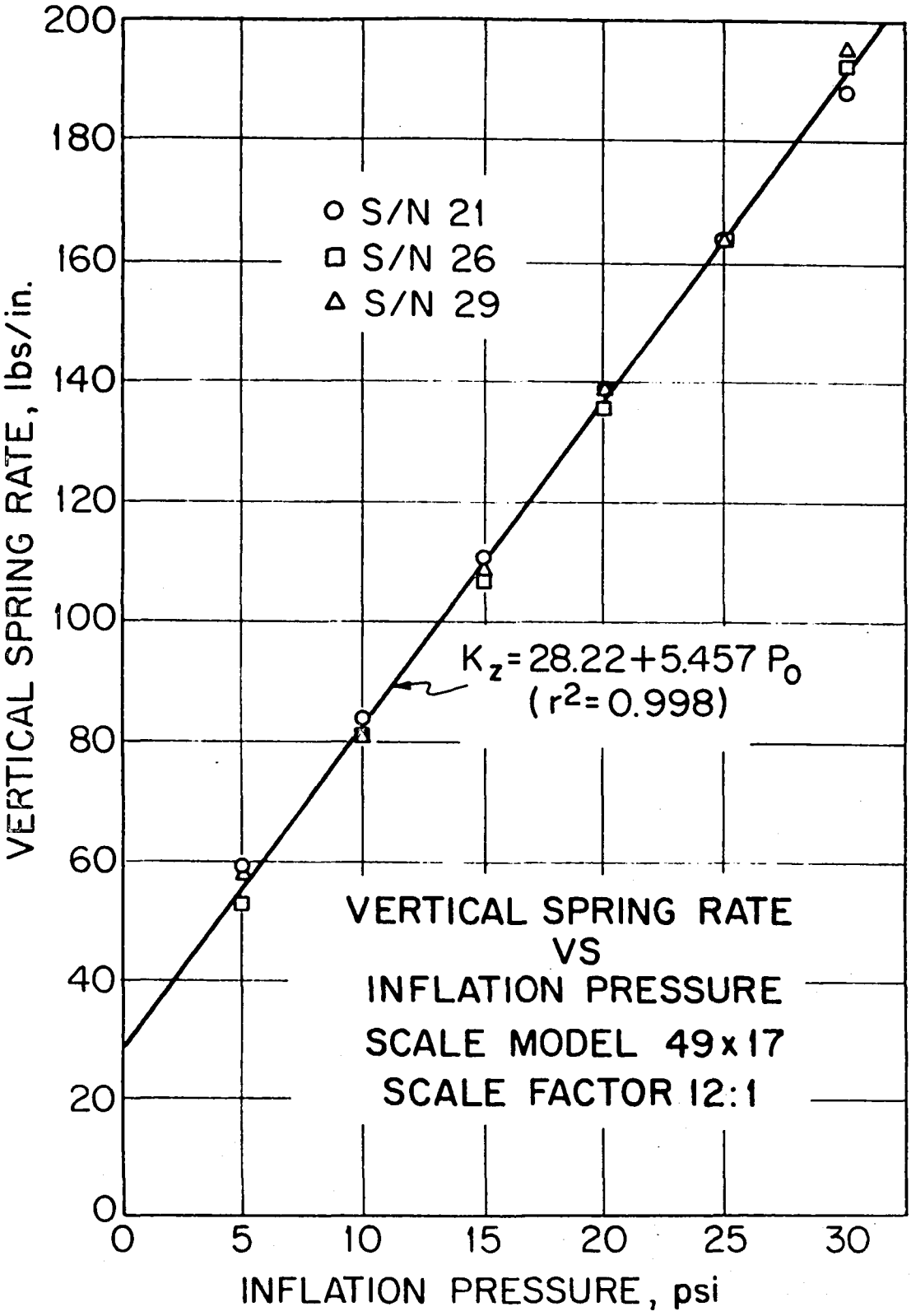

Figure A-3. Vertical spring rate vs inflation pressure for 49 x 17 tire models.

1. Report No. NASA CR-165720	2. Government Accession No.	3. Recipient's Catalog No.
4. Title and Subtitle A COMPARISON OF SOME STATIC AND DYNAMIC MECHANICAL PROPERTIES OF 18x5.5 AND 49x17 TYPE VII AIRCRAFT TIRES AS MEASURED BY THREE TEST FACILITIES		5. Report Date July 1981 6. Performing Organization Code
7. Author(s) Richard N. Dodge and Samuel K. Clark		8. Performing Organization Report No. 10. Work Unit No.
9. Performing Organization Name and Address The University of Michigan Department of Mechanical Engineering and Applied Mechanics Ann Arbor, Michigan 48109		11. Contract or Grant No. NSG-1494
12. Sponsoring Agency Name and Address National Aeronautics and Space Administration Washington, D.C. 20546		13. Type of Report and Period Covered Contractor Report 14. Sponsoring Agency Code

15. Supplementary Notes

Langley Technical Monitor: John L. McCarty
Final Report

16. Abstract Mechanical properties of 49x17 and 18x5.5 type VII aircraft tires were measured during static, slow rolling, and high-speed tests, and comparisons were made between data as acquired on indoor drum dynamometers and on an outdoor test track. In addition, mechanical properties were also obtained from scale model tires and compared with corresponding properties from full-size tires. While the tests covered a wide range of tire properties, results seem to indicate that speed effects are not large, scale models may be used for obtaining some but not all tire properties, and that predictive equations developed in NASA TR R-64 are still useful in estimating most mechanical properties.

17. Key Words (Suggested by Author(s))	18. Distribution Statement
Tires, aircraft Landing gear	Unclassified - Unlimited Subject Category 03

19. Security Classif. (of this report)	20. Security Classif. (of this page)	21. No. of Pages	22. Price
Unclassified	Unclassified	85	A05

For sale by the National Technical Information Service, Springfield, Virginia 22161